ABSTRACT

Title of dissertation: CONVERGENCE OF ADAPTIVE
FINITE ELEMENT METHODS

Khamron Mekchay, Doctor of Philosophy, 2005

Dissertation directed by: Professor Ricardo H. Nochetto
Department of Mathematics

We develop adaptive finite element methods (AFEMs) for elliptic problems, and prove their convergence, based on ideas introduced by Dörfler [7], and Morin, Nochetto, and Siebert [15, 16]. We first study an AFEM for general second order linear elliptic PDEs, thereby extending the results of Morin et al [15, 16] that are valid for the Laplace operator. The proof of convergence relies on quasi-orthogonality, which accounts for the bilinear form not being a scalar product, together with novel error and oscillation reduction estimates, which now do not decouple. We show that AFEM is a contraction for the sum of energy error plus oscillation. Numerical experiments, including oscillatory coefficients and both coercive and non-coercive convection-diffusion PDEs, illustrate the theory and yield optimal meshes. The role of oscillation control is now more crucial than in [15, 16] and is discussed and documented in the experiments.

We next introduce an AFEM for the Laplace-Beltrami operator on C^1 graphs in R^d ($d \geq 2$). We first derive a posteriori error estimates that account for both the energy error in H^1 and the geometric error in W_∞^1 due to approximation of the

surface by a polyhedral one. We devise a marking strategy to reduce the energy and geometric errors as well as the geometric oscillation. We prove that AFEM is a contraction on a suitably scaled sum of these three quantities as soon as the geometric oscillation has been reduced beyond a threshold. The resulting AFEM converges without knowing such threshold or any constants, and starting from any coarse initial triangulation. Several numerical experiments illustrate the theory.

Finally, we introduce and analyze an AFEM for the Laplace-Beltrami operator on parametric surfaces, thereby extending the results for graphs. Note that, due to the nature of parametric surfaces, the geometric oscillation is now measured in terms of the differences of tangential gradients rather than differences of normals as for graphs. Numerical experiments with closed surfaces are provided to illustrate the theory.

CONVERGENCE OF ADAPTIVE
FINITE ELEMENT METHODS

by

Khamron Mekchay

Dissertation submitted to the Faculty of the Graduate School of the
University of Maryland, College Park in partial fulfillment
of the requirements for the degree of
Doctor of Philosophy
2005

Advisory Commmittee:

Professor Ricardo H. Nochetto, Chair/Advisor
Dr. Georg Dolzmann
Professor Howard C. Elman
Professor Jian-Guo Liu
Professor John E. Osborn

ACKNOWLEDGMENTS

I owe my gratitude to all the people who have made this thesis possible and because of whom my graduate experience has been one that I will cherish forever.

First and foremost I'd like to thank my advisor, Professor Ricardo H. Nochetto for giving me an invaluable opportunity to work on challenging and extremely interesting projects over the past three and a half years. He has always made himself available for help and advice, and there has never been an occasion when I've knocked on his door and he hasn't given me time. It has been a pleasure to work with and learn from such an extraordinary individual.

I would also like to thank Professor John E. Osborn, Dr. Georg Dolzmann, Professor Howard C. Elman, Professor Jian-Guo Liu, and Dr. Tobias von Petersdorff for agreeing to serve on my thesis committee and for sparing their invaluable time reviewing the manuscript. Thanks also to Dr. Pedro Morin from IMAL, Argentina, for his great ideas and advice that shade the light on some projects and numerical experiments.

I owe my deepest thanks to my family - my parents and my fiancee Premsuda Sricharmorn, who have always stood by me, and have pulled me through against impossible odds at times. Words cannot express the gratitude I owe them. I would also like to thank Sangwan Chan-ngern, Rasmeloungon family who are like family members to me.

My officemates and friends in Mathematics departments have been a crucial factor in my finishing smoothly. I'd like to express my gratitude to Gunay Dogan, Chensong Zhang, Ju-Yi Yen for their friendship and support.

It is impossible to remember all, and I apologize to those I've inadvertently left out.

TABLE OF CONTENTS

Overview

Adaptive procedure for numerical solution of partial differential equations (PDEs) started in the late 1970's and are now standard tools in science and engineering. Adaptivity is an effective tool for obtaining approximate solutions of good quality at relatively low computational costs, especially in the presence if singularities. *Adaptive finite element methods (AFEMs)* are indeed a meaningful approach toward multi-scale phenomena that makes realistic computations feasible.

A key ingredient of adaptivity is *a posteriori error estimation.* A posteriori error estimates are computable estimates for the error in suitable norms, typically in energy norm, in terms of the approximate solution and data of the problem. They in fact provide the basis for adaptive mesh refinement and quantitative error control to reach the ultimate goal - equidistribute the local discretization error. This can be rephrased in terms of optimizing the computational effort for a given accuracy, which in turn corresponds to avoiding overrefinement. We refer to the books of Ainsworth and Oden [1] and Verfürth [23] for an extensive review on a posteriori error estimation.

For elliptic PDEs, AFEM boils down to iterations of the form

$$\text{SOLVE} \rightarrow \text{ESTIMATE} \rightarrow \text{MARK} \rightarrow \text{REFINE}.$$

Given a current mesh and data, SOLVE finds the approximate solution; ESTIMATE computes error estimates in suitable norms based on *a posteriori error estimators*; MARK marks elements for refinement, thus hoping to reach the ultimate goal; REFINE refines the current mesh to obtain a finer, hopefully enhanced, mesh. Ide-

ally, AFEMs produce an infinite sequence of approximate solutions, and the question arises whether this sequence converges to the exact solution. A complete answer in $1d$ was given by Babuška and Vogelius [2]; this result and techniques do not extend to several dimensions though. For multidimensional problems, Dörfler [7] introduced a marking strategy and established a connection between consecutive discrete solutions which turn out to be crucial for convergence. Dörfler did not construct, however, a convergent AFEM in the sense described above. More recently, Morin et al [15, 16] introduced the notion of *data oscillation*, incorporated an additional marking to account for it, and proved convergence of the resulting AFEM. These results, however, are only valid for second order elliptic operators with piecewise constant coefficients and without lower order terms; the Laplace operator is a chief example.

In this thesis we extend these results upon developing AFEM and proving their convergence for general second order linear elliptic PDEs and for the Laplace-Beltrami operator on surfaces. The study of AFEM for general second order linear elliptic PDEs extends [15, 16] to variable coefficients and non-symmetric noncoercive bilinear forms; this could be used as a basis for further work on AFEM for *nonlinear* elliptic PDEs. The interest in solving the Laplace-Beltrami operator on surfaces comes from problems in physics, biophysics, engineering problems, and image processing, where elliptic PDEs are to be solved on surfaces instead of flat domains. We deal first with the simpler case of graphs, and later with the general case of parametric surfaces.

Thesis Outline

We organize the presentation of this thesis into three parts. In Chapter 1, we develop and prove convergence of AFEM for general second order linear elliptic PDEs. We introduce the concept of *quasi-orthogonality* to account for non-symmetric bilinear forms corresponding to convection-diffusion PDEs. Since oscillations now depend also on the approximate solution, due to the presence of variable coefficients and lower order terms, they are coupled with the error. This is an essential difficulty, typical of general operators, that was not addressed in [15, 16]. We study this issue in detail. We prove convergence upon showing that AFEM is a contraction for a suitably scaled sum of energy error and oscillation. We conclude this chapter with several numerical experiments to illustrate the theory and shed light on the more prominent role of oscillation.

In Chapter 2, we develop AFEM for the Laplace-Beltrami operator on graphs. We start with differential geometry properties of graphs that are useful for the a posteriori error analysis. We derive a posteriori error estimates that account for both the energy error in H^1 and the geometric error in W_∞^1 due to approximation of the graph by a polyhedral one. We devise a marking strategy to reduce the energy and geometric errors as well as the geometric oscillation. We prove that AFEM is a contraction on a suitably scaled sum of these three quantities as soon as the geometric oscillation has been reduced beyond a threshold; this threshold measures closeness between exact and discrete surfaces or, equivalently, geometric resolution of the underlying finite element mesh. Our AFEM converges without knowing such

threshold or any constants, and starting from any coarse initial triangulation. Several numerical experiments illustrate the theory.

In Chapter 3, we extend the results of Chapter 2 to the Laplace-Beltrami operator on parametric surfaces. The development and analysis are similar to those of graphs. Starting from basic differential geometry, we discuss the local representation of the surface within the finite element context and how conforming refinement of macro-elements gives rise to a conforming discretization of the surface. This matter is crucial for both the formulation of AFEM and its analysis. We next derive a posteriori error estimates. We point out that both the geometric error and oscillation for parametric surfaces are different from those used for graphs. We prove convergence of the resulting AFEM and conclude with numerical experiments that illustrate the theory.

Chapter 1

AFEM for General Second Order Linear Elliptic PDEs

1.1 Introduction and Main Result

Let Ω be a polyhedral bounded domain in $\mathbb{R}^d$, $(d = 2, 3)$. We consider a homogeneous Dirichlet boundary value problem for a general second order elliptic partial differential equation (PDE):

$$\mathcal{L}u = -\nabla\cdot(\mathbf{A}\nabla u) + \mathbf{b}\cdot\nabla u + c\,u = f \quad \text{in } \Omega, \tag{1.1.1}$$

$$u = 0 \quad \text{on } \partial\Omega; \tag{1.1.2}$$

the choice of boundary condition is made for ease of presentation, since similar results are valid for other boundary conditions. We also assume

- $\mathbf{A} : \Omega \mapsto \mathbb{R}^{d\times d}$ is Lipschitz and symmetric positive definite with smallest eigenvalue a_- and largest eigenvalue a_+, i.e.,

$$a_-(x)\,|\xi|^2 \le \mathbf{A}(x)\xi\cdot\xi \le a_+(x)\,|\xi|^2, \quad \forall\xi \in \mathbb{R}^d,\ x \in \Omega; \tag{1.1.3}$$

- $\mathbf{b} \in [L^\infty(\Omega)]^d$ is divergence free ($\nabla\cdot\mathbf{b} = 0$ in Ω);

- $c \in L^\infty(\Omega)$ is nonnegative ($c \ge 0$ in Ω);

- $f \in L^2(\Omega)$.

The purpose of this chapter is to prove the following convergence results for adaptive finite element methods (AFEM) for (1.1.1-1.1.2), and document their performance computationally.

Theorem 1.1 (Convergence of AFEM). *Let $\{u_k\}_{k\in\mathbb{N}_0}$ be a sequence of finite element solutions corresponding to a sequence of nested finite element spaces $\{\mathbb{V}_k\}_{k\in\mathbb{N}_0}$ produced by the AFEM of §3.5, which involves loops of the form*

$$\mathsf{SOLVE} \to \mathsf{ESTIMATE} \to \mathsf{MARK} \to \mathsf{REFINE}.$$

There exist constants $\sigma, \gamma > 0$, and $0 < \xi < 1$, depending solely on the shape regularity of meshes, the data, the parameters used by AFEM, and a number $0 < s \leq 1$ dictated by the interior angles of $\partial\Omega$, such that if the initial meshsize h_0 satisfies $h_0^s \|\mathbf{b}\|_{L^\infty} < \sigma$, then for any two consecutive iterations k and $k+1$ we have

$$\|u - u_{k+1}\|^2 + \gamma\, \mathsf{osc}_{k+1}(\Omega)^2 \leq \xi^2 \left(\|u - u_k\|^2 + \gamma\, \mathsf{osc}_k(\Omega)^2 \right). \tag{1.1.4}$$

Therefore, AFEM converges with a linear rate ξ, namely

$$\|u - u_k\|^2 + \gamma\, \mathsf{osc}_k(\Omega)^2 \leq C_0\, \xi^{2k},$$

where $C_0 := \|u - u_0\|^2 + \gamma\, \mathsf{osc}_0(\Omega)^2$.

Hereafter, $\|\cdot\|$ denotes the energy norm induced by the operator $\mathcal{L}$ and $\mathsf{osc}(\Omega)$, the oscillation term, stands for information missed by the averaging process associated to FEM. This convergence result extends those of Morin et al. [15, 16] in several ways:

• We deal with a full second order linear elliptic PDE with variable coefficients $\mathbf{A}, \mathbf{b}$ and c, whereas in [15, 16] $\mathbf{A}$ is assumed to be piecewise constant and $\mathbf{b}$ and c to vanish.

• The underlying bilinear form $\mathcal{B}$ is non-symmetric due to the first order term $\mathbf{b}\cdot\nabla u$. Since $\mathcal{B}$ is no longer a scalar product as in [15, 16], the Pythagoras equality relating u, u_k and u_{k+1} fails; we prove a *quasi-orthogonality* property instead.

• The oscillation terms depend on discrete solutions in addition to data. Therefore, oscillation and error cannot be reduced separately as in [15, 16].

• The oscillation terms do not involve the oscillation of the jump residuals. This is achieved by exploiting positivity and continuity of $\mathbf{A}$.

• Since error and oscillation are now coupled, in order to prove convergence we need to handle them together. This leads to a novel argument and result, the contraction property (1.1.4), according to which both error and oscillation decrease together.

This chapter is organized as follows. In section 2 we introduce the bilinear form, the energy norm, recall existence and uniqueness of solutions, and state the quasi-orthogonality property. In section 3 we describe the procedures used in AFEM, namely, SOLVE, ESTIMATE, MARK, and REFINE, state new error and oscillation reduction estimates, present the adaptive algorithm AFEM and prove its convergence. In section 4 we prove the quasi-orthogonality property of section 2 and the error and oscillation reduction estimates of section 3. In section 5 we present three numerical experiments to illustrate properties of AFEM. We conclude in section 6 with extensions to $\mathbf{A}$ piecewise Lipschitz, with discontinuities aligned with the initial mesh, as well as non-coercive bilinear form $\mathcal{B}$ due to $\nabla \cdot \mathbf{b} \neq 0$ and a numerical experiment.

1.2 Discrete Solution and Quasi-Orthogonality

For an open set $G \subset \mathbb{R}^d$ we denote by $H^1(G)$ the usual Sobolev space of functions in $L^2(G)$ whose first derivatives are also in $L^2(G)$, endowed with the norm

$$\|u\|_{H^1(G)} := \left(\|u\|_{L^2(G)} + \|\nabla u\|_{L^2(G)} \right)^{1/2};$$

we use the symbols $\|\cdot\|_{H^1}$ and $\|\cdot\|_{L^2}$ when $G = \Omega$. Moreover, we denote by $H_0^1(G)$ the space of functions in $H^1(G)$ that vanish on the boundary in the trace sense.

A weak solution of (1.1.1) and (1.1.2) is a function u satisfying

$$u \in H_0^1(\Omega) : \qquad \mathcal{B}[u, v] = \langle f, v \rangle \qquad \forall\, v \in H_0^1(\Omega), \qquad (1.2.1)$$

where $\langle u, v \rangle := \int_\Omega uv$ for any $u, v \in L^2(\Omega)$, and the bilinear form is defined on $H_0^1(\Omega) \times H_0^1(\Omega)$ as

$$\mathcal{B}[u, v] := \langle \mathbf{A}\nabla u, \nabla v \rangle + \langle \mathbf{b} \cdot \nabla u + c\, u, v \rangle. \qquad (1.2.2)$$

By Cauchy-Schwarz inequality one can easily show the *continuity* of the bilinear form

$$|\mathcal{B}[u, v]| \leq C_B \|u\|_{H^1} \|v\|_{H^1},$$

where C_B depends only on the data. Combining Poincaré inequality with the divergence free condition $\nabla \cdot \mathbf{b} = 0$, one has *coercivity* in $H_0^1(\Omega)$

$$\mathcal{B}[v, v] \geq \int_\Omega a_- |\nabla v|^2 + cv^2 \geq c_B \|v\|_{H^1}^2,$$

where c_B depends only on the data. Existence and uniqueness of (1.2.1) thus follows from Lax-Milgram theorem. [10].

We define the energy norm on $H_0^1(\Omega)$ by $\|v\|^2 := \mathcal{B}[v,v]$, which is equivalent to $H_0^1(\Omega)$-norm $\|\cdot\|_{H^1}$. In fact we have

$$c_B \|v\|_{H^1}^2 \leq \|v\|^2 \leq C_B \|v\|_{H^1}^2 \qquad \forall\, v \in H_0^1(\Omega). \qquad (1.2.3)$$

1.2.1 Discrete Solutions on Nested Meshes

Let $\{\mathcal{T}_H\}$ be a shape regular family of nested conforming meshes over Ω: that is there exists a constant γ^* such that

$$\frac{H_T}{\rho_T} \leq \gamma^* \qquad \forall\, T \in \bigcup_H \mathcal{T}_H, \qquad (1.2.4)$$

where, for each $T \in \mathcal{T}_H$, H_T is the diameter of T, and ρ_T is the diameter of the biggest ball contained in T; the global meshsize is $h_H := \max_{T \in \mathcal{T}_H} H_T$.

Let $\{\mathbb{V}_H\}$ be a corresponding family of nested finite element spaces consisting of continuous piecewise polynomials over $\mathcal{T}_H$ of fixed degree $n \geq 1$, that vanish on the boundary. Let u_H be a discrete solution of (1.2.1) satisfying

$$u_H \in \mathbb{V}_H : \qquad \mathcal{B}[u_H, v_H] = \langle f, v_H \rangle \qquad \forall\, v_H \in \mathbb{V}_H; \qquad (1.2.5)$$

the effect of quadrature is not considered in this chapter. Existence and uniqueness of this problem follows from Lax-Milgram theorem, since $\mathbb{V}_H \subset H_0^1(\Omega)$.

1.2.2 Quasi-Orthogonality

Consider two consecutive nested meshes $\mathcal{T}_H \subset \mathcal{T}_h$, i.e. $\mathcal{T}_h$ is a refinement of $\mathcal{T}_H$. For the corresponding spaces $\mathbb{V}_H \subset \mathbb{V}_h \subset H_0^1(\Omega)$, let $u_h \in \mathbb{V}_h$ and $u_H \in \mathbb{V}_H$ be the discrete solutions. Since the bilinear form is non-symmetric, it is not a scalar

product and the orthogonality relation between $u - u_H$ and $u_h - u_H$, the so-called Pythagoras equality, fails to hold. We have instead a perturbation result referred to as quasi-orthogonality provided that the initial mesh is fine enough. This result is stated below and the proof is given in section 4.

Lemma 1.2.1 (Quasi-orthogonality). *Let $f \in L^2(\Omega)$. There exist a constant $C^* > 0$, solely depending on the shape regularity constant γ^*, the data $\mathbf{A}, \mathbf{b}$, and c, and a number $0 < s \leq 1$ dictated only by the interior angles of $\partial\Omega$, such that if the meshsize h_0 of the initial mesh satisfies $C^* h_0^s \|\mathbf{b}\|_{L^\infty} < 1$, then*

$$\|u - u_h\|^2 \leq \Lambda_0 \|u - u_H\|^2 - \|u_h - u_H\|^2, \qquad (1.2.6)$$

where $\Lambda_0 := (1 - C^* h_0^s \|\mathbf{b}\|_{L^\infty})^{-1}$. The equality holds provided $\mathbf{b} = 0$ in Ω.

1.3   Adaptive Algorithm

The Adaptive procedure consists of loops of the form

$$\boxed{\text{SOLVE} \rightarrow \text{ESTIMATE} \rightarrow \text{MARK} \rightarrow \text{REFINE.}}$$

The procedure SOLVE solves (1.2.5) for the discrete solution u_H. The procedure ESTIMATE determines the element indicators $\eta_H(T)$ and oscillation $\mathsf{osc}_H(T)$ for all elements $T \in \mathcal{T}_H$. Depending on their relative size, these quantities are later used by the procedure MARK to mark elements T, and thereby create a subset $\widehat{\mathcal{T}}_H$ of $\mathcal{T}_H$ of elements to be refined. Finally, procedure REFINE partitions those elements in $\widehat{\mathcal{T}}_H$ and a few more to maintain mesh conformity. These procedures are discussed more in detail below.

1.3.1 Procedure SOLVE : Linear Solver

We employ linear solvers, either direct or iterative methods, such as preconditioned GMRES, CG, and BICG, to solve linear system (1.2.5). In other words, given a mesh $\mathcal{T}_k$, an initial guess u_{k-1} for the solution, and the data $\mathbf{A}, \mathbf{b}, c, f$, SOLVE computes the discrete solution

$$\boxed{u_k := \mathsf{SOLVE}(\mathcal{T}_k, u_{k-1}, \mathbf{A}, \mathbf{b}, c, f)}$$

1.3.2 Procedure ESTIMATE : A Posteriori Error Estimate

Since we assume exact numerical integration, subtracting (1.2.5) from (1.2.1) yields Galerkin orthogonality

$$\mathcal{B}[u - u_H, v_H] = 0 \qquad \forall\, v_H \in \mathbb{V}_H. \tag{1.3.1}$$

In addition to $\mathcal{T}_H$, let $\mathcal{S}_H$ denote the set of interior faces (edges or sides) of the mesh (triangulation) $\mathcal{T}_H$. We consider the *residual* $\mathcal{R}(u_H) \in H^{-1}(\Omega)$ defined by

$$\mathcal{R}(u_H) := f + \nabla\!\cdot\!(\mathbf{A}\nabla u_H) - \mathbf{b}\cdot\nabla u_H - c\,u_H,$$

and its relation to the error $\mathcal{L}(u - u_H) = \mathcal{R}(u_H)$. It is clear that to estimate $\|u - u_H\|$ we can equivalently deal with $\|\mathcal{R}(u_H)\|_{H^{-1}(\Omega)}$. To this end, we integrate by parts elementwise the bilinear form $\mathcal{B}[u - u_H, v]$ to obtain the *error representation formula*

$$\mathcal{B}[u - u_H, v] = \sum_{T \in \mathcal{T}_H} \int_T R_T(u_H)v + \sum_{S \in \mathcal{S}_H} \int_S J_S(u_H)v \qquad \forall\, v \in H_0^1(\Omega), \tag{1.3.2}$$

11

where the *element residual* $R_T(u_H)$ and the *jump residual* $J_S(u_H)$ are defined as

$$R_T(u_H) := f + \nabla \cdot (\mathbf{A} \nabla u_H) - \mathbf{b} \cdot \nabla u_H - c\, u_H \qquad \text{in } T \in \mathcal{T}_H, \quad (1.3.3)$$

$$J_S(u_H) := -\mathbf{A} \nabla u_H^+ \cdot \nu^+ - \mathbf{A} \nabla u_H^- \cdot \nu^- := [\![\mathbf{A} \nabla u_H]\!]_S \cdot \nu_S \quad \text{on } S \in \mathcal{S}_H, \quad (1.3.4)$$

where S is the common side of elements T^+ and T^- with unit outward normals ν^+ and ν^-, respectively, and $\nu_S = \nu^-$. Whenever convenient, we will use the abbreviations $R_T = R_T(u_H)$ and $J_S = J_S(u_H)$.

Upper Bound

For $T \in \mathcal{T}_H$ and $S \in \mathcal{S}_h$ an interior face, we define the *local error indicator* $\eta_H(T)$ by

$$\eta_H(T)^2 := H_T^2 \, \|R_T(u_H)\|_{L^2(T)}^2 + \sum_{S \subset \partial T} H_S \, \|J_S(u_H)\|_{L^2(S)}^2 . \qquad (1.3.5)$$

Given a subset $\omega \subset \Omega$, we define the *error estimator* $\eta_H(\omega)$ by

$$\eta_H(\omega)^2 := \sum_{T \in \mathcal{T}_H,\, T \subset \omega} \eta_H(T)^2 .$$

Hence, $\eta_H(\Omega)$ is the error estimator of Ω with respect to the mesh $\mathcal{T}_H$. Using (1.3.1),(1.3.2) and properties of Clément interpolation, as shown in [1, 5, 23], we obtain the upper bound of the error in terms of the estimator,

$$\|u - u_H\|^2 \leq C_1 \eta_H(\Omega)^2, \qquad (1.3.6)$$

where the constant $C_1 > 0$ depends only on the shape regularity γ^*, coercivity constant c_B and continuity constant C_B of the bilinear form.

Lower Bound

Using the explicit construction of Verfürth [1, 23] via bubble functions and positivity and continuity of A, we can get a local lower bound of the error in terms of local indicators and oscillation. That is, there exist constants $C_2, C_3 > 0$, depending only on the shape regularity γ^*, C_B , and c_B, such that

$$C_2 \, \eta_H(T)^2 - C_3 \sum_{T \subset \omega_T} H_T^2 \left\| R_T - \overline{R_T} \right\|^2_{L^2(T)} \leq \|u - u_H\|^2_{H^1(\omega_T)}, \qquad (1.3.7)$$

where the domain ω_T consists of all elements sharing at least a side with T, and $\overline{R_T}$ is any polynomial approximation of R_T on T. However, for the purpose of proving Lemmas 1.3.1 and 1.3.2 below, we will assume that $\overline{R_T} \in \mathbb{P}_{n-1}(T)$ is the L^2-projection of R_T. We define the *oscillation* on the elements $T \in \mathcal{T}_H$ by

$$\mathsf{osc}_H(T)^2 := H_T^2 \left\| R_T - \overline{R_T} \right\|^2_{L^2(T)}, \qquad (1.3.8)$$

and for a subset $\omega \subset \Omega$, we define

$$\mathsf{osc}_H(\omega)^2 := \sum_{T \in \mathcal{T}_H, \, T \subset \omega} \mathsf{osc}_H(T)^2 .$$

Remark 1.3.1. We see from (1.3.7) that if the oscillation $\mathsf{osc}_H(\omega_T)$ is small compared to the indicator $\eta_H(T)$, then a large $\eta_H(T)$ implies a large local error $\|u - u_H\|_{H^1(\omega_T)}$. This explains why refining elements with large indicators usually tends to equidistribute the errors, which is an ultimate goal of adaptivity. This idea is employed by the procedure MARK of §1.3.3.

Remark 1.3.2. The oscillation $\mathsf{osc}_H(T)$ does not involve oscillation of the jump residual $J_S(u_H)$ as is customary [1, 23]. This result follows from the positivity and continuity of **A**, and is explained in §1.4.2.

Remark 1.3.3. The oscillation $\mathsf{osc}_H(T)$ depends on $R_T = R_T(u_H)$, which in turn depends on the discrete solution u_H. This is a fundamental difference with Morin et al. [15, 16], where the oscillation is purely data oscillation. It is not clear now that the oscillation will decrease when the mesh $\mathcal{T}_H$ will be refined because u_H will also change. Controlling the decay of $\mathsf{osc}_H(T)$ is thus a major challenge addressed in this work; see §1.3.3 and §1.3.4. It is not possible to show that oscillation will always decrease as the mesh gets refined as in [15, 16].

For a given mesh $\mathcal{T}_H$ and discrete solution u_H, along with input data $\mathbf{A}, \mathbf{b}, c$ and f, the procedure ESTIMATE computes indicators $\eta_H(T)$ and oscillations $\mathsf{osc}_H(T)$ for all elements $T \in \mathcal{T}_H$ according to (1.3.5) and (1.3.8):

$$\boxed{\{\eta_H(T), \mathsf{osc}_H(T)\}_{T \in \mathcal{T}_H} = \mathsf{ESTIMATE}(\mathcal{T}_H, u_H, \mathbf{A}, \mathbf{b}, c, f)}$$

1.3.3 Procedure MARK

Our goal is to devise a marking procedure, namely to identify a subset $\widehat{\mathcal{T}}_H$ of the mesh $\mathcal{T}_H$ such that, after refining, both error and oscillation will be reduced. We use two strategies for this: Marking Strategy E deals with the error estimator, and Marking Strategy O does so with the oscillation.

Marking Strategy E : Error Reduction

This strategy was introduced by Dörfler [7] to enforce error reduction.

> Marking Strategy E. Given a parameter $0 < \theta < 1$, construct a subset $\widehat{\mathcal{T}}_H$ of $\mathcal{T}_H$ such that
>
> $$\sum_{T \in \widehat{\mathcal{T}}_H} \eta_H(T)^2 \geq \theta^2 \eta_H(\Omega)^2, \qquad (1.3.9)$$
>
> and mark all elements in $\widehat{\mathcal{T}}_H$ for refinement.

We will see later that Marking Strategy E guarantees error reduction in the absence of oscillation terms. Since the latter account for information missed by the averaging process associated with the finite element method, we need a separate procedure to guarantee oscillation reduction.

Marking Strategy O: Oscillation Reduction

This procedure was introduced by Morin et al. [15, 16] as a separate means for reducing oscillation.

> Marking Strategy O. Given a parameter $0 < \hat{\theta} < 1$ and the subset $\widehat{\mathcal{T}}_H \subset \mathcal{T}_H$ produced by Marking Strategy E, enlarge $\widehat{\mathcal{T}}_H$ such that
>
> $$\sum_{T \in \widehat{\mathcal{T}}_H} \mathsf{osc}_H(T)^2 \geq \hat{\theta}^2 \mathsf{osc}_H(\Omega)^2, \qquad (1.3.10)$$
>
> and mark all elements in $\widehat{\mathcal{T}}_H$ for refinement.

Given a mesh $\mathcal{T}_H$ and all information about the local error indicators $\eta_H(T)$, and oscillation $\mathsf{osc}_H(T)$, together with user parameters θ and $\hat{\theta}$, MARK generates a subset $\widehat{\mathcal{T}}_H$ of $\mathcal{T}_H$

$$\widehat{\mathcal{T}}_H = \mathsf{MARK}(\theta, \hat{\theta} \; ; \; \mathcal{T}_H, \{\eta_H(T), \mathsf{osc}_H(T)\}_{T \in \mathcal{T}_H})$$

1.3.4 Procedure REFINE

The following Interior Node Property, due to Morin et al [15, 16], is known to be necessary for error and oscillation reduction.

Interior Node Property. Refine each marked element $T \in \widehat{\mathcal{T}}_H$ to obtain a new mesh $\mathcal{T}_h$ compatible with $\mathcal{T}_H$ such that

T and the $d + 1$ adjacent elements $T' \in \mathcal{T}_H$ of T, as well as their common sides, contain a node of the finer mesh $\mathcal{T}_h$ in their interior.

In addition to the Interior Node Property, we assume that the refinement is done in such a way that the new mesh $\mathcal{T}_h$ is conforming, which guarantees that both $\mathcal{T}_H$ and $\mathcal{T}_h$ are nested. With this property, we have a reduction factor $\gamma_0 < 1$ of element size, i.e. if $T \in \mathcal{T}_h$ is obtained by refining $T' \in \widehat{\mathcal{T}}_H$, then $h_T \leq \gamma_0 H_{T'}$. For example, when $d = 2$ with triangular elements, to have Interior Node Property we can use the three newest bisections for each single refinement step, whence $\gamma_0 \leq 1/2$.

Given a mesh $\mathcal{T}_H$ and a marked set $\widehat{\mathcal{T}}_H$, REFINE constructs the refinement $\mathcal{T}_h$ satisfying the Interior Node Property:

$$\boxed{\mathcal{T}_h = \mathsf{REFINE}(\mathcal{T}_H, \widehat{\mathcal{T}}_H)}$$

Combining the marking strategies of §1.3.3 with the Interior Node Property, we obtain the following two crucial results whose proofs are given in §1.4.

Lemma 1.3.1 (Error Reduction). *There exist constants C_4 and C_5, depending only on the shape regularity constant γ^* and θ, such that*

$$\eta_H(T)^2 \leq C_4 \, \|u_h - u_H\|_{H^1(\omega_T)}^2 + C_5 \mathsf{osc}_H(\omega_T)^2 \qquad \forall \, T \in \widehat{\mathcal{T}}_H. \qquad (1.3.11)$$

16

We realize that the local energy error between consecutive discrete solutions is bounded below by the local indicators for elements in the marked set $\widehat{\mathcal{T}}_H$, provided the oscillation term is sufficiently small relative to the energy error.

Lemma 1.3.2 (Oscillation Reduction). *There exist constants $0 < \rho_1 < 1$ and $0 < \rho_2$, depending only on γ^* and $\hat{\theta}$, such that*

$$\mathsf{osc}_h(\Omega)^2 \leq \rho_1 \mathsf{osc}_H(\Omega)^2 + \rho_2 \left\| u_h - u_H \right\|^2. \tag{1.3.12}$$

We have that oscillation reduces with a factor $\rho_1 < 1$ provided the energy error between consecutive discrete solutions is relatively small.

Remark 1.3.4 *(Coupling of error and oscillation).* Lemmas 1.3.1 and 1.3.2 seem to lead to conflicting demands on the relative sizes of error and oscillation. These two concepts are indeed coupled, which contrasts with [15, 16], where oscillation depends only on data and reduces separately from the error. This suggests that we must handle them together, this being the main contribution of this chapter. We make this assertion explicit in Theorem 1.1 below.

1.3.5 Adaptive Algorithm AFEM

The adaptive algorithm consists of the loops of procedures SOLVE, ESTIMATE, MARK, and REFINE, consecutively, given that the parameters θ and $\hat{\theta}$ are chosen according to Marking Strategies E and O.

<div style="border:1px solid">

AFEM.

Choose parameters $0 < \theta, \hat{\theta} < 1$.

1. Pick an initial mesh $\mathcal{T}_0$, initial guess $u_{-1} = 0$, and set $k = 0$.

2. $u_k = \mathsf{SOLVE}(\mathcal{T}_k, u_{k-1}, \mathbf{A}, \mathbf{b}, c, f)$.

3. $\{\eta_k(T), \mathsf{osc}_k(T)\}_{T \in \mathcal{T}_k} = \mathsf{ESTIMATE}(\mathcal{T}_k, u_k, \mathbf{A}, \mathbf{b}, c, f))$.

4. $\widehat{\mathcal{T}}_k = \mathsf{MARK}(\theta, \hat{\theta} \; ; \; \mathcal{T}_k, \{\eta_k(T), \mathsf{osc}_k(T)\}_{T \in \mathcal{T}_k})$.

5. $\mathcal{T}_{k+1} = \mathsf{REFINE}(\mathcal{T}_k, \widehat{\mathcal{T}}_k)$.

6. Set $k = k + 1$ and go to step 2.

</div>

Theorem 1.1 (Convergence of AFEM). *Let $\{u_k\}_{k \in \mathbb{N}_0}$ be a sequence of finite element solutions corresponding to a sequence of nested finite element spaces $\{\mathbb{V}^k\}_{k \in \mathbb{N}_0}$ produced by AFEM. There exist constants $\sigma, \gamma > 0$, and $0 < \xi < 1$, depending solely on the mesh regularity constant γ^*, data, parameters θ and $\hat{\theta}$, and a number $0 < s \leq 1$ dictated by interior angles of $\partial\Omega$, such that if the initial meshsize h_0 satisfies $h_0^s \|\mathbf{b}\|_{L^\infty} < \sigma$, then for any two consecutive iterations k and $k+1$, we have*

$$\|u - u_{k+1}\|^2 + \gamma \, \mathsf{osc}_{k+1}(\Omega)^2 \leq \xi^2 \left(\|u - u_k\|^2 + \gamma \, \mathsf{osc}_k(\Omega)^2 \right). \qquad (1.3.13)$$

Therefore AFEM converges with a linear rate ξ, namely,

$$\|u - u_k\|^2 + \gamma \, \mathsf{osc}_k(\Omega)^2 \leq C_0 \, \xi^{2k},$$

where $C_0 := \|u - u_0\|^2 + \gamma \, \mathsf{osc}_0(\Omega)^2$.

Proof. We just prove the contraction property (1.3.13), which obviously implies the decay estimate. For convenience, we introduce the notation

$$e_k := \|u - u_k\|, \qquad \varepsilon_k := \|u_{k+1} - u_k\|, \qquad \mathsf{osc}_k := \mathsf{osc}_k(\Omega).$$

The idea is to use the quasi-orthogonality (1.2.6) and replace the term $\|u_{k+1} - u_k\|^2$ using new results of error and oscillation reduction estimates (1.3.11) and (1.3.12). We proceed in three steps as follows.

Step 1. We first get a lower bound for ε_k in terms of e_k. To this end, we use Marking Strategy E and the upper bound (1.3.6) to write

$$\theta^2 e_k^2 \le C_1 \theta^2 \eta_k(\Omega)^2 \le C_1 \sum_{T \in \widehat{\mathcal{T}_k}} \eta_k(T)^2.$$

Adding (1.3.11) of Lemma 1.3.1 over all marked elements $T \in \widehat{\mathcal{T}_k}$, and observing that each element can be counted at most $D := d + 2$ times due to overlap of the sets ω_T, together with $\|v\|_{H^1}^2 \le c_B^{-1} \|v\|^2$ for all $v \in H_0^1(\Omega)$, we arrive at

$$\theta^2 e_k^2 \le \frac{DC_1 C_4}{c_B} \varepsilon_k^2 + DC_1 C_5 \, \mathsf{osc}_k^2.$$

If $\Lambda_1 := \frac{\theta^2 c_B}{DC_1 C_4}, \Lambda_2 := \frac{C_5 c_B}{C_4}$, then this implies the lower bound for ε_k^2,

$$\varepsilon_k^2 \ge \Lambda_1 e_k^2 - \Lambda_2 \mathsf{osc}_k^2. \tag{1.3.14}$$

Step 2. If h_0 is sufficiently small so that the quasi-orthogonality (1.2.6) of Lemma 1.2.1 holds with $\Lambda_0 = (1 - C^* h_0^s \|\mathbf{b}\|_{L^\infty})^{-1}$, then

$$e_{k+1}^2 \le \Lambda_0 e_k^2 - \varepsilon_k^2.$$

Replacing the fraction $\beta \varepsilon_k^2$ of ε_k^2 via (1.3.14) we obtain

$$e_{k+1}^2 \le (\Lambda_0 - \beta \Lambda_1) e_k^2 + \beta \Lambda_2 \mathsf{osc}_k^2 - (1 - \beta) \varepsilon_k^2,$$

where $0 < \beta < 1$ is a constant to be chosen suitably. We now assert that it is possible to chose h_0 compatible with Lemma 1.2.1 and also that

$$0 < \alpha := \Lambda_0 - \beta\Lambda_1 < 1.$$

A simple calculation shows that this is the case provided

$$C^* h_0^s \|\mathbf{b}\|_{L^\infty} < \frac{\beta\Lambda_1}{(1+\beta\Lambda_1)} < 1,$$

i.e., $h_0^s \|\mathbf{b}\|_{L^\infty} < \sigma$ with $\sigma := \frac{\beta\Lambda_1}{C^*(1+\beta\Lambda_1)}$. Consequently

$$e_{k+1}^2 \leq \alpha e_k^2 + \beta\Lambda_2 \mathsf{osc}_k^2 - (1-\beta)\varepsilon_k^2. \tag{1.3.15}$$

Step 3. To remove the last term of (1.3.15) we resort to the oscillation reduction estimate of Lemma 1.3.2

$$\mathsf{osc}_{k+1}^2 \leq \rho_1 \mathsf{osc}_k^2 + \rho_2 \varepsilon_k^2.$$

We multiply it by $(1-\beta)/\rho_2$ and add it to (1.3.15) to deduce

$$e_{k+1}^2 + \frac{1-\beta}{\rho_2}\mathsf{osc}_{k+1}^2 \leq \alpha\, e_k^2 + \left(\beta\Lambda_2 + \frac{\rho_1}{\rho_2}(1-\beta)\right)\mathsf{osc}_k^2.$$

If $\gamma := \frac{1-\beta}{\rho_2}$, then we would like to choose $\beta < 1$ in such a way that

$$\beta\Lambda_2 + \rho_1\gamma = \mu\gamma$$

for some $\mu < 1$. A simple calculation yields

$$\beta = \frac{\frac{\mu-\rho_1}{\rho_2}}{\Lambda_2 + \frac{\mu-\rho_1}{\rho_2}},$$

and shows that $\rho_1 < \mu < 1$ guarantees that $0 < \beta < 1$. Therefore,

$$e_{k+1}^2 + \gamma\,\mathsf{osc}_{k+1}^2 \leq \alpha\, e_k^2 + \mu\gamma\,\mathsf{osc}_k^2,$$

and the asserted estimate (1.3.13) follows upon taking $\xi = \max(\alpha, \mu) < 1$. □

20

Remark 1.3.5 *(Comparison with [15, 16])*. In [15, 16] the oscillation is independent of discrete solutions, i.e. $\rho_2 = 0$, and is reduced by the factor $\rho_1 < 1$ in (1.3.12). Consequently, Step 3 above is avoided by setting $\beta = 1$, and the decay of e_k and osc_k is monitored separately. Since this is no longer possible, e_k and osc_k are now combined and decreased together.

Remark 1.3.6 *(Splitting of ε_k)*. The idea of splitting ε_k is already used by Chen and Jia [4] in examining one time step for the heat equation. This is because a mass (zero order) term naturally occurs, which did not take place in [15, 16]. The elliptic operator is just the Laplacian in [4].

Remark 1.3.7 *(Effect of Convection)*. Assuming that $h_0^s \|\mathbf{b}\|_{L^\infty} < \sigma$ implies that the local Péclet number is sufficiently small for the Galerkin method not to exhibit oscillations. This appears to be essential for u_0 to contain relevant information and guide correctly the adaptive process. This restriction is difficult to verify in practice because it involves unknown constants. However, starting from coarser meshes than needed in theory does not seem to be a problem in our examples (see §1.5.3-Experiment 2 where we carefully express the constant σ in terms of data).

Remark 1.3.8 *(Vanishing Convection)*. If $\mathbf{b} = 0$, then Theorem 1.1 has no restriction on the initial mesh. This thus extends the convergent result of Morin et al. [15, 16] to variable diffusion coefficient and zero order terms.

Remark 1.3.9 *(Optimal β)*. The choice of β can be optimized. In fact, we can easily see that

$$\alpha = \Lambda_0 - \beta\Lambda_1, \qquad \mu = \rho_1 + \frac{\beta}{1-\beta}\rho_2\Lambda_2$$

yields a unique value $0 < \beta_* < 1$ for which $\alpha = \mu$ and the contraction constant ξ of Theorem 1.1 is minimal. This β_* depends on geometric constant $\Lambda_0, \Lambda_1, \Lambda_2$ as well on $\theta, \hat{\theta}$ and h_0, but it is not computable.

1.4   Proofs of Lemmas

Let $\widehat{\mathcal{T}}_H \subset \mathcal{T}_H$ be a set of marked elements obtained from procedure MARK. Let $\mathcal{T}_h$ be a refined mesh obtained from procedure REFINE, and let $\mathbb{V}_H \subset \mathbb{V}_h$ be nested spaces corresponding to compatible meshes $\mathcal{T}_H$ and $\mathcal{T}_h$, respectively. For convenience, set

$$e_h := u - u_h, \qquad e_H := u - u_H, \qquad \varepsilon_H := u_h - u_H.$$

1.4.1   Proof of Lemma 1.2.1: Quasi-Orthogonality

In view of Galerkin orthogonality (1.3.1), i.e. $\mathcal{B}[e_h, v_h] = 0$, $v_h \in \mathbb{V}_h$, we have

$$\|e_H\|^2 = \|e_h\|^2 + \|\varepsilon_H\|^2 + \mathcal{B}[\varepsilon_H, e_h].$$

If $\mathbf{b} = 0$, then $\mathcal{B}$ is symmetric and $\mathcal{B}[\varepsilon_H, e_h] = \mathcal{B}[e_h, \varepsilon_H] = 0$. For $\mathbf{b} \neq 0$, instead, $\mathcal{B}[\varepsilon_H, e_h] \neq 0$, and we must account for this term. It is easy to see that $\nabla \cdot \mathbf{b} = 0$ and integration by parts yield

$$\mathcal{B}[\varepsilon_H, e_h] = \mathcal{B}[e_h, \varepsilon_H] + \langle \mathbf{b} \cdot \nabla \varepsilon_H, e_h \rangle - \langle \mathbf{b} \cdot \nabla e_h, \varepsilon_H \rangle = 2 \langle \mathbf{b} \cdot \nabla \varepsilon_H, e_h \rangle.$$

Hence

$$\|e_h\|^2 = \|e_H\|^2 - \|\varepsilon_H\|^2 - 2 \langle \mathbf{b} \cdot \nabla \varepsilon_H, e_h \rangle.$$

Using Cauchy-Schwarz inequality and replacing the $H^1(\Omega)$-norm by the energy norm we have, for any $\delta > 0$ to be chosen later,

$$-2 \langle \mathbf{b} \cdot \nabla \varepsilon_H, e_h \rangle \leq \delta \| e_h \|_{L^2}^2 + \frac{\| \mathbf{b} \|_{L^\infty}^2}{\delta c_B} \| \varepsilon_H \|^2 .$$

We then realize the need to relate $L^2(\Omega)$ and energy norms to replace $\| e_h \|_{L^2}$ by $\| e_h \|$. This requires a standard duality argument whose proof is reported in [5].

Lemma 1.4.1 (Duality). *Let $f \in L^2(\Omega)$ and $u \in H^{1+s}(\Omega)$ for some $0 < s \leq 1$ be the solution of (1.2.1), where s depends on the interior angles of $\partial \Omega$ ($s = 1$ if Ω is convex). Then, there exists a constant C_D, depending only on the shape regularity constant γ^* and the data of (1.1.1) such that*

$$\| e_h \|_{L^2} \leq C_D h^s \| e_h \|_{H^1} . \tag{1.4.1}$$

Inserting this estimate in the preceding two bounds, and using $h \leq h_0$, the meshsize of the initial mesh, in conjunction with (1.2.3) we deduce

$$\left(1 - \delta C_D^2 c_B^{-1} h_0^{2s} \right) \| e_h \|^2 \leq \| e_H \|^2 - \left(1 - \| \mathbf{b} \|_{L^\infty}^2 (\delta c_B)^{-1} \right) \| \varepsilon_H \|^2 .$$

We now choose $\delta = \frac{\| \mathbf{b} \|_{L^\infty}}{C_D h_0^s}$ to equate both parenthesis, as well as h_0 sufficiently small for $\delta C_D^2 h_0^{2s} c_B^{-1} = C^* h_0^s \| \mathbf{b} \|_{L^\infty} < 1$ with $C^* := C_D/c_B$. We end up with

$$\| e_h \|^2 \leq \frac{1}{1 - C^* h_0^s \| \mathbf{b} \|_{L^\infty}} \| e_H \|^2 - \| \varepsilon_H \|^2 .$$

This implies (1.2.6) and concludes the proof. $\qquad \square$

1.4.2 Proof of Lemma 1.3.1 : Error Reduction

Upon restricting the test function v in (1.3.2) to $\mathbb{V}_h \supset \mathbb{V}_H$, we obtain the error representation

$$\mathcal{B}[\varepsilon_H, v_h] = \sum_{T \in \mathcal{T}_H} \int_T \overline{R_T} v_h + \int_T (R_T - \overline{R_T}) v_h + \sum_{S \in \mathcal{S}_H} \int_S J_S\, v_h \qquad \forall\, v_h \in \mathbb{V}_h, \quad (1.4.2)$$

where we use the abbreviations $R_T = R_T(u_H)$ and $J_S = J_S(u_H)$, and $\overline{R_T} = \Pi_T^{n-1} R_T$ denotes the L_2-projection of R_T onto the space of polynomials $\mathbb{P}_{n-1}(T)$ over the element $T \in \mathcal{T}_H$. Except for avoiding the oscillation terms of the jump residual J_S, the proof goes back to [7, 15, 16]. We proceed in three steps.

Step 1 (Interior Residual). Let $T \in \mathcal{T}_H$, and let x_T be an interior node of T generated by the procedure REFINE. Let $\psi_T \in \mathbb{V}_h$ be a bubble function which satisfies $\psi_T(x_T) = 1$, vanishes on ∂T, and $0 \le \psi_T \le 1$; hence $\mathsf{supp}\,(\psi_T) \subset T$. Since $\overline{R_T} \in \mathbb{P}_{n-1}(T)$ and $\psi_T > 0$ in a polyhedron of measure comparable with that of T, we have

$$C \left\|\overline{R_T}\right\|_{L^2(T)}^2 \le \int_T \psi_T\, \overline{R_T}^2 = \int_T \overline{R_T}(\psi_T\, \overline{R_T}).$$

Since $\psi_T \overline{R_T}$ is a piecewise polynomial of degree $\le n$ over $\mathcal{T}_h$, it is thus an admissible test function in (1.4.2) which vanishes outside T (and in particular on all $S \in \mathcal{S}_H$). Therefore

$$C \left\|\overline{R_T}\right\|_{L^2(T)}^2 \le \mathcal{B}[\varepsilon_H, \psi_T \overline{R_T}] + \int_T (\overline{R_T} - R_T)\psi_T \overline{R_T}$$

$$\le C \left(H_T^{-1} \left\|\varepsilon_H\right\|_{H^1(T)} + \left\|R_T - \overline{R_T}\right\|_{L^2(T)} \right) \left\|\overline{R_T}\right\|_{L^2(T)},$$

because of an inverse inequality for $\psi_T \overline{R_T}$. This, together with the triangle inequal-

24

ity, yields the desired estimate for $H_T^2 \|R_T\|_{L^2(T)}^2$:

$$H_T^2 \|R_T\|_{L^2(T)}^2 \le C \left(\|\varepsilon_H\|_{H^1(T)}^2 + H_T^2 \|R_T - \overline{R_T}\|_{L^2(T)}^2 \right). \qquad (1.4.3)$$

Step 2 (Jump Residual). Let $S \in \mathcal{S}_H$ be an interior side of $T_1 \in \widehat{\mathcal{T}}_H$, and let $T_2 \in \mathcal{T}_H$ be the other element sharing S. Let x_S be an interior node of S created by the procedure REFINE. Let $\psi_S \in \mathbb{V}_h$ be a bubble function in $\omega_S := T_1 \cup T_2$ such that $\psi_S(x_S) = 1$, ψ_S vanishes on $\partial\omega_S$, and $0 \le \psi_S \le 1$; hence $\mathsf{supp}\,(\psi_S) \subset \omega_S$.

Since u_H is continuous, then $[\![\nabla u_H]\!]_S$ is parallel to ν_S, i.e. $[\![\nabla u_H]\!]_S = j_S\, \nu_S$. Moreover, the coefficient matrix $\mathbf{A}(x)$ being continuous implies

$$J_S = \mathbf{A}(x)\,[\![\nabla u_H]\!]_S \cdot \nu_S = j_S\, \mathbf{A}(x)\nu_S \cdot \nu_S = a(x)\, j_S,$$

where $a(x) := \mathbf{A}(x)\nu_S \cdot \nu_S$ satisfies $0 < \underline{a}_S \le a(x) \le \overline{a}_S$ with $\underline{a}_S, \overline{a}_S$ the smallest and largest eigenvalues of $\mathbf{A}(x)$ on S. Consequently,

$$\|J_S\|_{L^2(S)}^2 \le \overline{a}_S^2 \int_S j_S^2 \le C\overline{a}_S^2 \int_S j_S^2 \psi_S \le C\frac{\overline{a}_S^2}{\underline{a}_S} \int_S (j_S\,\psi_S)J_S, \qquad (1.4.4)$$

where the second inequality follows from j_S being a polynomial and $\psi_S > 0$ in a polygon of measure comparable with that of S.

We now extend j_S to ω_S by first mapping to the reference element, next extending constantly along the normal to $\hat{S}$, and finally mapping back to ω_S. The resulting extension $\mathsf{E}_h(j_S)$ is a piecewise polynomial of degree $\le n-1$ in ω_S so that $\psi_S\mathsf{E}_h(j_S) \in \mathbb{V}_h$, and satisfies $\|\psi_S\mathsf{E}_h(j_S)\|_{L^2(\omega_S)} \le CH_S^{1/2}\|j_S\|_{L^2(S)}$. Since $v_h = \psi_S\mathsf{E}_h(j_S)$ is an admissible test function in (1.4.2) which vanishes on all sides of

$\mathcal{S}_H$ but S, we arrive at

$$\int_S J_S(j_S \psi_S) = \mathcal{B}[\varepsilon_H, v_h] - \int_{T_1} R_{T_1} \, v_h - \int_{T_2} R_{T_2} \, v_h$$
$$\leq C \left(H_S^{-1/2} \|\varepsilon_H\|_{H_S^1(\omega_S)} + H_S^{1/2} \sum_{i=1}^2 \|R_{T_i}\|_{L^2(T_i)} \right) \|j_S\|_{L^2(S)}. \tag{1.4.5}$$

Therefore

$$H_S \|J_S\|_{L^2(S)}^2 \leq C \left(\|\varepsilon_H\|_{H^1(\omega_S)}^2 + \sum_{i=1}^2 H_{T_i}^2 \|R_{T_i}\|_{L^2(T_i)}^2 \right). \tag{1.4.6}$$

Step 3 (Final Estimate). To remove the interior residual from the right hand side of (1.4.6) we observe that both T_1 and T_2 contain an interior node according to procedure REFINE. Hence, (1.4.3) implies

$$H_S \|J_S\|_{L^2(S)}^2 \leq C \left(\|\varepsilon_H\|_{H^1(\omega_S)}^2 + \sum_{i=1}^2 H_{T_i}^2 \left\|R_{T_i} - \overline{R_{T_i}}\right\|_{L^2(T_i)}^2 \right). \tag{1.4.7}$$

The asserted estimate for $\eta_H(T)^2$ is thus obtained by adding this bound to (1.4.3). The constant C depends on the shape regularity constant γ^* and the ratio $\overline{a}_S^2/\underline{a}_S$ of largest and smallest eigenvalues of $\mathbf{A}(x)$ for $x \in S$. $\qquad\square$

Remark 1.4.1 *(Positivity).* The use of $\mathbf{A}(x)$ being positive definite in (1.4.4) avoids having oscillation terms on S. This comes at the expense of a constant depending on $\overline{a}_S^2/\underline{a}_S$. If we were to proceed in the usual manner, as in [1, 18, 23], we would end up with oscillation of the form

$$H_S^{1/2} \|(\mathbf{A} - \mathbf{A}(x_S)) [\![\nabla u_H]\!]_S \cdot \nu_S\|_{L^2(S)} = H_S^{1/2} \|(a - a(x_S))j_S\|_{L^2(S)}$$
$$\leq C H_S^{3/2} \|\mathbf{A}\|_{W_\infty^1(S)} \|j_S\|_{L^2(S)}$$
$$\leq C H_S \left\|H_S^{1/2} J_S\right\|_{L^2(S)},$$

where $C > 0$ also depends on the ratio $\overline{a}_S/\underline{a}_S$ dictated by the variation of $a(x)$ on S. This oscillation can be absorbed into the term $H_S^{1/2} \|J_S\|_{L^2(S)}$ provided that the meshsize H_S is sufficiently small; see [18]. We do not need this assumption in our present discussion.

Remark 1.4.2 (*Continuity of* **A**). The continuity of **A** is instrumental in avoiding jump oscillations, which in turn makes computations simpler. However, jump oscillations cannot be avoided when **A** exhibits discontinuities across inter-element boundaries of the initial mesh. We get instead of (1.4.7)

$$CH_S \|J_S\|_{L^2(S)}^2 \leq \|\varepsilon_H\|_{H^1(\omega_S)}^2 + \sum_{i=1}^{2} H_{T_i}^2 \left\|R_{T_i} - \overline{R_{T_i}}\right\|_{L^2(T_i)}^2 + H_S \left\|J_S - \overline{J_S}\right\|_{L^2(S)}^2, \quad (1.4.8)$$

where $\overline{J_S}$ is the best L^2-projection of J_S onto $\mathbb{P}_{n-1}(S)$. To obtain estimate (1.4.8) we proceed as follows. Starting from a polynomial $\overline{J_S}$, we get an estimate similar to that of (1.4.4)

$$C \left\|\overline{J_S}\right\|_{L^2(S)}^2 \leq \int_S \psi_S \overline{J_S}^2 = \int_S J_S(\psi_S \overline{J_S}) + \int_S (\overline{J_S} - J_S)(\psi_S \overline{J_S}). \quad (1.4.9)$$

In contrast to (1.4.4), we see that the oscillation term $(\overline{J_S} - J_S)$ cannot be avoided when **A** has a discontinuity across S. We estimate the first term on the right hand side of (1.4.9) exactly as we have argued with (1.4.5) and thereby arrive at

$$\int_S J_S(\overline{J_S}\psi_S) \leq C \left(H_S^{-1/2} \|\varepsilon_H\|_{H_S^1(\omega_S)} + H_S^{1/2} \sum_{i=1}^{2} \|R_{T_i}\|_{L^2(T_i)} \right) \left\|\overline{J_S}\right\|_{L^2(S)}.$$

This and a further estimate of the second term on the right hand side of (1.4.9), yield

$$H_S \left\|\overline{J_S}\right\|_{L^2(S)}^2 \leq C \left(\|\varepsilon_H\|_{H^1(\omega_S)}^2 + \sum_{i=1}^{2} H_{T_i}^2 \|R_{T_i}\|_{L^2(T_i)}^2 + H_S \left\|J_S - \overline{J_S}\right\|_{L^2(S)}^2 \right),$$

whence the assertion (1.4.8) follows using triangle inequality for $\|J_S\|_{L^2(S)}$. Combining with (1.4.3), we deduce an estimate for $\eta_H(T)$ similar to (1.3.11), namely,

$$\eta_H(T)^2 \leq C \left(\|\varepsilon_H\|^2_{H^1(\omega_T)} + \mathsf{osc}_H(\omega_T)^2 \right),$$

with the new oscillation term involving jumps on interior sides

$$\mathsf{osc}_H(T)^2 := H_T^2 \left\| R_T - \overline{R_T} \right\|^2_{L^2(T)} + \sum_{S \subset \partial T} H_S \left\| J_S - \overline{J_S} \right\|^2_{L^2(S)}. \tag{1.4.10}$$

In §1.6.1 we discuss the case of a discontinuous $\mathbf{A}$. We show an oscillation reduction property of $\mathsf{osc}_H(T)$, defined by (1.4.10), similar to Lemma 1.3.2.

1.4.3 Proof of Lemma 1.3.2 : Oscillation Reduction

The proof hinges on the Marking Strategy O and the Interior Node Property. We point out that if $T \in \mathcal{T}_h$ is contained in $T' \in \widehat{\mathcal{T}}_H$, then REFINE gives a reduction factor $\gamma_0 < 1$ of element size:

$$h_T \leq \gamma_0 H_{T'}. \tag{1.4.11}$$

The proof proceeds in three steps as follows.

Step 1 (Relation between Oscillations). We would like to relate $\mathsf{osc}_h(T')$ and $\mathsf{osc}_H(T')$ for any $T' \in \mathcal{T}_H$. To this end, we note that for all $T \in \mathcal{T}_h$ contained in T', we can write

$$R_T(u_h) = R_T(u_H) - \mathcal{L}_T(\varepsilon_H) \qquad \text{in } T,$$

where $\varepsilon_H = u_h - u_H$ as before and

$$\mathcal{L}_T(\varepsilon_H) := -\nabla \cdot (\mathbf{A}\nabla \varepsilon_H) + \mathbf{b} \cdot \nabla \varepsilon_H + c\, \varepsilon_H \qquad \text{in } T.$$

By Young's inequality, we have for all $\delta > 0$

$$\mathsf{osc}_h(T)^2 = h_T^2 \left\| R_T(u_h) - \overline{R_T(u_h)} \right\|_{L^2(T)}^2$$

$$\leq (1+\delta)h_T^2 \left\| R_T(u_H) - \overline{R_T(u_H)} \right\|_{L^2(T)}^2 + (1+\delta^{-1})h_T^2 \left\| \mathcal{L}_T(\varepsilon_H) - \overline{\mathcal{L}_T(\varepsilon_H)} \right\|_{L^2(T)}^2,$$

where $\overline{R_T(u_h)}$, $\overline{R_T(u_H)}$, and $\overline{\mathcal{L}_T(\varepsilon_H)}$ are L^2-projections of $R_T(u_h)$, $R_T(u_H)$, and $\mathcal{L}_T(\varepsilon_H)$ onto polynomials of degree $\leq n-1$ on T. We next observe that

$$\left\| \mathcal{L}_T(\varepsilon_H) - \overline{\mathcal{L}_T(\varepsilon_H)} \right\|_{L^2(T)} \leq \|\mathcal{L}_T(\varepsilon_H)\|_{L^2(T)}$$

and that, according to (1.4.11),

$$h_T \leq \gamma_{T'} H_{T'}$$

provided $\gamma_{T'} = \gamma_0$ if $T' \in \widehat{\mathcal{T}}_H$ and $\gamma_{T'} = 1$ otherwise. Therefore, if $\mathcal{T}_h(T')$ denotes all $T \in \mathcal{T}_h$ contained in T',

$$\mathsf{osc}_h(T')^2 = \sum_{T \in \mathcal{T}_h(T')} \mathsf{osc}_h(T)^2$$

$$\leq (1 + \delta)\gamma_{T'}^2 \mathsf{osc}_H(T')^2 + (1 + \delta^{-1}) \sum_{T \in \mathcal{T}_h(T')} h_T^2 \|\mathcal{L}_T(\varepsilon_H)\|_{L^2(T)}^2, \tag{1.4.12}$$

since $R_T(u_H) = R_{T'}(u_H)$ and $\overline{R_T(u_H)}$ is the L^2-projection of $R_{T'}(u_H)$ in T.

Step 2 (Estimate of $\mathcal{L}_T(\varepsilon_H)$). In order to estimate $\|\mathcal{L}_T(\varepsilon_H)\|_{L^2(T)}$ in terms of $\|\varepsilon_H\|_{H^1(T)}$, we first split it as follows

$$\|\mathcal{L}_T(\varepsilon_H)\|_{L^2(T)} \leq \|\nabla \cdot (\mathbf{A}\nabla\varepsilon_H)\|_{L^2(T)} + \|\mathbf{b} \cdot \nabla\varepsilon_H\|_{L^2(T)} + \|c\,\varepsilon_H\|_{L^2(T)}.$$

We denote these terms N_A, N_B, and N_C, respectively. Since

$$N_A \leq \|(\nabla \cdot \mathbf{A}) \cdot \nabla\varepsilon_H\|_{L^2(T)} + \|\mathbf{A} : H(\varepsilon_H)\|_{L^2(T)}$$

29

where $H(\varepsilon_H)$ is the Hessian of ε_H in T, invoking the Lipschitz continuity of $\mathbf{A}$ together with an inverse estimate in T, we infer that

$$N_A \le C_A \left(\|\nabla \varepsilon_H\|_{L^2(T)} + h_T^{-1} \|\nabla \varepsilon_H\|_{L^2(T)} \right),$$

where C_A depends on $\mathbf{A}$ and the shape regularity constant γ^*. Besides, we readily have

$$N_B \le C_B \|\nabla \varepsilon_H\|_{L^2(T)}, \qquad N_C \le C_C \|\varepsilon_H\|_{L^2(T)},$$

where C_B, C_C depend on $\mathbf{b}$, c. Combining these estimates, we arrive at

$$h_T^2 \|\mathcal{L}_T(\varepsilon_H)\|_{L^2(T)}^2 \le C_* \|\varepsilon_H\|_{H^1(T)}^2. \tag{1.4.13}$$

Step 3 (Choice of δ). We insert (1.4.13) into (1.4.12) and add over $T' \in \mathcal{T}_H$. Recalling the definition of $\gamma_{T'}$ and utilizing (1.3.10), we deduce

$$\sum_{T' \in \mathcal{T}_H} \gamma_{T'}^2 \mathsf{osc}_H(T')^2 = \gamma_0^2 \sum_{T' \in \widehat{\mathcal{T}}_H} \mathsf{osc}_H(T')^2 + \sum_{T' \in \mathcal{T}_H \setminus \widehat{\mathcal{T}}_H} \mathsf{osc}_H(T')^2$$

$$= \mathsf{osc}_H(\Omega)^2 - (1 - \gamma_0^2) \sum_{T' \in \widehat{\mathcal{T}}_H} \mathsf{osc}_H(T')^2$$

$$\le (1 - (1 - \gamma_0^2)\hat{\theta}^2)) \mathsf{osc}_H(\Omega)^2,$$

where $\hat{\theta}$ is the user's parameter in (1.3.10). Moreover, since $C_* \|\varepsilon_H\|_{H^1}^2 \le C_o \|\|\varepsilon_H\|\|^2$ with $C_o = C_* c_B^{-1}$ in light of (1.2.3), we end up with

$$\mathsf{osc}_h(\Omega)^2 \le (1 + \delta)(1 - (1 - \gamma_0^2)\hat{\theta}^2)\mathsf{osc}_H(\Omega)^2 + (1 + \delta^{-1})C_o \|\|\varepsilon_H\|\|^2.$$

To complete the proof, we finally choose δ sufficiently small so that

$$\rho_1 = (1 + \delta)(1 - (1 - \gamma_0^2)\hat{\theta}^2) < 1, \qquad \rho_2 = (1 + \delta^{-1})C_o. \qquad \square$$

1.5 Numerical Experiments

We test performance of the adaptive algorithm AFEM with several examples. We are thus able to study how meshes adapt to various effects from lack of regularity of solutions and convexity of domains to data smoothness, boundary layers, changing boundary conditions, etc. For simplicity, we strict to the case of piecewise linear finite element on polygonal domains in $\mathbb{R}^2$. The implementation is done using the ALBERT toolbox of Schmidt and Siebert [20, 21].

1.5.1 Implementation

We employ the four main procedures as given by Morin et al. [15, 16]: SOLVE, ESTIMATE, MARK, and REFINE. We slightly modified the built-in adaptive solver for elliptic problems of ALBERT toolbox [20] to make it work for the general PDE (1.1.1) and mixed boundary conditions, as follows:

• SOLVE: We used built-in solvers provided by ALBERT, such as GMRES and CG.

• ESTIMATE: We modified ALBERT for computing the estimator so that it works for (1.1.1), and added procedures for computing oscillations which are not provided.

• MARK: We employed Marking Strategies E and O to find a marked set $\widehat{\mathcal{T}}_H$.

• REFINE: We employed the three newest bisections for each refinement step to enforce the Interior Node Property.

Remark 1.5.1 *(Quadrature).* Computations of integrals involving non-constant functions $f, \mathbf{A}, \mathbf{b}, c, g$, and the exact solution u, use a quadrature rule of order 5. Our experiments indicate that increasing the quadrature order does not change the re-

31

sults. We refer to [5, 20, 21] for details on quadrature.

For convenience of presentation, we introduce the following notation:

- $\mathsf{DOF_k} :=$ number of elements in $\mathcal{T}_k$;

- $\mathsf{EOC_e} := \frac{\log(e_{k-1}/e_k)}{\log(\mathsf{DOF_k}/\mathsf{DOF_{k-1}})}$, experimental order of convergence, $e_k := \|u - u_k\|$;

- $\mathsf{EOC_\eta} := \frac{\log(\eta_{k-1}/\eta_k)}{\log(\mathsf{DOF_k}/\mathsf{DOF_{k-1}})}$, experimental order of convergence of $\eta_k := \eta_k(\Omega)$;

- $\mathsf{RF_E} := \frac{e_k}{e_{k-1}}$ and $\mathsf{RF_O} := \frac{\mathsf{osc}_k}{\mathsf{osc}_{k-1}}$, reduction factors of the error and the oscillation;

- $\mathsf{Eff} := \eta_k/e_k$, effectivity index, i.e. the ratio between the estimator and the error;

- $\mathsf{M_E}$ and $\mathsf{M_O}$ are the number of marked elements due to Marking Strategy E and the additional marked elements due to Marking Strategy O, respectively.

The experimental order of convergence $\mathsf{EOC_e}$ measures how the error e_k decreases as $\mathsf{DOF_k}$ increases. In fact we have $e_k \approx C\,\mathsf{DOF_k}^{-\mathsf{EOC_e}}$.

1.5.2 Experiment 1 : Oscillatory Coefficients and Nonconvex Domain

We consider the PDE (1.1.1) with Dirichlet boundary condition $u = g$ on the nonconvex L-shape domain $\Omega := (-1,1)^2 \setminus [0,1] \times [-1,0]$. We also take the exact solution

$$u(r) = r^{\frac{2}{3}} \sin(\frac{2}{3}\theta),$$

where $r^2 := x^2 + y^2$ and $\theta := \tan^{-1}(y/x) \in [0, 2\pi)$. We deal with variable coefficients $\mathbf{A}(x,y) = a(x,y)\mathbf{I}$, $\mathbf{b}(x,y) = \mathbf{0}$, and $c(x,y)$ defined by

$$a(x,y) = \frac{1}{4 + P(\sin(\frac{2\pi x}{\epsilon}) + \sin(\frac{2\pi y}{\epsilon}))} \,, \tag{1.5.1}$$

$$c(x,y) = A_c(\cos^2(lx) + \cos^2(lx)) \,, \tag{1.5.2}$$

32

where P, ϵ, A_c, and l are parameters. The functions f in (1.1.1) and g are defined accordingly. The results are shown in Tables 1.5.1 and 1.5.2 and Figure 1.5.1. The observations and conclusions of this experiment are as follows:

k	$\mathsf{DOF_k}$	$\|u - u_k\|$	$\mathsf{EOC_e}$	$\mathsf{RF_E}$	$\mathsf{RF_O}$	Eff	$\mathsf{M_E}$	$\mathsf{M_O}$
-	24	2.181e-01	–	–	–	4.504	3	0
1	65	1.481e-01	0.388	0.679	0.446	2.994	10	0
2	229	1.056e-01	0.268	0.713	0.558	2.475	11	0
3	423	8.812e-02	0.295	0.834	0.652	2.222	13	0
4	651	5.083e-02	1.276	0.577	0.314	2.053	37	0
5	1156	3.305e-02	0.750	0.650	0.444	2.028	89	0
6	2299	2.206e-02	0.588	0.668	0.408	1.980	253	0
7	5148	1.445e-02	0.525	0.655	0.658	1.965	771	0
8	12678	7.991e-03	0.657	0.553	0.175	1.957	1833	0
9	29979	4.911e-03	0.566	0.615	0.426	2.032	-	-

Table 1.5.1: Experiment 1 (Oscillatory coefficients and nonconvex domain): The parameters of AFEM are $\theta = \hat{\theta} = 0.5$, and those controlling the oscillatory coefficients are $P = 1.8, \epsilon = 0.4, A_c = 4.0, l = 1.0$, as described in (1.5.1) and (1.5.2). The experimental order of convergence $\mathsf{EOC_e}$ is close to the optimal rate of 0.5, which indicates quasi-optimal meshes. The oscillation reduction factor $\mathsf{RF_O}$ is smaller than the error reduction factor $\mathsf{RF_E}$, which confirms that oscillation decreases faster than error. The effectivity index Eff is approximately 2.0. There are no additional marked elements from oscillation for this $\theta = 0.5$ i.e. $\mathsf{M_O} = 0$. However, this is not the case if $\theta < 0.3$, see §5.3.

• AFEM gives an optimal rate of convergence of order ≈ 0.5, while standard uniform refinement achieves the suboptimal rate of 0.3 as expected from theory.

• Both AFEM and FEM with uniform refinement perform with effectivity index Eff ≈ 2.0, which give the estimate of constant $C_1 \approx 0.5$ for upper bound (1.3.6); no weights have been used in (1.3.5). For AFEM, the reduction factors of error and oscillation are approximately 0.7 and 0.5 as DOF increases (Table 1.5.1). The oscillation thus decreases faster than the error and becomes insignificant asymptotically for k large. In addition, AFEM outperforms FEM in terms of CPU time vs. energy error.

DOF_k	$\|u - u_k\|$	EOC_e	RF_E	RF_O	Eff
384	1.005e-01	0.400	0.574	0.300	2.398
1536	4.809e-02	0.532	0.478	0.195	2.127
6144	2.597e-02	0.444	0.540	0.182	1.984
24576	1.551e-02	0.372	0.597	0.242	1.845
98304	9.585e-03	0.347	0.618	0.264	1.745

Table 1.5.2: Experiment 1 (Oscillatory coefficients and nonconvex domain): Standard uniform refinement is performed using the same values for parameters P, ϵ, A_c, and l as that of AFEM given in Table 1.5.1 above. EOC_e is now suboptimal and close to the expected value 1/3. The effectivity index Eff is around 2, which is about the same as AFEM. We need about 10^5 DOFs to get the error around 10^{-2}, whereas for AFEM we need only 10^4 DOFs.
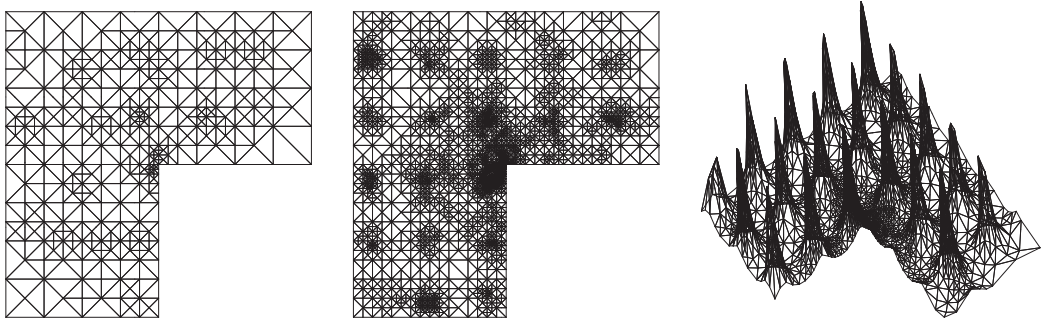

Figure 1.5.1: Experiment 1 (Oscillatory coefficients and nonconvex domain): Parameters of AFEM are $\theta = \hat{\theta} = 0.5$, and those of oscillatory coefficients are $P = 1.8, \epsilon = 0.4, A_c = 1.0, l = 1.0$. The sequence of graded meshes after 4 and 7 iterations shows that mesh refinement is dictated by geometric (corner) singularities as well as periodic variations of the diffusion coefficient but not much from the zero order term. Also on the right, 3-D plot of diffusion coefficient $a(x,y)$ of (1.5.1) interpolated onto the mesh of iteration 7. This shows the combined effect of rapidly varying $a(x,y)$ and exact solution $u = r^{\frac{2}{3}} \sin(\frac{2}{3}\theta)$: meshes are refined more where $a(x,y)$ has large gradient.

• Figure 1.5.1 depicts the effect of a corner singularity and rapid variation of diffusion coefficient $a(x,y)$ in mesh grading; c does not play much of a role.

• The number of additional marked elements M_O due to Marking strategy O depends on parameters θ and $\hat{\theta}$. For this example, $M_O = 0$ because the parameter θ is sufficiently big, hence the condition for Marking strategy O is automatically satisfied. Similar experiments for $\theta < 0.3$ and $\hat{\theta} = 0.5$ yield $M_O \neq 0$ and M_O becomes even dominant for $\theta = 0.1$; see Experiment 2 for more details.

Effects of Oscillatory Coefficient A

In this section we study the behavior of the solution due to the effects of oscillatory coefficient A. We conduct the same experiment as above but without knowing the exact solution. We assume that the forcing term $f = 1.0$ and the Dirichlet boundary condition $g = 0$. We consider a very oscillating coefficient A controlled by parameters $P = 1.99$ and $\epsilon = 0.2$ as defined in (1.5.1). We perform AFEM with parameters $\theta = \hat{\theta} = 0.6$. The results are shown in Figures 1.5.2 with observations and conclusions below.
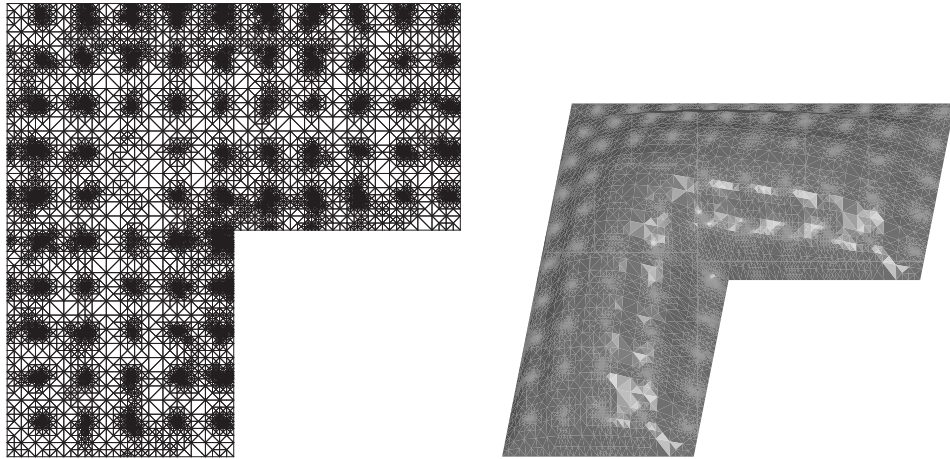
Figure 1.5.2: Experiment 1: (Effect of Oscillatory Coefficients): The mesh and solution after 10 iterations. The solution behaves according to the coefficient A, namely the solution has bumps mimicking the variation of A. As in the previous Experiment, the mesh refinement is based on the variation of A, being more pronounced where A changes more rapidly. It also shows that the effect of oscillatory A dominates the effect of corner singularity.

- The approximate solutions are affected by the oscillatory coefficient A, namely, the solutions have bumps according to the way A varies; see Figure 1.5.2.

- The mesh refinement follows the variation of A, namely, more grading when A changes more rapidly, except around the point $(-0.5, 0.5)$ where the solution seems

to be smooth; see Figure 1.5.2.

• Due to the very highly oscillating character of A, which exhibits a maximum of 50 and minimum of ≈ 0.125, in a lattice with spacing $\epsilon = 0.2$, the effect of A dominates the effect of corner singularity.

1.5.3   Experiment 2 : Convection Dominated-Diffusion

We consider the convection dominated-diffusion elliptic model problem (1.1.1) with Dirichlet boundary condition $u = g$ on convex domain $\Omega := (0, 1)^2$, with isotropic diffusion coefficient $\mathbf{A} = \epsilon \mathbf{I}$, $\epsilon = 10^{-3}$, convection velocity $\mathbf{b} = (y, \frac{1}{2} - x)$ and $c = f = 0$; note that $\nabla \cdot \mathbf{b} = 0$. The Dirichlet boundary condition $g(x, y)$ on $\partial \Omega$, a pulse, is the continuous piecewise linear function given by

$$g(x, y) = \begin{cases} 1 & \{.2 + \tau \leq x \leq .5 - \tau;\ y = 0\}, \\ 0 & \partial \Omega \setminus \{.2 \leq x \leq .5;\ y = 0\}, \\ \text{linear} & \{(.2 \leq x \leq .2 + \tau)\ \text{or}\ (.5 - \tau \leq x \leq .5); y = 0\}, \end{cases} \quad (1.5.3)$$

where τ is a parameter. This problem models the transport of a pulse from $\partial \Omega$ inside Ω and back to $\partial \Omega$. Results are reported in Table 1.5.3 and Figures 1.5.3, 1.5.4 for parameters $\theta = 0.3, \hat{\theta} = 0.6, \tau = 0.005$, starting from a coarser mesh than what we would need in theory. To see whether oscillation plays any role in AFEM, Table 1.5.4 shows results of AFEM without using Marking Strategy O. Observations and conclusions follow:

• Tables 1.5.3 and 1.5.4 document the role of oscillation in AFEM. Without marking due to oscillation $\mathsf{M_O} = 0$, estimator $\eta(\Omega)$ still reduces at optimal rate but oscillation

DOF_k	$\eta_k(\Omega)$	EOC_η	RF_O	M_E	M_O
64	1.74e-1	-	-	2	5
147	9.48e-2	0.73	0.27	8	7
360	2.35e-2	1.55	0.33	4	9
500	1.68e-2	1.02	0.50	5	15
762	1.12e-2	0.95	0.43	10	23
1170	8.58e-3	0.62	0.52	15	70
2173	6.10e-3	0.55	0.48	22	137
3862	4.75e-3	0.43	0.48	30	298
7149	3.45e-3	0.51	0.50	80	600
13981	2.60e-3	0.42	0.51	-	-

Table 1.5.3: Experiment 2: AFEM with parameters $\theta = 0.3, \hat\theta = 0.6$, and $\tau = 0.005$. The optimal decay ≈ 0.5 of estimator $\eta(\Omega)$ is computational evidence of optimal meshes. The reduction factor of oscillation $RF_O := osc_k/osc_{k-1}$ gives an estimate of constant $\rho_1 \approx 0.5$ in Lemma 1.3.2. In contrast to Experiment 1, the additional marking M_O due to oscillation dominates M_E from Marking Strategy E. This controls RF_O, the decay of oscillations, which decrease together with the error according to Theorem 1.1.

DOF_k	$\eta_k(\Omega)$	EOC_η	RF_O
64	1.74e-1	-	-
95	1.02e-1	1.34	0.59
244	3.81e-2	1.31	0.86
414	1.75e-2	4.09	0.62
654	9.42e-3	1.18	0.70
834	9.05e-3	0.16	0.59
1577	5.43e-3	0.89	0.93
2970	3.56e-3	0.51	0.92
4250	2.84e-3	0.62	0.82
6502	2.15e-3	0.65	0.59
10209	1.66e-3	0.57	0.62

Table 1.5.4: Experiment 2: AFEM performance without Marking Strategy O, using the same parameters as for Table 1.5.3. The reduction factor of oscillation RF_O is not as stable as our AFEM shown in Table 1.5.3. The estimator still reduces at the optimal rate but requires a few more iterations to reach the same level as that of our AFEM.

reduction RF_O is not stable. The factor RF_O approximates ρ_1 of Lemma 1.3.2 and

thus controls the oscillation decay between consecutive iterations. In fact Table 1.5.4

indicates that lack of control of $\mathsf{RF_O}$ leads to more iterations for the same estimator.

• Tables 1.5.3 and 1.5.4 also illustrate the need of Marking Strategy O to control the reduction rate of oscillations and confirm the convergence theory of AFEM. Our experiments show that the ratio $\mathsf{M_E}/\mathsf{M_O}$ depends inversely on the ratio $\theta/\hat{\theta}$. If $\theta = \hat{\theta}$, then $\mathsf{M_E}$ dominates $\mathsf{M_O}$.

• Comparison of computational cost is measured using CPU time used by each procedure. In average, about 80% of total CPU time is used by SOLVE; the other procedures $\mathsf{ESTIMATE}$, MARK and REFINE use about 5-10%.

• In theory, the initial meshsize h_0 must satisfy

$$C^* B h_0 < \frac{\beta \Lambda_1}{1 + \beta \Lambda_1} = \beta_0,$$

where $B = \|\mathbf{b}\|_{L^\infty}$, $\beta_0 = O(1)$, and C^* is the constant from Lemma 1.4.1. In this particular case, we can express C^* in terms of ϵ and B quite explicitly. We first observe that H^2-regularity theory gives [10]

$$\begin{cases} \mathcal{L}\varphi = \zeta & \text{in } \Omega \\ \varphi = 0 & \text{on } \partial\Omega \end{cases} \implies \|\varphi\|_{H^2(\Omega)} \le C_R B^{1/2} \epsilon^{-3/2} \|\zeta\|_{L^2(\Omega)}$$

with $C_R > 0$ independent of data. We also note that C_D of Lemma 1.4.1 satisfies

$$C_I C_R \left(\frac{B}{\epsilon}\right)^{\frac{3}{2}} h_0 \le \frac{1}{2} \implies C_D = 2 C_I C_R \left(\frac{B}{\epsilon}\right)^{\frac{1}{2}},$$

where C_I is an interpolation constant solely dependent on shape regularity. This results from the usual duality argument and the fact that $\nabla \cdot \mathbf{b} = 0$, namely

$$|\langle e_h, \zeta \rangle| = |\mathcal{B}[e_h, \varphi]| \le C_I h_0 \left(\epsilon \|\nabla e_h\|_{L^2} + B \|e_h\|_{L^2} \right) \|\varphi\|_{H^2}.$$

We finally recall that $C^* = C_D/\epsilon$ (see section 1.4.1), to arrive at

$$h_0 < \frac{\beta_0}{2C_I C_R} \left(\frac{\epsilon}{B}\right)^{3/2},$$

which is consistent with the previous restriction on h_0. We stress that this implies $h_0 \approx 10^{-4}$ in theory, whereas $h_0 \approx 10^{-1}$ works in examples; see Figures 1.5.3-1.5.4.
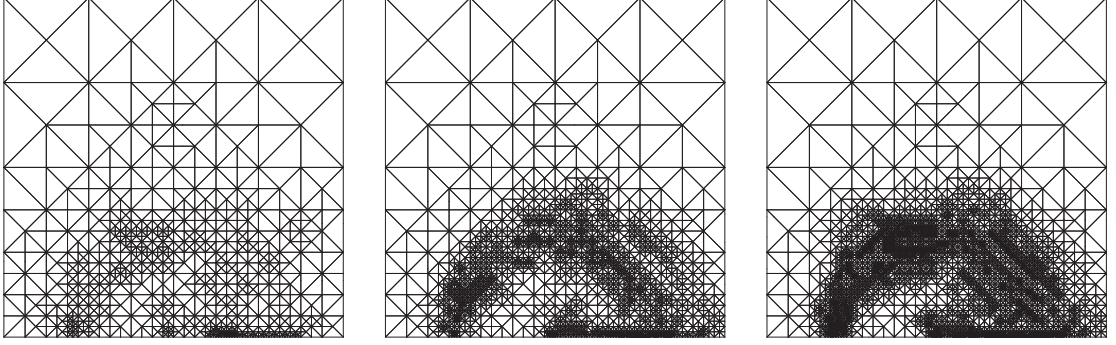

Figure 1.5.3: Experiment 2 (Convection-Dominated Diffusion with $\epsilon = 10^{-3}, \mathbf{b} = (y, \frac{1}{2} - x)$): Adaptively refined meshes after 5, 7, and 8 iterations corresponding to Table 1.5.3 starting from a uniform mesh coarser than required in theory. After a few iterations, AFEM detects the region of rapid variation (circular transport of a pulse) and boundary layer in the outflow, whereas the rest of the mesh remains unchanged. Refinement in smooth region is caused by early oscillations.
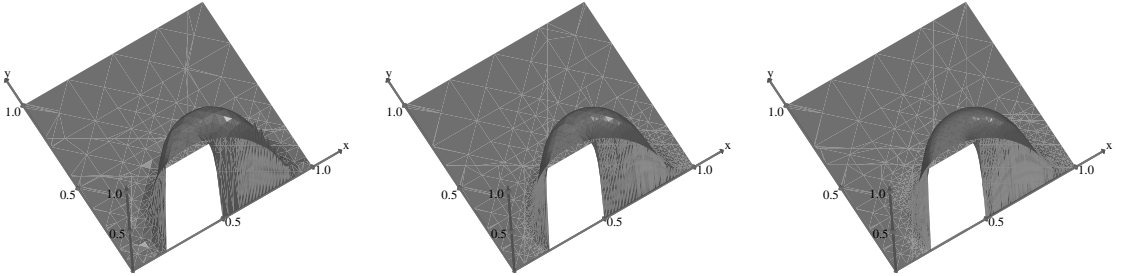
Figure 1.5.4: Experiment 2 (Convection-Dominated Diffusion with $\epsilon = 10^{-3}, \mathbf{b} = (y, \frac{1}{2} - x)$): plots of solutions after 5, 7, and 8 iterations. No oscillations (of Galerkin solutions) are detected after a few iterations even though AFEM is not stabilized.

- The local Péclet number $P_e = \frac{h_0 B}{\epsilon}$ is about 10^2 at the beginning. Since $P_e > 1$, and the Galerkin method is not stabilized, oscillations are observed in the first few iterations but cured later by AFEM via local refinement; see Figure 1.5.4, which displays solutions without oscillations for iterations 7 and 8. Figure 1.5.3 depicts

several graded meshes and confirms that mesh refinement is localized around the pulse location and outflow boundary layer. Minor refinement in the smooth region is caused by early oscillations.

1.5.4   Experiment 3 : Drift-Diffusion Model

We consider a model problem that comes from a mathematical model in semi-conductors and chemotaxis.

$$-\nabla{\cdot}(\nabla u + \chi u \nabla \psi) = 0 \qquad \text{in } \Omega := (0,1)^2,$$

$$u = g \qquad \text{on } \Gamma \subset \partial\Omega,$$

$$\partial_\nu u = 0 \qquad \text{on } \partial\Omega \setminus \Gamma,$$

where χ is a constant. The radial function ψ is defined in Ω by

$$\psi(x,y) := \begin{cases} 1 & \{\sqrt{x^2 + y^2} \le r_1\}, \\ \alpha & \{\sqrt{x^2 + y^2} \ge r_1 + \alpha\}, \\ \text{linear} & \{r_1 < \sqrt{x^2 + y^2} < r_1 + \alpha\}, \end{cases}$$

where α is a small parameter and $r_1 < 1$ is a constant. The Dirichlet boundary condition on Γ is assumed to be

$$g(x,y) = \begin{cases} 1 & \{x = 0; 0 \le y \le 0.5\} \bigcup \{y = 0; 0 \le x \le 0.5\}, \\ 0 & \{x = 1; 0.5 \le y \le 1\} \bigcup \{y = 1; 0.5 \le x \le 1\}. \end{cases}$$

We resort to the following transformation (exponential fitting) to symmetrize the problem

$$\rho := \exp(\chi\psi)u \implies -\nabla\cdot(\exp(-\chi\psi)\nabla\rho) = 0,$$

which gives a simpler form of model problem with variable scalar coefficient $a = \exp(-\chi\psi)$. We apply AFEM to solve for ρ and obtain solution u via $u = \exp(-\chi\psi)\rho$. The experiment is performed using parameters $\chi = 10.0, r_1 = 0.75$, and $\alpha = 0.04$ for the model problem, and parameters $\theta = 0.6, \hat{\theta} = 0.75$ for AFEM. Results are reported in Tables 1.5.5, 1.5.6 and Figure 1.5.5. Conclusions and observations follow:

DOF_k	$\eta_k(\Omega)$	EOC_η	RF_O
1154	6.645	1.880	0.267
1546	3.824	1.888	0.252
2448	2.144	1.259	0.206
4032	1.455	0.776	0.285
6790	1.086	0.560	0.340
12188	0.737	0.663	0.253
23386	0.518	0.540	0.287
45728	0.363	0.529	0.261

DOF_k	$\eta_k(\Omega)$	EOC_η	RF_O
1024	179.831	3.186	0.009
2048	30.769	2.547	0.026
4096	11.031	1.479	0.096
8192	3.983	1.469	0.106
16384	2.173	0.874	0.188
32768	1.296	0.745	0.216
65536	0.874	0.567	0.250

Table 1.5.5: Experiment 3 (Drift-Diffusion Model): Performance of AFEM with parameter $\theta = 0.6$, $\hat{\theta} = 0.75$, and model parameters $\chi = 10$, $r_1 = 0.75$ and $\alpha = 0.04$. The optimal decay ≈ 0.5 of estimator $\eta(\Omega)$ is computational evidence of quasi-optimal meshes. AFEM outperforms uniform refinement (compare with Table 1.5.6).

Table 1.5.6: Experiment 3 (Drift-Diffusion Model): Performance of FEM with uniform refinement and the same parameters χ, r_1 and α as for AFEM given in Table 1.5.5. To have estimator around 0.9, uniform refinement needs about 65,000 DOFs, whereas AFEM needs only around 10,000 DOFs.

• From Tables 1.5.5, 1.5.6 we see again that AFEM outperforms FEM with standard uniform refinement. Since the decay of estimator $\eta(\Omega)$ is optimal, we have computational evidence of optimal meshes.

• Figure 1.5.5 displays discrete solution u_8 and graded meshes after 8 and 10 itera-
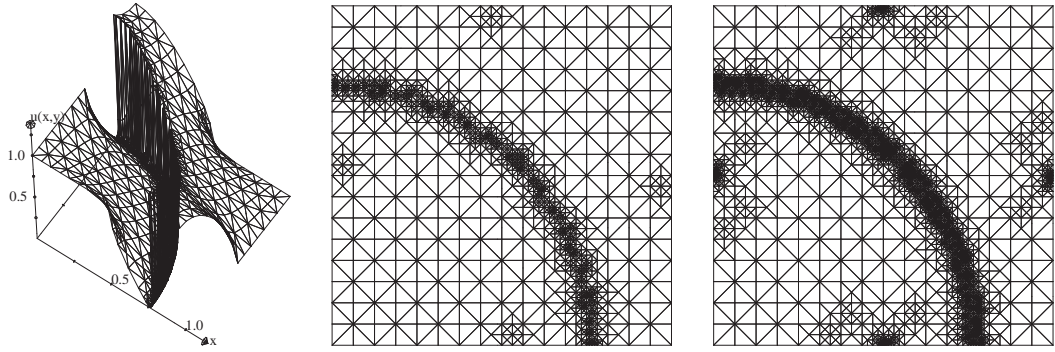
Figure 1.5.5: Experiment 3 (Drift-Diffusion Model): Discrete solution u_8 and refined meshes after 8 and 10 iterations. Mesh grading is quite pronounced in the internal layer where $\nabla\psi$ does not vanish, and at the midpoints of the boundary sides, where boundary conditions change. The solution $u(x,y)$ has a thin transition layer where $\nabla\psi \neq 0$, and meshes are highly refined there.

tions; note the drastic variation of u_8 across the annulus $r_1 < r < r_1 + \alpha$. Meshes adapt well to lack of smoothness, namely refinement concentrates in the transition layer, where $\nabla\psi$ does not vanish, and at the midpoints of boundary sides, where boundary conditions change.

1.6 Extensions

We extend the model problem (1.1.1) by considering now $\mathbf{A}$ with discontinuities aligned with the initial mesh and a non-divergence-free $\mathbf{b}$. Note that if $\nabla\cdot\mathbf{b} \neq 0$, then the bilinear form $\mathcal{B}$ may be non-coercive if $c - \frac{1}{2}\nabla\cdot\mathbf{b} \not\geq 0$.

1.6.1 Discontinuous $\mathbf{A}$

We first observe that Lemma 1.4.1, and thus Lemma 1.2.1, still holds because the regularity H^{1+s} required in the duality argument is valid, see [11] for example. The continuity of $\mathbf{A}$ is used instead for obtaining error and oscillation reduction

estimates, Lemma 1.3.1 and Lemma 1.3.2, in that the element oscillation $\mathsf{osc}_H(T)$ does not involve oscillation of jump residual on ∂T. Remark 1.4.2 shows that when $\mathbf{A}$ has discontinuities across element faces, we still obtain error reduction estimate (1.3.11) of Lemma 1.3.1, but this time the oscillation is defined by (1.4.10) and involves oscillation of jump residual. To prove convergence it suffices to show the oscillation reduction estimate (1.3.12), for the new concept of element oscillation, namely $\mathsf{osc}_H(T)^2 = \mathsf{osc}_{R,H}(T)^2 + \sum_{S \subset \partial T} \mathsf{osc}_{J,H}(S)^2$ with

$$\mathsf{osc}_{R,H}(T)^2 := H_T^2 \left\| R_T(u_H) - \overline{R_T(u_H)} \right\|_{L^2(T)}^2 \qquad \forall\, T \in \mathcal{T}_H,$$

$$\mathsf{osc}_{J,H}(S)^2 := H_S \left\| J_S(u_H) - \overline{J_S(u_H)} \right\|_{L^2(S)}^2 \qquad \forall\, S \in \mathcal{S}_H.$$

We proceed in three steps as follows.

Step 1 (Oscillation of Interior Residual). Invoking the same arguments as in the proof of Lemma 1.3.2 in section 1.4.3, we obtain an oscillation reduction estimate for interior residual

$$\mathsf{osc}_{R,h}(T')^2 \le (1 + \delta)\gamma_{T'}^2 \mathsf{osc}_{R,H}(T')^2 + C_*(1 + \delta^{-1}) \left\| \varepsilon_H \right\|_{H^1(T')}^2 \qquad \forall\, T' \in \mathcal{T}_H,$$

where $\mathsf{osc}_{R,h}(T')$ is defined to be $\mathsf{osc}_h(T')$ in (1.4.12).

Step 2 (Oscillation of Jump Residual). To obtain estimate for $\mathsf{osc}_{J,h}(S)$ we write

$$J_S(u_h) = \gamma_S \left[\!\left[\mathbf{A}\nabla u_H \right]\!\right]_S \cdot \nu_S + \left[\!\left[\mathbf{A}\nabla \varepsilon_H \right]\!\right]_S \cdot \nu_s = \gamma_S J_S(u_H) + J_S(\varepsilon_H),$$

where $\gamma_S = 1$ if $S \subset S' \in \mathcal{S}_H$ and $\gamma_S = 0$ otherwise, since $\mathbf{A}\nabla u_H$ is continuous on S in the second case. Using Young's inequality, we have for all $\delta > 0$

$$\mathsf{osc}_{J,h}(S)^2 \le (1 + \delta)\gamma_S h_S \left\| J_S(u_H) - \overline{J_S(u_H)} \right\|_{L^2(S)}^2$$
$$+ (1 + \delta^{-1}) h_S \left\| J_S(\varepsilon_H) - \overline{J_S(\varepsilon_H)} \right\|_{L^2(S)}^2,$$

where $\overline{J_S(u_H)}$ and $\overline{J_S(\varepsilon_H)}$ are L^2-projections of $J_S(u_H)$ and $J_S(\varepsilon_H)$ onto $\mathbb{P}_{n-1}(S)$.

For the second term we observe that

$$
\begin{aligned}
\left\| J_S(\varepsilon_H) - \overline{J_S(\varepsilon_H)} \right\|_{L^2(S)} &\leq \| J_S(\varepsilon_H) \|_{L^2(S)} = \| [\![\mathbf{A} \nabla \varepsilon_H]\!]_S \cdot \nu_S \|_{L^2(S)} \\
&\leq \left\| \mathbf{A}^+ \nabla \varepsilon_H^+ \cdot \nu_S \right\|_{L^2(S)} + \left\| \mathbf{A}^- \nabla \varepsilon_H^- \cdot \nu_S \right\|_{L^2(S)} \\
&\leq \| \mathbf{A} \|_{L^\infty(\omega_S)} \left(\left\| \nabla \varepsilon_H^+ \right\|_{L^2(S)} + \left\| \nabla \varepsilon_H^- \right\|_{L^2(S)} \right) \\
&\leq C_A h_S^{-1/2} \| \varepsilon_H \|_{H^1(\omega_S)},
\end{aligned}
$$

where C_A depends on $\mathbf{A}$ and shape regularity constant γ^*. For simplicity, let $\mathcal{S}_h(T')$ denote all $S \in \mathcal{S}_h$ contained in $T' \in \mathcal{T}_H$; hence

$$
\begin{aligned}
\mathsf{osc}_{J,h}(T')^2 &= \sum_{S \in \mathcal{S}_h(T')} \mathsf{osc}_{J,h}(S)^2 \\
&\leq (1+\delta) \sum_{S \in \mathcal{S}_h(T')} \gamma_S h_S \left\| J_S(u_H) - \overline{J_S(u_H)} \right\|_{L^2(S)}^2 + (1+\delta^{-1}) C_A \| \varepsilon_H \|_{H^1(\omega_{T'})}^2.
\end{aligned}
$$

In light of reduction factor of element size $h_S \leq \gamma_{T'} H_{S'}$, and definitions of γ_S and $\gamma_{T'}$, we obtain

$$
\sum_{S \in \mathcal{S}_h(T')} \gamma_S h_S \left\| J_S(u_H) - \overline{J_S(u_H)} \right\|_{L^2(S)}^2 \leq \gamma_{T'} \sum_{S' \in \mathcal{S}_H(T')} H_{S'} \left\| J_{S'}(u_H) - \overline{J_{S'}(u_H)} \right\|_{L^2(S')}^2
$$

$$
= \gamma_{T'} \mathsf{osc}_{J,H}(T')^2,
$$

because for $S \subset S' \subset \partial T'$, we have $J_S(u_H) = J_{S'}(u_H)$ and $\overline{J_S(u_H)}$ is L^2-projection of $J_S(u_H)$ on S. Therefore

$$
\mathsf{osc}_{J,h}(T')^2 \leq (1+\delta) \gamma_{T'} \mathsf{osc}_{J,H}(T')^2 + (1+\delta^{-1}) C_A \| \varepsilon_H \|_{H^1(\omega_{T'})}^2 \qquad \forall\, T' \in \mathcal{T}_H.
$$

Step 3 (Choice of δ). Combining results from Steps 1 and 2 above using $\gamma_{T'} \leq 1$, $C_{**} = \max\{C_*, C_A\}$ and definition of $\mathsf{osc}_h(T)$, we arrive at

$$
\mathsf{osc}_h(T')^2 \leq (1+\delta) \gamma_{T'} \mathsf{osc}_H(T')^2 + C_{**}(1+\delta^{-1}) \| \varepsilon_H \|_{H^1(\omega_{T'})}^2.
$$

Proceeding as in Step 3 of the proof of Lemma 1.3.2, this time with Marking Strategy O performed according to the new definition of $\mathsf{osc}_H(T)$, we arrive at

$$\mathsf{osc}_h(\Omega)^2 \le (1+\delta)(1-(1-\gamma_0)\hat{\theta}^2)\mathsf{osc}_H(\Omega)^2 + C_o(1+\delta^{-1})\|\varepsilon_H\|^2,$$

with $C_o = C_{**}c_B^{-1}$. The assertion thus follows by choosing δ sufficiently small so that

$$\rho_1 := (1+\delta)(1-(1-\gamma_0)\hat{\theta}^2) < 1, \qquad \rho_2 := C_o(1+\delta^{-1}). \qquad \square$$

1.6.2   Non-coercive $\mathcal{B}$

In this section we prove convergence of AFEM for the case $c - \frac{1}{2}\nabla\cdot\mathbf{b} \not\ge 0, c \ge 0$; the case $c < 0$ can be treated as well. According to what we have so far, the assumption of $\nabla\cdot\mathbf{b} = 0$ is used for proving quasi-orthogonality and for having equivalence between energy norm $\|v\|^2 := \mathcal{B}[v,v]$ and H^1-norm as in (1.2.3), where $\mathcal{B}$ is coercive. Since now $\mathcal{B}$ may be non-coercive, we cannot define energy norm in this manner. We instead define energy norm by $\|v\|^2 := \int_\Omega \mathbf{A}\nabla v \cdot \nabla v + c\, v^2$, and we have equivalence of norms

$$c_E \|v\|_{H^1(\Omega)}^2 \le \|v\|^2 \le C_E \|v\|_{H^1(\Omega)}^2, \tag{1.6.1}$$

where constants c_E and C_E depend only on data $\mathbf{A}, c$ and Ω. The lack of coercivity is now replaced by Gårding's inequality

$$\|v\|^2 - \gamma_G \|v\|_{L^2(\Omega)}^2 \le \mathcal{B}[v,v] \qquad \forall\, v \in H_0^1(\Omega), \tag{1.6.2}$$

where $\gamma_G = \|\nabla\cdot\mathbf{b}\|_\infty / 2$. To see this we integrate by parts the middle term of $\mathcal{B}[v,v]$,

$$\int_\Omega \mathbf{b}\cdot\nabla v\, v = \frac{1}{2}\int_\Omega \mathbf{b}\cdot\nabla(v^2) = -\int_\Omega \frac{\nabla\cdot\mathbf{b}}{2}v^2 \qquad \forall\, v \in H_0^1(\Omega).$$

The same calculation leads to the sharp upper bound for $\mathcal{B}[v, v]$:

$$\mathcal{B}[v, v] \leq \|v\|^2 + \gamma_G \|v\|_{L^2(\Omega)}^2 \qquad \forall \, v \in H_0^1(\Omega). \qquad (1.6.3)$$

Existence and uniqueness of weak solutions follows from the maximum principle for $c \geq 0$ [10]. Schatz showed in [19] that the discrete problem (1.2.5) has a unique solution if the meshsize h is sufficiently small, i.e. $h \leq h^*$ for some constant h^* depending on shape regularity and data but not computable; the results in [19] are valid also for graded meshes. Assuming $h_0 \leq h^*$, to prove convergence of AFEM it thus suffices to prove quasi-orthogonality. We follow the steps of Lemma 1.2.1.

Using the same notation as in §4 for e_h, e_H and ε_H, expanding $\mathcal{B}[e_H, e_H]$, and noticing that $e_H = e_h + \varepsilon_H$ and $\mathcal{B}[e_h, \varepsilon_H] = 0$, we arrive at

$$\mathcal{B}[e_h, e_h] = \mathcal{B}[e_H, e_H] - \mathcal{B}[\varepsilon_H, \varepsilon_H] - \mathcal{B}[\varepsilon_H, e_h], \qquad (1.6.4)$$

where this time integration by parts yields

$$\mathcal{B}[\varepsilon_H, e_h] = \mathcal{B}[e_h, \varepsilon_H] + \langle \mathbf{b} \cdot \nabla \varepsilon_H, e_h \rangle - \langle \mathbf{b} \cdot \nabla e_h, \varepsilon_H \rangle$$

$$= 2 \langle \mathbf{b} \cdot \nabla \varepsilon_H, e_h \rangle + \langle \nabla \cdot \mathbf{b} \, e_h, \varepsilon_H \rangle.$$

Consequently, using Cauchy-Schwarz inequality and (1.6.1), we have for all $\delta > 0$

$$|\mathcal{B}[\varepsilon_H, e_h]| \leq (2 \|\mathbf{b}\|_\infty \|\nabla \varepsilon_H\|_{L^2} + \|\nabla \cdot \mathbf{b}\|_\infty \|\varepsilon_H\|_{L^2}) \, \|e_h\|_{L^2} \leq C_b^2 \delta \, \|\varepsilon_H\|^2 + \delta^{-1} \|e_h\|_{L^2}^2 \, ,$$

where constant $C_b = \max\{2 \|\mathbf{b}\|_\infty, \|\nabla \cdot \mathbf{b}\|_\infty\} c_E^{-1}/2$.

Using (1.6.2) and (1.6.3) to estimate terms $\mathcal{B}[e_h, e_h], \mathcal{B}[e_H, e_H], \mathcal{B}[\varepsilon_H, \varepsilon_H]$ in (1.6.4), and combining with the previous estimate, we infer that

$$\|e_h\|^2 - (\gamma_G + \delta^{-1}) \|e_h\|_{L^2}^2 \leq \|e_H\|^2 + \gamma_G \|e_H\|_{L^2}^2 - (1 - C_b^2 \delta) \|\varepsilon_H\|^2 + \gamma_G \|\varepsilon_H\|_{L^2}^2 \, .$$

Since $\|\varepsilon_H\|_{L^2}^2 \leq 2\|e_h\|_{L^2}^2 + 2\|e_H\|_{L^2}^2$, estimates for $\|e_h\|_{L^2}$ and $\|e_H\|_{L^2}$ of the form (1.4.1), obtained via duality, with $C_6 := \frac{C_D}{\sqrt{c_E}}$ imply

$$\Lambda_h \ \|e_h\|^2 \leq \Lambda_H \ \|e_H\|^2 - \Lambda_\varepsilon \ \|\varepsilon_H\|^2, \tag{1.6.5}$$

where $\Lambda_h = 1 - C_6^2 h_0^{2s}(3\gamma_G + \delta^{-1})$, $\Lambda_H = 1 + 3\gamma_G C_6^2 h_0^{2s}$, and $\Lambda_\varepsilon = 1 - C_b^2 \delta$.

Consequently, to get $\Lambda_h = \Lambda_\varepsilon$, we choose δ depending on h_0 so that

$$\delta(h_0) = \frac{C_G h_0^{2s} + \sqrt{C_G^2 h_0^{4s} + 4 C_b^2 C_6^2 h_0^{2s}}}{2 C_b^2} > 0,$$

where $C_G = 3\gamma_G C_6^2$. We further choose h_0 sufficiently small so that $C_b^2 \delta(h_0) < 1$, whence $\Lambda_h = \Lambda_\varepsilon > 0$. This can be achieved for $h_0^s \leq \min\{C_6 C_b C_G^{-1}, (3C_6 C_b)^{-1}\}$ because

$$C_b^2 \delta(h_0) = \frac{C_G}{2} h_0^{2s} + C_b C_6 h_0^s \sqrt{1 + h_0^{2s} C_G^2 (4 C_b^2 C_6^2)^{-1}}$$

$$\leq 2 C_b C_6 h_0^s \big(1 + h_0^s C_G (4 C_b C_6)^{-1}\big) < 3 C_b C_6 h_0^s \leq 1.$$

We conclude that if the meshsize h_0 of the initial mesh satisfies

$$h_0^s \leq \min\{C_6 C_b C_G^{-1}, (3C_6 C_b)^{-1}, (h^*)^s\}, \tag{1.6.6}$$

then quasi-orthogonality holds, i.e. for $\Lambda_0 := \Lambda_H / \Lambda_h$,

$$\|e_h\|^2 \leq \Lambda_0 \|e_H\|^2 - \|\varepsilon_H\|^2, \tag{1.6.7}$$

and Λ_0 can be made arbitrarily close to 1 by decreasing h_0. Convergence of AFEM finally follows as in Theorem 1.1.

1.6.3 Experiment 4 : Non-coercive $\mathcal{B}$

We repeat Experiment 2 in §1.5.3 with $\mathbf{b} = (x-1, y+1)$, and thus $\mathcal{B}$ is non-coercive because $c - \frac{1}{2}\nabla\cdot\mathbf{b} = -1$. For a better view of solutions we change the

boundary condition $g(x, y)$ to be 1 on x-axis from $(.4+\tau)$ to $(.8-\tau)$, with τ defined as in (1.5.3). Results of AFEM with $\theta = \hat{\theta} = 0.5, \tau = 0.005$ are reported in Figure 1.6.1. Observations and conclusions follow.
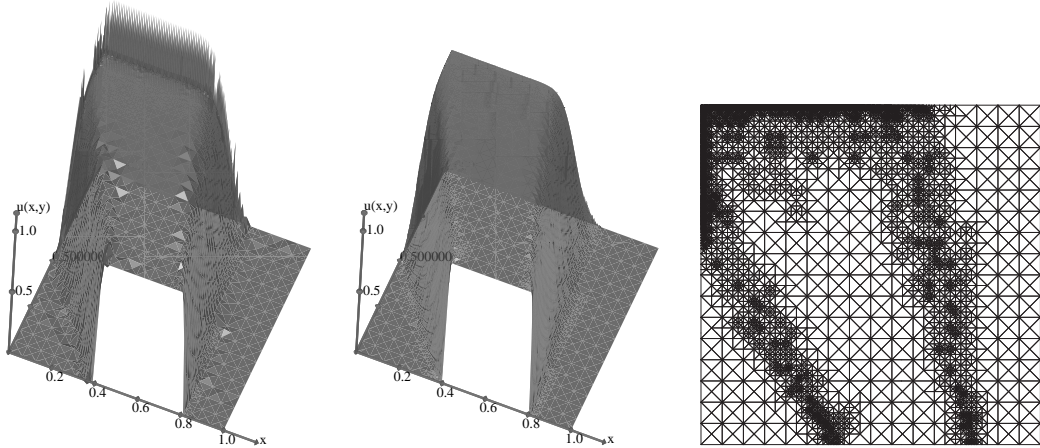

Figure 1.6.1: Experiment 4 (Non-coercive $\mathcal{B}$ with $\epsilon = 10^{-3}, \mathbf{b} = (x - 1, y + 1)$): 3-D plots of solutions after 4 and 6 iterations and graded mesh after 6 iterations. Oscillations of Galerkin solutions are observed near internal and boundary layers in a first few iterations but AFEM eliminates them after 6 iterations.

• Figure 1.6.1 shows oscillations of Galerkin solution near internal and boundary layers after 4 iterations. AFEM detects this effect and corrects it after 6 iterations by selective local refinement which does not spread in regions of smoothness.

•The resulting graded meshes are optimal and capture internal layers (diffuse boundary of pulse g being transported) and outflow boundary layer, even though the initial uniform mesh is far coarser than required by theory; see (1.6.6) which is a restriction similar to that discussed in §1.5.3-Experiment 2. Moreover, the performance of AFEM as to the estimator decay and oscillation control is analogous to §1.5.3-Experiment 2.

Chapter 2

AFEM for the Laplace-Beltrami Operator on Graphs:

A Posteriori Error Analysis and Convergence

2.1 Introduction

We consider a surface $\Gamma \subset \mathbb{R}^d$ described as the graph of a function $z(\mathbf{x})$ defined on a bounded polygonal region $\Omega \subset \mathbb{R}^{d-1}$, $d \geq 2$, namely,

$$\Gamma := \left\{ (\mathbf{x}, z(\mathbf{x})) \in \mathbb{R}^d \mid \mathbf{x} \in \Omega \subset \mathbb{R}^{d-1} \right\},$$

where $z : \Omega \to \mathbb{R}$ is a C^1 function. We develop the theory under the assumption of C^1, as opposed to C^2, regularity. In general we may allow z to be $C^{0,1}$ with discontinuities of ∇z aligned with polygonal lines on Ω. For example in $\mathbb{R}^3$, we can allow Γ to be a polyhedral surface, a graph of a piecewise polynomial function. We will not dwell on this matter though.

We consider the Dirichlet boundary value problem for the Laplace-Beltrami operator Δ_Γ on Γ

$$-\Delta_\Gamma u = f \text{ on } \Gamma,$$

$$u = 0 \text{ on } \partial\Gamma,$$

(2.1.1)

where $f \in L^2(\Gamma)$. Note that a non-zero Dirichlet boundary condition can be treated similarly to [17]. We next introduce the weak formulation, the FEM, and give an outline of the chapter along with our main result.

49

2.1.1 Variational Formulation

Given a function $v : \Gamma \to \mathbb{R}$ we define its lift $\tilde{v} : \Omega \times \mathbb{R} \to \mathbb{R}$ to be the obvious extension

$$\tilde{v}(\mathbf{x}, x_d) := v(\mathbf{x}, z(\mathbf{x})). \tag{2.1.2}$$

We denote by $\nabla \tilde{v} \in \mathbb{R}^d$ the gradient of $\tilde{v}$, and point our that it is a row vector. If Q is the elementary surface area and ν is the unit normal vector to Γ, namely,

$$Q := \sqrt{1 + |\nabla z|^2}, \qquad \nu := \frac{1}{Q}(-\nabla z, 1). \tag{2.1.3}$$

We indicate with $\nabla_\Gamma v \in \mathbb{R}^d$ the tangential gradient of v on Γ (or that part of $\nabla \tilde{v}$ tangent to Γ),

$$\nabla_\Gamma v = \nabla \tilde{v} - (\nabla \tilde{v} \cdot \nu)\nu = \nabla \tilde{v}(\mathbf{I} - \nu \otimes \nu). \tag{2.1.4}$$

Likewise, the tangential divergence of a vector field $\mathbf{q} : \Omega \times \mathbb{R} \to \mathbb{R}^d$ is given by

$$\mathrm{div}_\Gamma \mathbf{q} = \mathrm{div}\mathbf{q} - \nu D\mathbf{q}\,\nu^T, \tag{2.1.5}$$

where $D\mathbf{q}$ stands for the differential matrix of $\mathbf{q}$; hence, we have

$$\Delta_\Gamma v = \mathrm{div}_\Gamma \nabla_\Gamma v = \Delta \tilde{v} - (\nabla \tilde{v} \cdot \nu)(\nabla \cdot \nu) - \nu D^2 \tilde{v} \nu^T, \tag{2.1.6}$$

where $D^2 \tilde{v} \in \mathbb{R}^{d \times d}$ is the Hessian of $\tilde{v}$. To formulate (2.1.1) weakly, we now introduce Sobolev spaces on the surface Γ.

$$H^1(\Gamma) := \left\{ f \in L^2(\Gamma) \mid \nabla_\Gamma f \in L^2(\Gamma) \right\},$$

$$H_0^1(\Gamma) := \left\{ f \in H^1(\Gamma) \mid f \text{ has zero trace on } \partial\Gamma \right\}.$$

A weak solution of (2.1.1) is a function $u : \Gamma \to \mathbb{R}$ satisfying

$$u \in H_0^1(\Gamma) : \qquad \int_\Gamma \nabla_\Gamma u \cdot \nabla_\Gamma \varphi = \int_\Gamma f\varphi \qquad \forall\, \varphi \in H_0^1(\Gamma). \tag{2.1.7}$$

50

2.1.2 The Finite Element Method on Graphs

To approximate (2.1.7) via the FEM we proceed as follows. We first partition Ω into shape regular simplices, thereby giving rise to a graded triangulation (or mesh) $\mathcal{T}_h(\Omega)$ of local meshsize h. We next let $\mathbb{V}_h(\Omega)$ be a finite element space over $\mathcal{T}_h(\Omega)$ consisting of C^0 piecewise polynomial functions of degree $n \geq 1$. Each node of $\mathcal{T}_h(\Omega)$ is lifted to a point on Γ and all nodes on Γ are connected through a function $z_h \in \mathbb{V}_h(\Omega)$, the interpolant of z in $\mathbb{V}_h(\Omega)$; the image $\Gamma_h := \{(\mathbf{x}, z_h(\mathbf{x})) : \mathbf{x} \in \Omega\}$ is thus a 'polyhedral' approximation to Γ. This induces a pair $(\mathcal{T}_h(\Gamma_h), \mathbb{V}_h(\Gamma_h))$ as follows. We have a one-to-one correspondence between elements $\hat{T} \in \mathcal{T}_h(\Omega)$ and elements $T \in \mathcal{T}_h(\Gamma_h)$ via $T = \left\{(\mathbf{x}, z_h(\mathbf{x})) : \mathbf{x} \in \hat{T}\right\}$. The space $\mathbb{V}_h(\Gamma_h)$ is simply the lift of $\mathbb{V}_h(\Omega)$ via (2.1.2) where z is replaced by z_h. We point out that we insist on the same polynomial degree $n \geq 1$ for both surface and solution approximation. For later usage, we also denote by $\mathcal{T}_h(\Gamma)$ a partition of Γ into curved elements $\tilde{T} := \left\{(\mathbf{x}, z(\mathbf{x})) : \mathbf{x} \in \hat{T}\right\}$, and by $\mathring{\mathbb{V}}_h(\Gamma_h) := \mathbb{V}_h(\Gamma_h) \cap H_0^1(\Gamma_h)$.

We are now ready to introduce the FEM for the Laplace-Beltrami operator on graphs. If $F_h \in L^2(\Gamma_h)$ is a suitable approximation of f, then the finite element function $u_h : \Gamma_h \to \mathbb{R}$ solves

$$u_h \in \mathring{\mathbb{V}}_h : \qquad \int_{\Gamma_h} \nabla_{\Gamma_h} u_h \cdot \nabla_{\Gamma_h} \varphi_h = \int_{\Gamma_h} F_h \varphi_h \qquad \forall\, \varphi_h \in \mathring{\mathbb{V}}_h. \tag{2.1.8}$$

This yields a *symmetric positive definite* (SPD) linear system which can be solved with standard linear algebra tools. We note that (2.1.8) can be thought of as a linear elliptic PDE with variable coefficients in Ω; see Remark 2.2.1. However, in light of implementation issues and generalizations to parametric surfaces, it is better

to think of (2.1.8) as defined on Γ_h.

2.1.3   Main Result and Outline

The main purpose of this chapter is to present a new AFEM for (2.1.1), discuss its design, prove its convergence, and document its performance computationally. For convenience, if $T \in \mathcal{T}_k(\Gamma_k)$, we define its corresponding elements $\hat{T} \in \mathcal{T}_k(\Omega)$ and $\tilde{T} \in \mathcal{T}_k(\Gamma)$ by

$$\hat{T} := \{\mathbf{x} \in \Omega \ : \ (\mathbf{x}, z_k(\mathbf{x})) \in T\}, \quad \tilde{T} := \{(\mathbf{x}, z(\mathbf{x})) \in \Gamma \ : \ (\mathbf{x}, z_k(\mathbf{x})) \in T\}, \quad (2.1.9)$$

and we also use $\mathring{\mathbb{V}}_k$ and $\mathcal{T}_k$ instead of $\mathring{\mathbb{V}}_k(\Gamma_k)$ and $\mathcal{T}_k(\Gamma_k)$, respectively. We now briefly state our main result and provide an outline of the chapter.

Let $(\mathring{\mathbb{V}}_k, \mathcal{T}_k)_{k=1}^\infty$ be a sequence created via adaptive loops of the form

$$\text{SOLVE} \rightarrow \text{ESTIMATE} \rightarrow \text{MARK} \rightarrow \text{REFINE} \qquad (2.1.10)$$

as described below. To argue about the approximation of Γ by Γ_k in W_∞^1, we introduce the *geometric oscillation* $\lambda_k := \max_{T \in \mathcal{T}_k} \lambda_k(T)$ where

$$\lambda_k(T) := \|\nu - \nu_k\|_{L^\infty(\hat{T})} \qquad \forall\, T \in \mathcal{T}_k, \qquad (2.1.11)$$

and the unit normals ν and ν_k to Γ and Γ_k are defined according to (2.1.3). We next introduce the *geometric error* $\zeta_k := (\sum_{T \in \mathcal{T}_k} \zeta_k^2(T))^{1/2}$ where

$$\zeta_k(T) := \lambda_k(T) \|\nabla_\Gamma u_k\|_{L^2(\tilde{T})} \qquad \forall\, T \in \mathcal{T}_k, \qquad (2.1.12)$$

the presence of the second factor is interesting and shows the interaction between the PDE and the surface. We note that, in contrast with λ_k, the accumulation in

ζ_k is in $\ell^2(\mathcal{T}_k)$. In defining the *energy error*

$$e_k := \|\nabla_\Gamma(u - u_k)\|_{L^2(\Gamma)}, \qquad (2.1.13)$$

we have decided to measure it on Γ and so use ∇_Γ; in doing this, we are implicitly employing the lift (2.1.2). We finally let the *data oscillation* be $\mathsf{osc}_k :=$ $(\sum_{T \in \mathcal{T}_k} \mathsf{osc}_k(T)^2)^{1/2}$ where

$$\mathsf{osc}_k^2(T) = h_T^2 \left\| F_k - \overline{F}_k \right\|_{L^2(T)}^2 \qquad \forall\, T \in \mathcal{T}_k, \qquad (2.1.14)$$

where $\overline{F}_k$ is the L^2-projection of F_k onto $\mathbb{P}_{n-1}(T)$. We are now ready to state the main result of this chapter, the convergence of the adaptive loop (2.1.10).

In §2.3 and 2.4 we design an AFEM with the following contraction property. Let $(\Gamma_0, \mathcal{T}_0)$ *be an arbitrary initial surface-triangulation pair of* Γ. *Then there exist an integer* $k_0 > 0$ *and constants* $\gamma_g, \gamma_o > 0$, *and* $\xi < 1$, *solely depending on* $(\Gamma_0, \mathcal{T}_0)$, *shape regularity and the user's parameters of AFEM, such that for any* $k \geq k_0$ *AFEM satisfies*

$$\mathcal{E}_{k+1} \leq \xi\, \mathcal{E}_k, \qquad (2.1.15)$$

where $\mathcal{E}_k^2 := e_k^2 + \gamma_g \zeta_k^2 + \gamma_o \mathsf{osc}_k^2$ *represents the combined error incurred by AFEM, namely the energy and geometric errors,* e_k, ζ_k, *as well as information missing in the averaging process* osc_k.

The existence of k_0 is related to sufficient resolution of Γ by Γ_k, a condition which is attained by AFEM automatically but not imposed directly on the initial pair $(\Gamma_0, \mathcal{T}_0)$. More precisely, what is needed is that λ_k be below a threshold dictated by the regularity of Γ.

The chapter is organized as follows. We start in §2.2 with a review of differential geometry on graphs. We discuss the procedure ESTIMATE in §2.3 and the procedures SOLVE, MARK and REFINE in §2.4. We prove the contraction property, and so convergence, of AFEM in §2.4. We conclude in §2.5 with several numerical experiments that shed light on the theory and document the performance of AFEM on graphs.

To avoid confusions with constants, we write $a \lesssim b$ to denote $a \leq C_0 b$, and $a \sim b$ to denote $C_1 b \leq a \leq C_2 b$ for some constants C_0, C_1, C_2.

2.2 Differential Geometry on Graphs

According to the lifting (2.1.2), a function $v : \Gamma \to \mathbb{R}$ induces a function $\hat{v} : \Omega \to \mathbb{R}$ upon setting $\hat{v}(\mathbf{x}) = v(\mathbf{x}, z(\mathbf{x})) = \tilde{v}(\mathbf{x}, x_d)$. Therefore, $\nabla \tilde{v} = (\nabla_\mathbf{x} \hat{v}, 0)$ and (2.1.4) becomes

$$\nabla_\Gamma v = \nabla \tilde{v} \, \tilde{\mathbf{D}} = \nabla_\mathbf{x} \hat{v} \, \mathbf{D}, \tag{2.2.1}$$

where $\tilde{\mathbf{D}} \in \mathbb{R}^{d \times d}$ and $\mathbf{D} \in \mathbb{R}^{d-1 \times d}$ are the matrices

$$\tilde{\mathbf{D}} := \mathbf{I}_{d \times d} - \nu \otimes \nu, \qquad \mathbf{D} = [\mathbf{I}_{d-1 \times d-1} \, \mathbf{0}] + \frac{1}{Q^2} \nabla z \otimes (-\nabla z, 1); \tag{2.2.2}$$

we see that $\mathbf{D}$ results from $\tilde{\mathbf{D}}$ upon eliminating its last row. When no confusion is possible, we will refer to the three functions $v, \tilde{v}, \hat{v}$ just as v. In view of (2.2.1) we can express (2.1.7) as an elliptic PDE with variable coefficients in Ω:

$$\int_\Gamma \nabla_\Gamma u \cdot \nabla_\Gamma \varphi = \int_\Omega \nabla_\mathbf{x} u \left(Q \mathbf{D} \mathbf{D}^T \right) \cdot \nabla_\mathbf{x} \varphi. \tag{2.2.3}$$

Moreover, a simple calculation shows that $\mathbf{DD}^T$ is SPD and has the form

$$\mathbf{DD}^T = \mathbf{I}_{d-1 \times d-1} - \frac{1}{Q^2}(\nabla z \otimes \nabla z). \tag{2.2.4}$$

Remark 2.2.1 (*PDE with Variable Coefficients*). If $\mathbf{A} := Q\mathbf{DD}^T$ and $F := Qf$, then (2.1.7) becomes

$$-\mathrm{div}(\mathbf{A}\nabla^T u) = F \qquad \text{in} \quad \Omega, \qquad u = 0 \qquad \text{on} \quad \partial\Omega,$$

where $\nabla^T u$ denotes the transpose of ∇u. The convergence of AFEM for this type of PDEs is studied in Chapter 1 and [13]; see also [15, 16]. However, we prefer to view the surface Γ as a geometric object to be discretized, and the PDE to be formulated directly on Γ and Γ_h. This is consistent with the a priori analysis of Dziuk [9], and extends naturally to parametric surfaces [14]. $\qquad\square$

Remark 2.2.2 (*Quadrature*). We could regard the approximation of Γ by Γ_h as quadrature in that the coefficient matrix $\mathbf{A}$ of Remark 2.2.1 is replaced by $\mathbf{A}_h := Q_h\mathbf{D}_h\mathbf{D}_h^T$. This is not, however, *interpolatory* quadrature because $\mathbf{A}$ is not evaluated at preassigned points: the value of $\mathbf{A}_h$ within an element depends on all the values of $z(\mathbf{x})$ at its nodes. To get intuition about the structure of the error committed in replacing $\mathbf{A}$ by $\mathbf{A}_h$, let $U_h \in H_0^1(\Omega)$ be the solution of the PDE in Ω

$$-\mathrm{div}(\mathbf{A}_h\nabla^T U_h) = F.$$

The error $e = u - U_h \in H_0^1(\Omega)$ thus satisfies

$$\int_\Omega \nabla e \mathbf{A} \cdot \nabla\varphi = \int_\Omega \nabla U_h(\mathbf{A}_h - \mathbf{A}) \cdot \nabla\varphi \qquad \forall \; \varphi \in H_0^1(\Omega),$$

whence

$$\int_\Omega \nabla e \mathbf{A} \cdot \nabla e \leq \int_\Omega \nabla U_h\Big((\mathbf{A}_h - \mathbf{A})\mathbf{A}^{-1}(\mathbf{A}_h - \mathbf{A})\Big) \cdot \nabla U_h.$$

We will see below how to bound $\mathbf{A}_h - \mathbf{A}$ in terms of the unit normals ν and ν_h. $\quad\square$

To write a sort of inverse formula to (2.2.1), we let $\mathbf{t}_i(\mathbf{x}) = (\mathbf{e}_i, \frac{\partial z(\mathbf{x})}{\partial x_i})^T \in \mathbb{R}^d$ be the tangent (column) vectors to Γ and $\mathbf{e}_i$ be the canonical basis of $\mathbb{R}^{d-1}$ for $1 \leq i \leq d-1$. If $\mathbf{G} \in \mathbb{R}^{d \times d-1}$ is given by

$$\mathbf{G}(\mathbf{x}) = [\mathbf{t}_1(\mathbf{x}), \mathbf{t}_2(\mathbf{x}), ..., \mathbf{t}_{d-1}(\mathbf{x})],$$

then the chain rule yields the relations

$$\nabla_{\mathbf{x}} \hat{v}(\mathbf{x}) = \nabla \tilde{v}(\mathbf{x}, z(\mathbf{x})) \mathbf{G}(\mathbf{x}) = \nabla_\Gamma v(\mathbf{x}, z(\mathbf{x})) \mathbf{G}(\mathbf{x}) \qquad \forall\, \mathbf{x} \in \Omega. \tag{2.2.5}$$

It is easy to verify by simple matrix multiplication that $\mathbf{D}$ and $\mathbf{G}$ are pseudo-inverses, namely,

$$\mathbf{DG} = \mathbf{I}_{d-1 \times d-1}, \qquad \mathbf{GD} = \mathbf{I}_{d \times d} - \nu \otimes \nu; \tag{2.2.6}$$

note that $(\mathbf{GD})^2 = \mathbf{GDD}^T \mathbf{G}^T = \mathbf{GD}$. Similar results also apply elementwise to z_h in place of z, namely $\mathbf{D}_h, \mathbf{G}_h$, and Q_h are defined for each $T \in \mathcal{T}_h(\Omega)$ via z_h.

With these relations at hand, we can now show how to transform integrals on Γ to Ω and back to Γ_h. If $T \in \mathcal{T}_h$ we recall the definitions of $\hat{T}$ and $\tilde{T}$ in (2.1.9) and note that abusing notation $\int_{\tilde{T}} vw = \int_{\hat{T}} Qvw = \int_T \frac{Q}{Q_h} vw$ as well as

$$\int_{\tilde{T}} \nabla_\Gamma v \cdot \nabla_\Gamma w = \int_{\hat{T}} Q \nabla_{\mathbf{x}} v \mathbf{DD}^T \cdot \nabla_{\mathbf{x}} w = \int_T \frac{Q}{Q_h} \nabla_{\Gamma_h} v (\mathbf{G}_h \mathbf{DD}^T \mathbf{G}_h^T) \cdot \nabla_{\Gamma_h} w. \tag{2.2.7}$$

Conversely

$$\int_T \nabla_{\Gamma_h} v \cdot \nabla_{\Gamma_h} w = \int_{\hat{T}} Q_h \nabla_{\mathbf{x}} v \mathbf{D}_h \mathbf{D}_h^T \cdot \nabla_{\mathbf{x}} w = \int_{\tilde{T}} \frac{Q_h}{Q} \nabla_\Gamma v (\mathbf{GD}_h \mathbf{D}_h^T \mathbf{G}^T) \cdot \nabla_\Gamma w. \tag{2.2.8}$$

This allows us to compare integrals over Γ and Γ_h. In fact, the following is valid for

all $v, w \in H^1(\Omega)$

$$\int_{\Gamma_h} \nabla_{\Gamma_h} v \cdot \nabla_{\Gamma_h} w - \int_\Gamma \nabla_\Gamma v \cdot \nabla_\Gamma w = \int_\Gamma \nabla_\Gamma v \underbrace{\frac{1}{Q} \mathbf{G}(Q_h \mathbf{D}_h \mathbf{D}_h^T - Q\mathbf{D}\mathbf{D}^T)\mathbf{G}^T}_{:=\mathcal{A}_h} \cdot \nabla_\Gamma w. \quad (2.2.9)$$

This is a consequence of (2.2.8) and (2.2.6), because $\nabla_\Gamma v \cdot \nu = 0$ whence $\nabla_\Gamma v \mathbf{GD} = \nabla_\Gamma v$. To estimate this difference, we thus have to bound the matrix $\mathcal{A}_h$.

Lemma 2.2.1 (Basic Estimates). *The following geometric estimates are valid*

$$|Q - Q_h| \le QQ_h|\nu - \nu_h|, \qquad \left| \frac{\nabla z \otimes \nabla z}{Q} - \frac{\nabla z_h \otimes \nabla z_h}{Q_h} \right| \le 3QQ_h|\nu - \nu_h|.$$

Proof. If follows from (2.1.3) that $\left| \frac{1}{Q} - \frac{1}{Q_h} \right| \le |\nu - \nu_h|$, hence

$$|Q - Q_h| \le QQ_h |\nu - \nu_h| .$$

To get the last estimate, we write

$$\frac{\nabla z \otimes \nabla z}{Q} - \frac{\nabla z_h \otimes \nabla z_h}{Q_h} = (Q - Q_h)\left(\frac{\nabla z}{Q} \otimes \frac{\nabla z}{Q} \right)$$
$$+ Q_h \left[\frac{\nabla z}{Q} \otimes \left(\frac{\nabla z}{Q} - \frac{\nabla z_h}{Q_h} \right) + \left(\frac{\nabla z}{Q} - \frac{\nabla z_h}{Q_h} \right) \otimes \frac{\nabla z_h}{Q_h} \right].$$

Again, (2.1.3) implies $\left| \frac{\nabla z}{Q} - \frac{\nabla z_h}{Q_h} \right| \le |\nu - \nu_h|$ and $\left| \frac{\nabla z}{Q} \right|, \left| \frac{\nabla z_h}{Q_h} \right| \le 1$, which prove the assertion. $\qquad\square$

Lemma 2.2.2 (Estimate of $\mathcal{A}_h$). *We have* $\|\mathcal{A}_h\|_{L^\infty(\hat{T})} \lesssim \|\nu - \nu_h\|_{L^\infty(\hat{T})}$ *for all* $\hat{T} \in \mathcal{T}_h(\Omega)$.

Proof. In view of (2.2.4), we can write

$$Q_h \mathbf{D}_h \mathbf{D}_h^T - Q\mathbf{D}\mathbf{D}^T = (Q_h - Q)\mathbf{I} - \left(\frac{1}{Q_h} \nabla z_h \otimes \nabla z_h - \frac{1}{Q} \nabla z \otimes \nabla z \right).$$

Since $\|\mathbf{G}\|_{L^\infty(T)} \lesssim Q$, and both Q and Q_h are bounded because $\Gamma \in C^1$, the assertion thus follows from Lemma 2.2.1. $\qquad\square$

Lemma 2.2.3 (Equivalence of Norms). *Let Γ_h be a polyhedral surface approximating Γ as decribed above. For all lifted functions $v : \Omega \times \mathbb{R} \to \mathbb{R}$, we have equivalence of norms*

$$\|v\|_{L^2(\Gamma)} \sim \|v\|_{L^2(\Gamma_h)}, \tag{2.2.10}$$

$$\|v\|_{H_0^1(\Gamma)} \sim \|v\|_{H_0^1(\Gamma_h)}. \tag{2.2.11}$$

Proof: We will prove this only for a single element $T \in \mathcal{T}_h$ and the results will follow by summing over all $T \in \mathcal{T}_h$. The assertion (2.2.10) holds trivially from the change of integrals

$$\int_{\tilde{T}} |v|^2 = \int_T \frac{Q}{Q_h} |v|^2.$$

Note that $0 < c \le \frac{Q}{Q_h} \le C$ for some constants c and C depending only on Γ. To prove (2.2.11), we use (2.2.7),

$$\int_{\tilde{T}} |\nabla_\Gamma v|^2 = \int_T \frac{Q}{Q_h} \nabla_{\Gamma_h} v (\mathbf{G}_h \mathbf{D} \mathbf{D}^T \mathbf{G}_h^T)(\nabla_{\Gamma_h} v)^T.$$

Since $\mathbf{D}\mathbf{D}^T$ is SPD, $\|\mathbf{G}_h\|$ is bounded away from zero, and $\nabla_{\Gamma_h} v \mathbf{G}_h$ is non-zero unless $\nabla_{\Gamma_h} v = \mathbf{0}$, therefore

$$\|\nabla_{\Gamma_h} v\|_{L^2(T)} \sim \|\nabla_\Gamma v\|_{L^2(\tilde{T})},$$

where constants depend only on the Γ. Note that the matching of vanishing boundaries follow from the lift (2.1.2). $\qquad \square$

2.3 Procedure ESTIMATE: A Posteriori Error Estimation

2.3.1 Error Representation

Employing weak formulations (2.1.7) and (2.1.8), we obtain an error representation

$$\int_\Gamma \nabla_\Gamma(u - u_h) \cdot \nabla_\Gamma \varphi = I_1 + I_2 + I_3, \qquad \forall\, \varphi \in H_0^1(\Gamma),\ \forall\, \varphi_h \in \mathring{\mathbb{V}}_h, \qquad (2.3.1)$$

where

$$I_1 := \sum_{T \in \mathcal{T}_h} \int_T \mathcal{R}_T(u_h)(\varphi - \varphi_h) - \sum_{S \in \mathcal{S}_h^o} \int_S \mathcal{J}_S(u_h)(\varphi - \varphi_h),$$

$$I_2 := \int_{\Gamma_h} \nabla_{\Gamma_h} u_h \cdot \nabla_{\Gamma_h} \varphi - \int_\Gamma \nabla_\Gamma u_h \cdot \nabla_\Gamma \varphi,$$

$$I_3 := \int_\Gamma f \varphi - \int_{\Gamma_h} F_h \varphi.$$

- I_1 is a *standard residual term* obtained by integrating by parts on each $T \in \mathcal{T}_h$ where *element residual* $\mathcal{R}_T$ and *jump residual* $\mathcal{J}_S$ are defined by

$$\mathcal{R}_T(u_h) := (\Delta_{\Gamma_h} u_h + F_h)|_T, \qquad (2.3.2)$$

$$\mathcal{J}_S(u_h) := (\nabla_{\Gamma_h} u_h)_S^+ \cdot n_S^+ + (\nabla_{\Gamma_h} u_h)_S^- \cdot n_S^-. \qquad (2.3.3)$$

Here n_S^+ and n_S^- are outward unit normals to S, with respect to T^+ and T^-, on the supporting planes containing T^+ and T^- respectively; T^+ and T^- are elements in $\mathcal{T}_h$ that share the side $S \in \mathcal{S}_h^o$ where $\mathcal{S}_h^o$ denotes the set of interior faces of $T \in \mathcal{T}_h$, see Figure 2.3.1. Similarly, $(\nabla_{\Gamma_h} u_h)_S^+$ and $(\nabla_{\Gamma_h} u_h)_S^-$ are tangential gradients of u_h considered on T^+ and T^- restricted to S, respectively. If $\mathbb{V}_h$ is a space of piecewise linear functions, then $\mathcal{R}_T = F_h|_T$ and $\mathcal{J}_S$ is constant on S, since $\nabla_{\Gamma_h} u_h$ is constant on T.
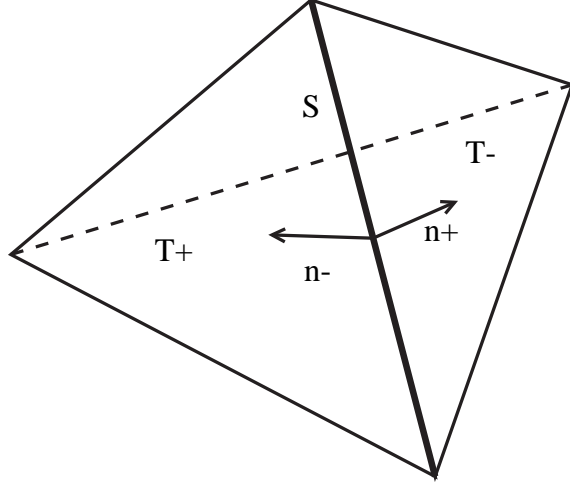
Figure 2.3.1: S is the common side shared by the elements T^+ and T^-, and n^+ and n^- are the normals to the side S on the supporting planes containing T^+ and T^-, respectively.

- I_2 is a *geometric consistency term* that accounts for the difference between Γ and Γ_h. According to (2.2.9), $I_2 = \int_\Gamma \nabla_\Gamma u_h \mathcal{A}_h \cdot \nabla_\Gamma \varphi$.

- I_3 is a consistency term that accounts for the difference of forcing functions f and F_h of the PDE on surfaces Γ and Γ_h, respectively. We choose F_h to balance this difference, thereby making $I_3 = 0$ upon defining

$$F_h(\mathbf{x}, z_h(\mathbf{x})) := \frac{Q(\mathbf{x})}{Q_h(\mathbf{x})} f(\mathbf{x}, z(\mathbf{x})). \tag{2.3.4}$$

Hence, we arrive at the error representation

$$\int_\Gamma \nabla_\Gamma (u - u_h) \cdot \nabla_\Gamma \varphi = \sum_{T \in \mathcal{T}_h} \int_T \mathcal{R}_T(u_h)(\varphi - \varphi_h) - \sum_{S \in \mathcal{S}_h^o} \int_S \mathcal{J}_S(u_h)(\varphi - \varphi_h)$$
$$+ \int_\Gamma \nabla_\Gamma u_h \mathcal{A}_h \cdot \nabla_\Gamma \varphi \qquad \forall\, \varphi \in H_0^1(\Gamma),\ \forall\, \varphi_h \in \mathring{\mathbb{V}}_h. \tag{2.3.5}$$

2.3.2 Upper Bound

The upper bound for the *energy error* $e_h := \|\nabla_\Gamma(u - u_h)\|_{L^2(\Gamma)}$ is obtained from (2.3.5) and Clement's interpolation for functions defined on a polyhedral surface.

Lemma 2.3.1 (Clemént Interpolation). *There exists a linear interpolation operator $\mathcal{I}_h : H_0^1(\Gamma_h) \to \mathring{\mathbb{V}}_h$ such that for $T \in \mathcal{T}_h$ and $S \in \mathcal{S}_h^o$ we have*

$$\|v - \mathcal{I}_h v\|_{L^2(T)} \le C h_T \|\nabla_{\Gamma_h} v\|_{L^2(\bar{\omega}_h(T))} \quad \forall v \in H_0^1(\Gamma_h), \tag{2.3.6}$$

$$\|v - \mathcal{I}_h v\|_{L^2(S)} \le C h_S^{1/2} \|\nabla_{\Gamma_h} v\|_{L^2(\bar{\omega}_h(T))} \quad \forall v \in H_0^1(\Gamma_h), \tag{2.3.7}$$

where C depends only on shape regularity constant, h_T and h_S are diameters of T and S respectively, and $\bar{\omega}_h(T) := \bigcup \{T' \in \mathcal{T}_h \mid T' \cap T \ne \varnothing\}$.

The proof of this lemma can be found in [5, 6]. Note that the shape regularity condition still holds for a polyhedral surface which is a piecewise polynomial interpolant of a C^1 graph.

Taking $\varphi = u - u_h \in H_0^1(\Gamma) \sim H_0^1(\Gamma_h)$, $\varphi_h = \mathcal{I}_h \varphi \in \mathring{\mathbb{V}}_h$ into (2.3.5), and using Lemmas 2.2.3 and 2.3.1, we obtain

$$\|\nabla_\Gamma (u - u_h)\|_{L^2(\Gamma)}^2 \le C_1 \sum_{T \in \mathcal{T}_h} \eta_h^2(T) + C_2 \sum_{T \in \mathcal{T}_h} \|\nabla_\Gamma u_h \mathcal{A}_h\|_{L^2(\tilde{T})}^2, \tag{2.3.8}$$

where the constants C_1 and C_2 depend only on shape regularity constant and Γ. Here we define the *energy error indicator* $\eta_h(T)$ by

$$\eta_h^2(T) := h_T^2 \|\mathcal{R}_T(u_h)\|_{L^2(T)}^2 + \sum_{\substack{S \in \mathcal{S}_h^o \\ S \subset \partial T}} h_S \|\mathcal{J}_S(u_h)\|_{L^2(S)}^2, \tag{2.3.9}$$

and the *energy error estimator* $\eta_h := (\sum_{T \in \mathcal{T}_h} \eta_h^2(T))^{1/2}$.

As a result of Lemma 2.2.2 and the definition of geometric error (2.1.12), we obtain the upper bound for the energy error.

Lemma 2.3.2 (Upper Bound). *There exist constants C_1 and C_2 depending only on shape regularity constant and the surface Γ such that*

$$\|\nabla_\Gamma(u - u_h)\|_{L^2(\Gamma)}^2 \le C_1 \eta_h^2 + C_2 \zeta_h^2. \tag{2.3.10}$$

Remark 2.3.1. If Γ is itself a polyhedral surface, then $\Gamma_h = \Gamma$. In this case we have $\zeta_h = 0$, and the estimate (2.3.10) does not involve a geometric error. The geometric error is necessary since it tells us how well the surface Γ is approximated by piecewise polynomial surface Γ_h. In fact, it is coupled with the energy error according to the term $\nabla_\Gamma u_h$.

2.3.3 Lower Bound

We obtain a local lower bound for the energy error by using the idea of bubble functions introduced by Verfürth [23] and later refined by Dörfler [7] in that continuous piecewise linear bubble functions are used. By proceeding as in [1, 7, 23] for estimating the local lower bound, we obtain the lemma below. Here we denote by $\omega_h(T)$, $T \in \mathcal{T}_h$, a subregion of Γ_h consisting of all elements in $\mathcal{T}_h$ that share a common side $S \in \mathcal{S}_h^o$ with T, and by $\tilde{T} \subset \Gamma$ a curved element as in (2.1.9).

Lemma 2.3.3 (Local Lower Bound). *There exist constants C_3, C_4, and C_5, depending on the shape regularity constant and Γ, such that for $T \in \mathcal{T}_h$,*

$$\eta_h^2(T) \le C_3 \sum_{\substack{T' \in \mathcal{T}_h \\ T' \subset \omega_h(T)}} \|\nabla_\Gamma(u - u_h)\|_{L^2(\tilde{T}')}^2 + C_4 \mathsf{osc}_h^2(\omega_h(T)) + C_5 \zeta_h^2(\omega_h(T)). \tag{2.3.11}$$

For $T \in \mathcal{T}_h$, let $\mathcal{S}_h^o(T) := \{S \in \mathcal{S}_h^o \mid S \subset \partial T\}$. We define the oscillation by

$$\mathsf{osc}_h^2(T) := h_T^2 \left\|\mathcal{R}_T(u_h) - \overline{\mathcal{R}}_T\right\|_{L^2(T)}^2 + h_T \sum_{S \in \mathcal{S}_h^o(T)} \left\|\mathcal{J}_S(u_h) - \overline{\mathcal{J}}_S\right\|_{L^2(S)}^2,$$

where $\overline{\mathcal{R}}_T$ and $\overline{\mathcal{J}}_S$ are L^2-projections of $\mathcal{R}_T(u_h)$ and $\mathcal{J}_S(u_h)$ onto $\mathbb{P}_m(T)$ and $\mathbb{P}_m(S)$, respectively, $m \geq 0$ is a fixed integer; $\mathbb{P}_m(T)$ and $\mathbb{P}_m(S)$ denote spaces of polynomial functions of degree $\leq m$ on T and S, respectively. For $\omega_h(T) \subset \Gamma_h$ we define $\mathsf{osc}_h^2(\omega_h(T)) := \sum_{T' \subset \omega_h(T)} \mathsf{osc}_h^2(T')$, and denote $\mathsf{osc}_h := \mathsf{osc}_h(\Gamma_h)$; the same notation also applies to $\zeta_h^2(\omega_h(T))$.

Remark 2.3.2. If we take $m = n - 1$ as in Lemma 2.4.4 stated in the next section, where n is the degree of $\mathbb{V}_h$, then by (2.3.2) and (2.3.3), $\mathcal{J}_S(u_h) \in \mathbb{P}_{n-1}(S)$, and $(\Delta_{\Gamma_h} u_h)|_T \in \mathbb{P}_{n-2}(T)$ imply that

$$\mathsf{osc}_h^2(T) = h_T^2 \left\| F_h - \overline{F}_h \right\|_{L^2(T)}^2, \tag{2.3.12}$$

where $\overline{F}_h$ is L^2-projection of F_h onto $\mathbb{P}_{n-1}(T)$.

According to the above two estimates (2.3.10) and (2.3.11), our adaptive algorithm will rely on four indicators $\eta_h(T), \zeta_h(T), \lambda_h(T)$ and $\mathsf{osc}_h(T)$. These indicators are important for designing a converging AFEM; see [7, 13, 15, 16]. We compute these values for all $T \in \mathcal{T}_h$ according to the definitions, and we call this procedure ESTIMATE, namely

$$\boxed{\{\eta_h(T), \zeta_h(T), \lambda_h(T), \mathsf{osc}_h(T)\}_{T \in \mathcal{T}_h} := \mathsf{ESTIMATE}(\Gamma, \Gamma_h, \mathcal{T}_h, F_h, u_h).}$$

2.4 AFEM

As outlined before in section 2.1.3, AFEM consists of loops of procedures SOLVE, ESTIMATE, MARK, and REFINE, consecutively. The procedure ESTIMATE has just been introduced in section 2.3. We now describe the other three procedures in detail.

2.4.1 Procedure SOLVE

In this procedure we solve the SPD linear system obtained from (2.1.8). Here we employ any standard linear solver, such as conjugate gradient CG with diagonal, hierarchical basis, or BPX preconditioning. In other words, given a pair of approximating surface-mesh $(\Gamma_k, \mathcal{T}_k)$, a forcing function F_k, and an initial guess for the solution u_{k-1}, SOLVE computes the discrete solution

$$u_k := \mathsf{SOLVE}(\Gamma_k, \mathcal{T}_k, F_k, u_{k-1}).$$

2.4.2 Procedure MARK

Given a pair of approximating surface-mesh $(\Gamma_k, \mathcal{T}_k)$, ideally this procedure will find a subset $\widehat{\mathcal{T}_k} \subset \mathcal{T}_k$ of marked elements according to the largest indicators of procedure ESTIMATE. Therefore, when we refine all elements in $\widehat{\mathcal{T}_k}$, we will get reductions for the errors and oscillations that will lead to convergence. The notion of energy error reduction was introduced by Dörfler [7], and further improved by Morin et al [15, 16] via the notion of data oscillation and its reduction. Here we introduce a similar concept to reduce the geometric error. The following marking strategy is just a combination of these ideas.

Marking Strategy: Given parameters $0 < \theta_e, \theta_g, \theta_o < 1$, construct a subset $\widehat{\mathcal{T}}_k$ of $\mathcal{T}_k$ such that the following inequalities hold:

$$(\text{M1}): \qquad \sum_{T \in \widehat{\mathcal{T}}_k} \eta_k^2(T) \geq \theta_e^2 \eta_k^2, \qquad (2.4.1)$$

$$(\text{M2}): \qquad \sum_{T \in \widehat{\mathcal{T}}_k} \zeta_k^2(T) \geq \theta_g^2 \zeta_k^2, \qquad (2.4.2)$$

$$(\text{M3}): \qquad \sum_{T \in \widehat{\mathcal{T}}_k} \mathsf{osc}_k^2(T) \geq \theta_o^2 \mathsf{osc}_k^2. \qquad (2.4.3)$$

The strategy (M1) is for the energy error reduction, (M2) is for geometric error reduction, and (M3) is for oscillation reduction. We refer to this procedure as

$$\widehat{\mathcal{T}}_k := \mathsf{MARK}(\{\eta_k(T), \zeta_k(T), \mathsf{osc}_k(T)\}_{T \in \mathcal{T}_k}).$$

2.4.3 Procedure REFINE

This procedure refines all elements in the marked set $\widehat{\mathcal{T}}_k$ of $\mathcal{T}_k$ to obtain a new (finer) pair of approximating surface-mesh $(\Gamma_{k+1}, \mathcal{T}_{k+1})$. The refinement step is performed according to two criteria. The first one was introduced by Morin et al [15, 16] to guaranteed energy error reduction:

Interior Node Property: Refine each marked element $T \in \widehat{\mathcal{T}}_k$ to obtain a new mesh $\mathcal{T}_{k+1}$ compatible with $\mathcal{T}_k$ such that

T and the adjacent elements $T' \in \mathcal{T}_k$ of T, as well as their common sides, contain a node of the finer mesh $\mathcal{T}_{k+1}$ in their interior.

The second criterium is new and deals with the geometric oscillation:

Geometric Oscillation Property: Given a reduction factor $\theta_\lambda < 1$, refine all $T \in \widehat{\mathcal{T}_k}$ such that for all $T' \in \mathcal{T}_{k+1}(T)$ we have

$$\lambda_{k+1}(T') \le \theta_\lambda \lambda_k(T),$$

where $\mathcal{T}_{k+1}(T) := \{T' \in \mathcal{T}_{k+1} \mid T' \text{ is obtained by refining } T\}$.

The procedure REFINE may also require additional steps to control the oscillations.

We describe the Refining Strategy in several steps as follows:

Refining Strategy: Given a sequence $\{a_k\} \searrow 0$, a marked set $\widehat{\mathcal{T}_k}$, geometric oscillations $\{\lambda_k(T)\}_{T \in \mathcal{T}_k}$, and a fixed reduction rate of element size $0 < \gamma_r < 1$;

1. Refine all $T \in \widehat{\mathcal{T}_k}$ according to Interior Node Property;

2. Refine more if needed for Geometric Oscillation Property;

3. Refine more if needed so that for any $T \in \mathcal{T}_k$

$$\lambda_{k+1}(T') \le \min\{a_k, \lambda_k(T)\} \qquad \forall\, T' \in \mathcal{T}_{k+1}(T);$$

4. Refine more if needed so that for any $T' \in \mathcal{T}_{k+1}(T)$, $T \in \mathcal{T}_k$,

$$\frac{|T_k'|}{|T'|} \le \gamma_T \left(\frac{|T|}{|T'|} \right)^{\frac{2}{d-1}} \qquad \text{where} \qquad \gamma_T := \begin{cases} \gamma_r & \text{if } T \in \widehat{\mathcal{T}_k} \\ 1 & \text{if } T \notin \widehat{\mathcal{T}_k} \end{cases}, \qquad (2.4.4)$$

and $T_k' := \{(\mathbf{x}, z_k(\mathbf{x})) \in \Gamma_k \mid (\mathbf{x}, z(\mathbf{x})) \in T'\} \subset T$, a lift of T' back to Γ_k.

We refine an element on a polyhedral surface Γ_k via a projection (or lift) from Γ_k to Γ along the (vertical) x_d-axis. If $(\mathbf{x}, z_k(\mathbf{x})) \in \Gamma_k$ is a new node obtained by refining $T \in \mathcal{T}_k$, then it is lifted to $(\mathbf{x}, z(\mathbf{x})) \in \Gamma$ to become a new node of Γ_{k+1}; see Figures 2.4.1 and 2.4.2. The new 'polyhedral' approximating surface is formed by
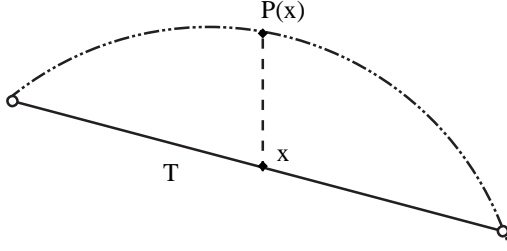
Figure 2.4.1: The element $T \in \mathcal{T}_k$ is bisected thereby giving rise to the new node x. This node is lifted (projected) to $P(x) \in \Gamma$ along the vertical axis.
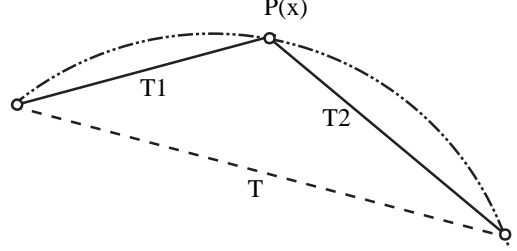
Figure 2.4.2: Two new elements $T1$ and $T2$ in $\mathcal{T}_{k+1}$ are formed joining the new node $P(x) \in \Gamma$ with the old nodes in Γ_k.

interpolating new nodes and old nodes via $z_{k+1} = \mathcal{I}_{k+1} z \in \mathbb{V}_{k+1}$. We refer to this procedure as

$$(\mathcal{T}_{k+1}, \Gamma_{k+1}) := \mathsf{REFINE}(\widehat{\mathcal{T}}_k, a_k, \gamma_r, \{\lambda_k(T)\}_{T \in \mathcal{T}_k}).$$

Note that, asymptotically, the new surface Γ_{k+1} is a better piecewise polynomial approximation of Γ than Γ_k in the sense that $\lambda_{k+1}(T') \leq \lambda_k(T)$ for all $T' \in \mathcal{T}_{k+1}(T)$. However, in the pre-asymptotic regime it can happen that this inequality is reversed.

Remark 2.4.1. Since for $T \in \mathcal{T}_k$, the corresponding $\tilde{T} \subset \Gamma$ is a smooth C^1 surface, hence steps 2 and 3 of `Refining Strategy` can be achieved by finite number of times. If Γ is C^2, then $\lambda_k(T)$ reduces proportionally to h_T, the diameter of T.

Remark 2.4.2. In step 3 of `Refining Strategy`, the sequence $a_k \searrow 0$ is needed to guarantee that $\lambda_k \searrow 0$, i.e., Γ_k gets closer and closer to Γ. However, in our results below, Lemma 2.4.3 and Theorem 2.1, we require only that λ_k decreases monotonically and is smaller than an unknown positive threshold. The condition $a_k \searrow 0$ might be stronger than needed. In fact, in numerical experiments, if Γ is C^2, then λ_k reduces monotonically without invoking step 3.

67

Remark 2.4.3. Step 4 of `Refining Strategy` is needed in order to have a reduction of oscillation, see Lemma 2.4.6, especially when we deal with general dimension $d \neq 3$. For $d = 3$, this step is trivial since $T'_k \subset T$, and if $T \in \widehat{\mathcal{T}}_k$ then $|T'_k| \leq \gamma_T |T|$ where $\gamma_T < 1$ depending only on the refinement method, and we can choose $\gamma_r := \max \{\gamma_T\} < 1$.

Remark 2.4.4. Step 4 of `Refining Strategy` can be achieved for $d \neq 3$ upon refining $T \in \mathcal{T}_k$ a finite (and fixed) number times. This is the case because $\frac{|T'_k|}{|T'|}$ is bounded by a constant depending only on $\frac{Q_k}{Q}$, whereas $\frac{|T|}{|T'|}$ increases by refinement.

2.4.4   Lemmas

The procedures MARK and REFINE lead to the following crucial results for proving the convergence of AFEM. For convenience we use the following notation. For any $\omega \subset \Gamma$,

$$e_k(\omega) := \|\nabla_\Gamma (u - u_k)\|_{L^2(\omega)}, \qquad \varepsilon_{k+1}(\omega) := \|\nabla_\Gamma (u_{k+1} - u_k)\|_{L^2(\omega)},$$

and use e_k, respectively ε_{k+1}, when $\omega = \Gamma$. We introduce also the bilinear forms

$$\mathcal{B}(u, v) := \int_\Gamma \nabla_\Gamma u \cdot \nabla_\Gamma v \quad \text{and} \quad \mathcal{B}_h(u, v) := \int_{\Gamma_h} \nabla_{\Gamma_h} u \cdot \nabla_{\Gamma_h} v. \tag{2.4.5}$$

Geometric Error Reduction

A trivial consequence Step 3 of `Refining Strategy` is the following result.

Lemma 2.4.1 (Geometric oscillation reduction). *For any sequence $\{a_k\}$ converging monotonically to 0 as $k \to \infty$ we have*

$$\lambda_k \to 0 \ \text{as} \ k \to \infty \ \text{monotonically.}$$

According to the definition (2.1.12), we have a local relation between geometric errors ζ_{k+1}, ζ_k, and ε_{k+1} as follows. For any $\delta > 0$,

$$\zeta_{k+1}^2(T') \leq \lambda_{k+1}^2(T') \left((1+\delta) \|\nabla_\Gamma u_k\|_{L^2(\tilde{T}')}^2 + (1+\delta^{-1})\varepsilon_{k+1}^2(\tilde{T}') \right), \qquad (2.4.6)$$

where $T' \in \mathcal{T}_{k+1}$ and $\tilde{T}' \subset \Gamma$ is its corresponding curved element. Employing Marking Strategy (M2), Geometric Oscillation Property, and Lemma 2.4.1, we obtain the reduction of geometric error. We state the result now but postpone its proof until §2.4.6.

Lemma 2.4.2 (Geometric error reduction). *There exist constants $0 < \rho_1 < 1$ and $\rho_2 > 0$ such that for any $k \geq 0$*

$$\zeta_{k+1}^2 \leq \rho_1 \zeta_k^2 + \rho_2 \lambda_k^2 \varepsilon_{k+1}^2. \qquad (2.4.7)$$

Quasi-Orthogonality

Since finite element space-mesh $(\mathbb{V}_k(\Gamma_k), \mathcal{T}_k(\Gamma_k))$'s are no longer nested, the usual orthogonality property fails. It is replaced by a quasi-orthogonality property. As expected, the geometric error ζ_k also plays a role in this result. We state here a lemma but postpone its proof until §2.4.6.

Lemma 2.4.3 (Quasi-orthogonality). *There exist constants $C_6, C_7 > 0$ and a number $k_* \geq 0$ such that $\Lambda_0 := (\frac{1}{2} - \rho_2 C_6 \lambda_{k_*}^2) \in [\frac{1}{4}, \frac{1}{2})$, and for any $k \geq k_*$*

$$e_{k+1}^2 \leq e_k^2 - \Lambda_0 \varepsilon_{k+1}^2 + C_7 \zeta_k^2. \qquad (2.4.8)$$

Remark 2.4.5 *(Threshold for λ_k).* For quasi-orthogonality we need that $\lambda_k \leq \lambda_*$ be sufficiently small (k is greater than some k_*) or, equivalently, that Γ_k be sufficiently

close to Γ; see the proof in §2.4.6. This is a natural a priori condition [9]. Since we do not have a procedure to quantify a posteriori when such a condition is achieved, we let sequence $\{a_k\}$ take care of this matter: it guarantees the eventual validity of $\lambda_k \leq \lambda_*$ regardless of the resolution of the initial mesh-surface approximation.

Energy Error Reduction

It is well documented that the reduction of energy error hinges on four concepts: the upper bound, a modified local lower bound, `Marking Strategy (M1)`, and `Interior Node Property`; see [13, 15, 16]. We discuss here the modified local lower bound which relies on a modified error equation, obtained from the error representation form (2.3.1) upon replacing Γ by Γ_{k+1}, u by u_{k+1}, φ by $\varphi_{k+1} \in \mathring{\mathbb{V}}_{k+1}$, and setting $\varphi_k = 0$, namely

$$\sum_{T \in \mathcal{T}_k} \int_T \mathcal{R}_T(u_k)\varphi_{k+1} - \sum_{S \in \mathcal{S}_k^o} \int_S \mathcal{J}_S(u_k)\varphi_{k+1} = \mathcal{B}_{k+1}(u_{k+1}, \varphi_{k+1}) - \mathcal{B}_k(u_k, \varphi_{k+1}), \quad (2.4.9)$$

where the bilinear form $\mathcal{B}_k$ is defined via (2.4.5).

To obtain the estimate, we follow the standard arguments used on flat domains [1, 23] with the help of piecewise linear bubble functions; see [7, 13, 15, 16]. Note that for graphs, the lift (2.1.2) of a C^0 piecewise linear bubble function on Ω is still a C^0 piecewise linear bubble function on Γ_k; hence, the standard arguments are still valid on surfaces Γ_k. However, due to discrepancy between surfaces Γ_k and Γ_{k+1}, the geometric error ζ_k also appears in this estimate. To see this let $\varphi_{k+1} := \psi_T \overline{\mathcal{R}}_T$, where $\overline{\mathcal{R}}_T$ is a L^2-projection of $\mathcal{R}_T(u_k)$ onto $\mathbb{P}_{n-1}(T)$ and ψ_T is a C^0 piecewise linear bubble function on T, namely $\mathsf{supp}\ \varphi_{k+1} \subseteq T$. Adding $\pm \int_\Gamma \nabla_\Gamma(u_{k+1} - u_k) \cdot \nabla_\Gamma \varphi_{k+1}$,

(2.4.9) becomes

$$\int_T \mathcal{R}_T(u_k)\varphi_{k+1} = \int_\Gamma \nabla_\Gamma(u_{k+1} - u_k) \cdot \nabla_\Gamma \varphi_{k+1}$$

$$+ \int_\Gamma \nabla_\Gamma u_{k+1}\mathcal{A}_{k+1} \cdot \nabla_\Gamma \varphi_{k+1} + \int_\Gamma \nabla_\Gamma u_k \mathcal{A}_k \cdot \nabla_\Gamma \varphi_{k+1},$$

which later gives an estimate involving the local geometric error terms ζ_k and ζ_{k+1}.

Moreover, we can estimate locally ζ_{k+1} in terms of ζ_k and ε_{k+1} according to (2.4.6), namely

$$\sum_{T' \in \mathcal{T}_{k+1}(T)} \zeta_{k+1}^2(T') \lesssim \zeta_k^2(T) + \varepsilon_{k+1}^2(\tilde{T}).$$

Following the usual arguments, we arrive at the estimate for the interior residual

$$h_T^2 \left\|\mathcal{R}_T(u_k)\right\|_{L^2(T)}^2 \lesssim \varepsilon_{k+1}^2(\tilde{T}) + \zeta_k^2(T) + h_T^2 \left\|\mathcal{R}_T(u_k) - \overline{\mathcal{R}}_T\right\|_{L^2(T)}^2.$$

The estimate for the jump residual is similarly obtained by following the standard arguments. Combining these two estimates, we thus obtain the lemma.

Lemma 2.4.4 (Modified local lower bound). *For any $T \in \widehat{\mathcal{T}}_k$, we have*

$$\eta_k^2(T) \le C_3 \sum_{\substack{T' \in \mathcal{T}_k \\ T' \subset \omega_k(T)}} \varepsilon_{k+1}^2(\tilde{T}') + C_4 \zeta_k^2(\omega_k(T)) + C_5 \mathsf{osc}_k^2(\omega_k(T)). \tag{2.4.10}$$

Applying the upper bound (2.3.10) and `Marking Strategy (M1)`, we have

$$e_k^2 \le C_1 \eta_k^2 + C_2 \zeta_k^2 \le \frac{C_1}{\theta_e^2} \sum_{T \in \widehat{\mathcal{T}}_k} \eta_k^2(T) + C_2 \zeta_k^2.$$

As a consequence of Lemma 2.4.4, using (2.4.10) to replace $\eta_k^2(T)$, we have the following corollary.

Corollary 2.4.5. *There exist constants $\Lambda_1, \Lambda_2, \Lambda_3 > 0$ depending only on θ_e, C_1, C_2, C_3, C_4 and C_5, such that*

$$e_k^2 \le \Lambda_1 \varepsilon_{k+1}^2 + \Lambda_2 \zeta_k^2 + \Lambda_3 \mathsf{osc}_k^2. \tag{2.4.11}$$

Oscillation Reduction

According to Remark 2.3.2 and Lemma 2.4.4 above, the element oscillation has the form

$$\mathsf{osc}_k^2(T) = h_T^2 \left\| F_k - \overline{F}_k \right\|_{L^2(T)}^2 .$$

Since it is convenient to work with area (measure) of the element T when surfaces are different, we re-define the oscillation to be

$$\mathsf{osc}_k^2(T) = |T|^{\frac{2}{d-1}} \left\| F_k - \overline{F}_k \right\|_{L^2(T)}^2 ,$$

since $h_T^2 \sim |T|^{\frac{2}{d-1}}$, where $d \geq 2$ denotes the dimension. The following lemma is a result of **Marking Strategy (M3)** and step 4 of **Refining Strategy**; the proof is given in §2.4.6.

Lemma 2.4.6 (Oscillation reduction). *There exists a constant $0 < \hat{\alpha} < 1$ depending on the surface Γ and a parameter θ_o from* **Marking Strategy (M3)** *such that*

$$\mathsf{osc}_{k+1}^2 \leq \hat{\alpha}\mathsf{osc}_k^2. \tag{2.4.12}$$

2.4.5 Algorithm and Convergence

Given parameters $\theta_e, \theta_g, \theta_o, \theta_\lambda, \gamma_r$, and the sequence $\{a_k\}$, the adaptive algorithm consists of consecutive loops of procedures SOLVE, ESTIMATE, MARK, and REFINE as follows.

Theorem 2.1 (Convergence of AFEM). *Let $(\Gamma_0, \mathcal{T}_0)$ be an arbitrary initial approximating surface-triangulation pair of Γ. Then there exist a number $k_0 \geq 0$, and positive constants γ_g, γ_o, and $\xi < 1$, such that for any $k \geq k_0$, AFEM satisfies*

$$\mathcal{E}_{k+1} \leq \xi \, \mathcal{E}_k, \tag{2.4.13}$$

where $\mathcal{E}_k^2 := e_k^2 + \gamma_g \zeta_k^2 + \gamma_o \mathsf{osc}_k^2$.

Proof: According to Lemma 2.4.3, there is k_* such that (2.4.8) holds, namely

$$e_{k+1}^2 \leq e_k^2 - \Lambda_0 \varepsilon_{k+1}^2 + C_7 \zeta_k^2 \qquad \forall k \geq k_*, \tag{2.4.14}$$

where $\frac{1}{4} \leq \Lambda_0 < \frac{1}{2}$. Since ε_{k+1} and ζ_k are coupled according to Lemma 2.4.2 and (2.4.11), we split the term $\Lambda_0 \varepsilon_{k+1}^2$ into two parts

$$\Lambda_0 \varepsilon_{k+1}^2 = \beta \Lambda_0 \varepsilon_{k+1}^2 + (1 - \beta) \Lambda_0 \varepsilon_{k+1}^2,$$

where the constant $\beta \in (0, 1)$ will be chosen later.

Step 1. Using (2.4.11), we can eliminate $\beta \Lambda_0 \varepsilon_{k+1}^2$ by the estimate

$$\frac{\beta \Lambda_0}{\Lambda_1} e_k^2 \leq \beta \Lambda_0 \varepsilon_{k+1}^2 + \frac{\Lambda_0 \Lambda_2}{\Lambda_1} \beta \zeta_k^2 + \frac{\Lambda_0 \Lambda_3}{\Lambda_1} \beta \mathsf{osc}_k^2,$$

and (2.4.14) becomes

$$e_{k+1}^2 \leq \alpha e_k^2 - (1-\beta)\Lambda_0 \varepsilon_{k+1}^2 + (C_7 + \Lambda_4 \beta)\zeta_k^2 + \Lambda_5 \beta \mathsf{osc}_k^2, \tag{2.4.15}$$

where $\alpha := 1 - \frac{\beta \Lambda_0}{\Lambda_1} < 1$, $\Lambda_4 := \frac{\Lambda_0 \Lambda_2}{\Lambda_1} > 0$, and $\Lambda_5 := \frac{\Lambda_0 \Lambda_3}{\Lambda_1} > 0$.

Step 2. To get rid of $(1-\beta)\Lambda_0 \varepsilon_{k+1}^2$, we use Lemma 2.4.2 inequality (2.4.7), namely

$$\frac{(1-\beta)\Lambda_0}{\rho_2 \lambda_{k_0}^2} \zeta_{k+1}^2 \leq \frac{\rho_1 (1-\beta)\Lambda_0}{\rho_2 \lambda_{k_0}^2} \zeta_k^2 + (1-\beta)\Lambda_0 \varepsilon_{k+1}^2 \qquad \forall k \geq k_0,$$

where $k_0 \geq k_*$ will be chosen later. Therefore, (2.4.15) becomes

$$e_{k+1}^2 + \gamma_g \zeta_{k+1}^2 \leq \alpha e_k^2 + \mu_0 \gamma_g \zeta_k^2 + \Lambda_5 \beta \mathsf{osc}_k^2, \tag{2.4.16}$$

where $\gamma_g := \frac{(1-\beta)\Lambda_0}{\rho_2 \lambda_{k_0}^2}$ and μ_0 satisfies

$$\mu_0 \gamma_g = C_7 + \Lambda_4 \beta + \rho_1 \gamma_g. \tag{2.4.17}$$

Step 3. From (2.4.17), writing γ_g in terms of β and solving for β, we have

$$\beta = \frac{\beta_0 - C_7}{\beta_0 + \Lambda_4} \qquad \text{where} \qquad \beta_0 := \frac{\Lambda_0 (\mu_0 - \rho_1)}{\rho_2 \lambda_{k_0}^2}.$$

Since $\rho_1 < 1$, we first choose $\rho_1 < \mu_0 < 1$ which gives $\beta_0 > 0$. Since $\lambda_k \searrow 0$, we can then choose $k_0 \geq k_*$ so that $\beta_0 > C_7$, which implies that $0 < \beta < 1$. Therefore, γ_g defined in (2.4.16) is a positive constant.

Step 4. Using (2.4.12) of Lemma 2.4.6, we can write (2.4.16) as

$$e_{k+1}^2 + \gamma_g \zeta_{k+1}^2 + \gamma_o \mathsf{osc}_{k+1}^2 \leq \alpha e_k^2 + \mu_0 \gamma_g \zeta_k^2 + \mu_1 \gamma_o \mathsf{osc}_k^2,$$

where γ_o is a constant to be determined and μ_1 satisfies

$$\mu_1\gamma_o = \gamma_o\hat{\alpha} + \Lambda_5\beta.$$

Since $\hat{\alpha} < 1$, we can choose $\hat{\alpha} < \mu_1 < 1$, which implies that $\gamma_o = \frac{\Lambda_5\beta}{\mu_1-\hat{\alpha}} > 0$. The assertion follows by setting $\xi = \sqrt{\max\{\alpha, \mu_0, \mu_1\}} < 1$. $\qquad\square$

2.4.6 Proofs of Lemmas

Proof of Lemma 2.4.2: Geometric error reduction

Proof: If $T' \in \mathcal{T}_{k+1}$, then by definition of $\zeta_{k+1}(T')$ we have for $\delta > 0$,

$$\zeta_{k+1}^2(T') := \lambda_{k+1}^2(T') \|\nabla_\Gamma u_{k+1}\|_{L^2(\tilde{T}')}^2 \tag{2.4.18}$$

$$\leq \lambda_{k+1}^2(T')\left((1+\delta)\|\nabla_\Gamma u_k\|_{L^2(\tilde{T}')}^2 + (1+\delta^{-1})\varepsilon_{k+1}^2(\tilde{T}')\right).$$

`Case 1.` If $T' \in \mathcal{T}_{k+1}(T)$ for some $T \in \widehat{\mathcal{T}}_k$, then $\lambda_{k+1}(T') \leq \theta_\lambda \lambda_k(T)$. Summing over all $T' \in \mathcal{T}_{k+1}(T)$ and using $\lambda_k(T) \leq \lambda_k$, we have

$$\sum_{T'\in\mathcal{T}_{k+1}(T)} \zeta_{k+1}^2(T') \leq (1+\delta)\theta_\lambda^2\zeta_k^2(T) + (1+\delta^{-1})\lambda_k^2\varepsilon_{k+1}^2(\tilde{T}).$$

`Case 2.` If $T' \in \mathcal{T}_{k+1}(T)$ for $T \notin \widehat{\mathcal{T}}_k$, then by using $\lambda_{k+1}(T') \leq \lambda_k(T)$ we have

$$\zeta_{k+1}^2(T') \leq \lambda_k^2(T)\left((1+\delta)\|\nabla_\Gamma u_k\|_{L^2(\tilde{T}')}^2 + (1+\delta^{-1})\varepsilon_{k+1}^2(\tilde{T}')\right),$$

and after summing over $T' \in \mathcal{T}_{k+1}(T)$

$$\sum_{T'\in\mathcal{T}_{k+1}(T)} \zeta_{k+1}^2(T') \leq (1+\delta)\zeta_k^2(T) + (1+\delta^{-1})\lambda_k^2\varepsilon_{k+1}^2(\tilde{T}).$$

Combining these two cases, we can write

$$\zeta_{k+1}^2 = \sum_{T \in \widehat{\mathcal{T}}_k} \left(\sum_{T' \in \mathcal{T}_{k+1}(T)} \zeta_{k+1}^2(T') \right) + \sum_{T \in \mathcal{T}_k \setminus \widehat{\mathcal{T}}_k} \left(\sum_{T' \in \mathcal{T}_{k+1}(T)} \zeta_{k+1}^2(T') \right)$$

$$\leq (1+\delta) \left(\zeta_k^2 - (1-\theta_\lambda^2) \sum_{T \in \widehat{\mathcal{T}}_k} \zeta_k^2(T) \right) + (1+\delta^{-1})\lambda_k^2 \varepsilon_{k+1}^2,$$

and by `Marking Strategy (M2)`

$$\zeta_{k+1}^2 \leq (1+\delta) \left(1 - (1-\theta_\lambda^2)\theta_g^2 \right) \zeta_k^2 + (1+\delta^{-1})\lambda_k^2 \varepsilon_{k+1}^2.$$

The assertion follows by choosing δ such that $\rho_1 := (1+\delta) \left(1 - (1-\theta_\lambda^2)\theta_g^2 \right) < 1$,

and taking $\rho_2 := (1+\delta^{-1}) > 0$. $\qquad\square$

Proof of Lemma 2.4.3: Quasi-orthogonality

Proof: By symmetry of the bilinear form $\mathcal{B}$ defined in (2.4.5), we have

$$e_{k+1}^2 = e_k^2 - \varepsilon_{k+1}^2 - 2\mathcal{B}(u - u_{k+1}, u_{k+1} - u_k).$$

Since for graphs $\varphi_{k+1} := u_{k+1} - u_k \in \mathring{\mathbb{V}}_{k+1}$, we thus have

$$\mathcal{B}(u - u_{k+1}, u_{k+1} - u_k) = \mathcal{B}(u, \varphi_{k+1}) - \mathcal{B}(u_{k+1}, \varphi_{k+1}) = \int_\Gamma f\varphi_{k+1} - \mathcal{B}(u_{k+1}, \varphi_{k+1}).$$

By definition of F_{k+1} in (2.3.4) and the weak form (2.1.8),

$$\int_\Gamma f\varphi_{k+1} = \int_{\Gamma_{k+1}} F_{k+1}\varphi_{k+1} = \mathcal{B}_{k+1}(u_{k+1}, \varphi_{k+1}).$$

Therefore, by (2.2.9)

$$\mathcal{B}(u - u_{k+1}, u_{k+1} - u_k) = \mathcal{B}_{k+1}(u_{k+1}, \varphi_{k+1}) - \mathcal{B}(u_{k+1}, \varphi_{k+1}) = \int_\Gamma \nabla_\Gamma u_{k+1} \mathcal{A}_{k+1} \cdot \nabla_\Gamma \varphi_{k+1}.$$

By Schwarz's inequality and the estimate $\|\nabla_\Gamma u_{k+1} \mathcal{A}_{k+1}\|_{L^2(\Gamma)} \lesssim \zeta_{k+1}$, we can bound

$$-2\mathcal{B}(u - u_{k+1}, \varphi_{k+1}) \leq C_6 \zeta_{k+1}^2 + \frac{1}{2}\varepsilon_{k+1}^2,$$

where $C_6 > 0$ depends only on Γ. Hence, by Lemma 2.4.2, we obtain

$$e_{k+1}^2 \leq e_k^2 - \left(\frac{1}{2} - C_6 \rho_2 \lambda_k^2\right)\varepsilon_{k+1}^2 + C_7 \zeta_k^2,$$

where $C_7 := C_6 \rho_1$. Since $\lambda_k \to 0$ as $k \to \infty$ by Lemma 2.4.1, there exists a number $k_* \geq 0$ such that $\Lambda_0 := \frac{1}{2} - C_6 \rho_2 \lambda_{k_*}^2 \in [\frac{1}{4}, \frac{1}{2})$. The assertion thus follows for $k \geq k_*$ by monotonicity of $\{\lambda_k\}$. $\qquad \square$

Proof of Lemma 2.4.6: Oscillation reduction

Proof: Let $T' \in \mathcal{T}_{k+1}(T)$ for some $T \in \mathcal{T}_k$, we have

$$\mathsf{osc}_{k+1}^2(T') = |T'|^{\frac{2}{d-1}} \left\|F_{k+1} - \overline{F}_{k+1}^{T'}\right\|_{L^2(T')}^2,$$

where $\overline{F}_{k+1}^{T'}$ is the L^2-projection of F_{k+1} onto $\mathbb{P}_{n-1}(T')$. Recall that

$$T'_k := \{(\mathbf{x}, z_k(\mathbf{x})) \in \Gamma_k \mid (\mathbf{x}, z(\mathbf{x})) \in T'\} \subset T,$$

a lift of T' back to Γ_k. By changing the surface of integration

$$\int_{T'} v = \int_{T'_k} v \frac{Q_{k+1}}{Q_k} = \frac{|T'|}{|T'_k|} \int_{T'_k} v.$$

Since on T', $F_{k+1} = F_k \frac{Q_k}{Q_{k+1}} = \frac{|T'_k|}{|T'|} F_k$, replacing $\overline{F}_{k+1}^{T'}$ by $\frac{|T'_k|}{|T'|}\overline{F}_k^T$, where $\overline{F}_k^T$ is the L^2-projection of F_k onto $\mathbb{P}_{n-1}(T)$, we have

$$\mathsf{osc}_{k+1}^2(T') \leq |T'|^{\frac{2}{d-1}} \frac{|T'_k|^2}{|T'|^2} \left\|F_k - \overline{F}_k^T\right\|_{L^2(T')}^2 = |T'|^{\frac{2}{d-1}} \frac{|T'_k|}{|T'|} \left\|F_k - \overline{F}_k^T\right\|_{L^2(T'_k)}^2.$$

By Step 4 of `Refining Strategy`, we thus have

$$|T'|^{\frac{2}{d-1}} \frac{|T'_k|}{|T'|} \leq \gamma_T |T|^{\frac{2}{d-1}},$$

where γ_T is defined in (2.4.4). By summing over all $T' \in \mathcal{T}_{k+1}(T)$, we arrive at

$$\sum_{T' \in \mathcal{T}_{k+1}(T)} \mathsf{osc}^2_{k+1}(T') \leq \gamma_T \, \mathsf{osc}^2_k(T).$$

Proceeding as in Lemma 2.4.2 and using `Marking Strategy (M3)`, we end up with

$$\mathsf{osc}^2_{k+1} \leq \left(1 - (1 - \gamma_r)\theta_o^2\right)\mathsf{osc}^2_k =: \hat{\alpha} \, \mathsf{osc}^2_k.$$

$\square$

2.5   Numerical Experiments

To illustrate our main result, we present some numerical experiments based on the AFEM described above. They are implemented within the FEM toolbox ALBERT developed by Schmidt and Siebert [20, 21].

For convenience of presentation, we use the following notation:

- e_k and ζ_k denote the energy and geometric errors, respectively, after k iterations.

- $|\mathcal{T}_k|$ denotes the number of elements in triangulation $\mathcal{T}_k$.

- $\mathsf{EOC}_e(k)$ and $\mathsf{EOC}_g(k)$ denote the experimental orders of convergence after k iterations, namely

$$\mathsf{EOC}_e(k) := \frac{\log(e_{k-1}/e_k)}{\log(|\mathcal{T}_k| / |\mathcal{T}_{k-1}|)} \quad \text{and} \quad \mathsf{EOC}_g(k) := \frac{\log(\zeta_{k-1}/\zeta_k)}{\log(|\mathcal{T}_k| / |\mathcal{T}_{k-1}|)}.$$

2.5.1   Experiment 1: Corner Singularity

In this experiment we consider a surface $\Gamma \subset \mathbb{R}^3$ as a graph of the function $z(x,y) = x^2 + y^2$ defined on the L-shape region $\Omega := [-1,1]^2 \setminus (0,1) \times (-1,1)$. To

78

test our algorithm, we assume that the exact solution is known and defined by

$$u(x, y, z) = u(r, \theta) = r^{2/3} \sin(\frac{2}{3}\theta),$$

where $r := \sqrt{x^2 + y^2}, \theta := \tan^{-1}(y/x)$. The forcing term $f = -\Delta_\Gamma u$ is given by (2.1.6).

We solve the Laplace-Beltrami operator on Γ together with Dirichlet boundary condition that is compatible with the solution. We implemented AFEM with parameters $\theta_e = \theta_g = 0.6$, $\theta_o = 0.5$, and $\theta_\lambda = 0.8$, and with $\{a_k\} = \{1/k\}$. Our results and comments are as follows.

k	$|\mathcal{T}_k|$	e_k	$\mathsf{EOC}_e(k)$	ζ_k	$\mathsf{EOC}_g(k)$
0	96	1.85e-01	–	2.01e-01	–
1	244	1.10e-01	0.558	1.29e-01	0.477
2	846	6.33e-02	0.443	7.17e-02	0.470
3	2288	3.82e-02	0.508	4.47e-02	0.476
4	6034	2.40e-02	0.480	2.85e-02	0.463
5	11982	1.61e-02	0.580	2.00e-02	0.514
6	32952	9.57e-03	0.515	1.44e-02	0.328
7	57416	7.00e-03	0.563	1.00e-02	0.653

Table 2.5.1: AFEM with parameters $\theta_e = \theta_g = 0.6$, $\theta_o = 0.5$, and $\theta_\lambda = 0.8$. Both the energy and geometric errors decay at the optimal rate at 0.5 despite the corner singularity; compare with FEM in Table 2.5.2 below.

$|\mathcal{T}_k|$	e_k	$\mathsf{EOC}_e(k)$	ζ_k	$\mathsf{EOC}_g(k)$
96	1.85e-01	–	2.01e-01	–
384	1.17e-01	0.329	1.01e-01	0.497
1536	7.42e-02	0.329	5.04e-02	0.499
6144	4.69e-02	0.331	2.52e-02	0.500
24576	2.96e-02	0.332	1.26e-02	0.500
98304	1.87e-02	0.332	6.30e-03	0.500

Table 2.5.2: FEM: The energy error decays slower than AFEM at the expected rate 0.33 due to corner singularity. The geometric error still decays at the optimal rate 0.5 due to the smoothness of the surface.
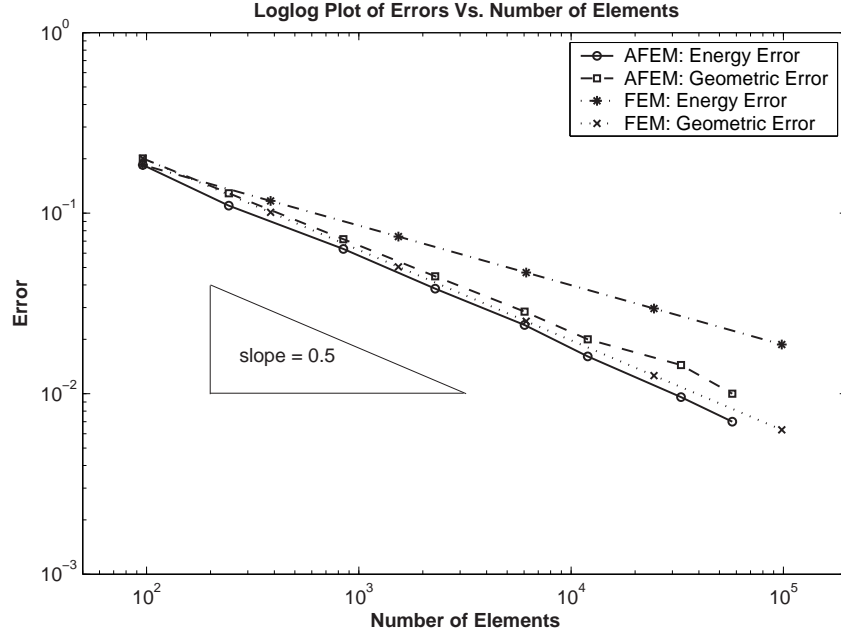
Figure 2.5.1: Experiment 1: Loglog plot of energy and geometric error vs. number of elements for both AFEM and FEM. AFEM is implemented with parameters $\theta_e = \theta_g = 0.6$, $\theta_o = 0.5$, and $\theta_\lambda = 0.8$. We see that energy and geometric errors from AFEM decay at the optimal rate of about 0.5 while the energy error from FEM does not, due to the corner singularity.

• Tables 2.5.1 and 2.5.2 show the decay of energy and geometric errors vs. number of elements, together with their experimental orders, for both AFEM and a standard FEM, respectively. AFEM performs at the optimal rate of 0.5 for both errors, while FEM performs only at the expected rate 0.3 for the energy error because of a corner singularity. This experiment confirms that AFEM performs optimally for corner singularities and smooth surfaces. See also Figure 2.5.1 for the log-log plot of errors vs. number.

• Figure 2.5.2 shows a sequence of meshes, polyhedral surfaces Γ_k, for $k = 1$, 3, and 5. The refinements are mostly dictated by the corner singularity at the origin but also by the surface. The zoom in near the origin shows that the refinement concentrate more near the origin.

80

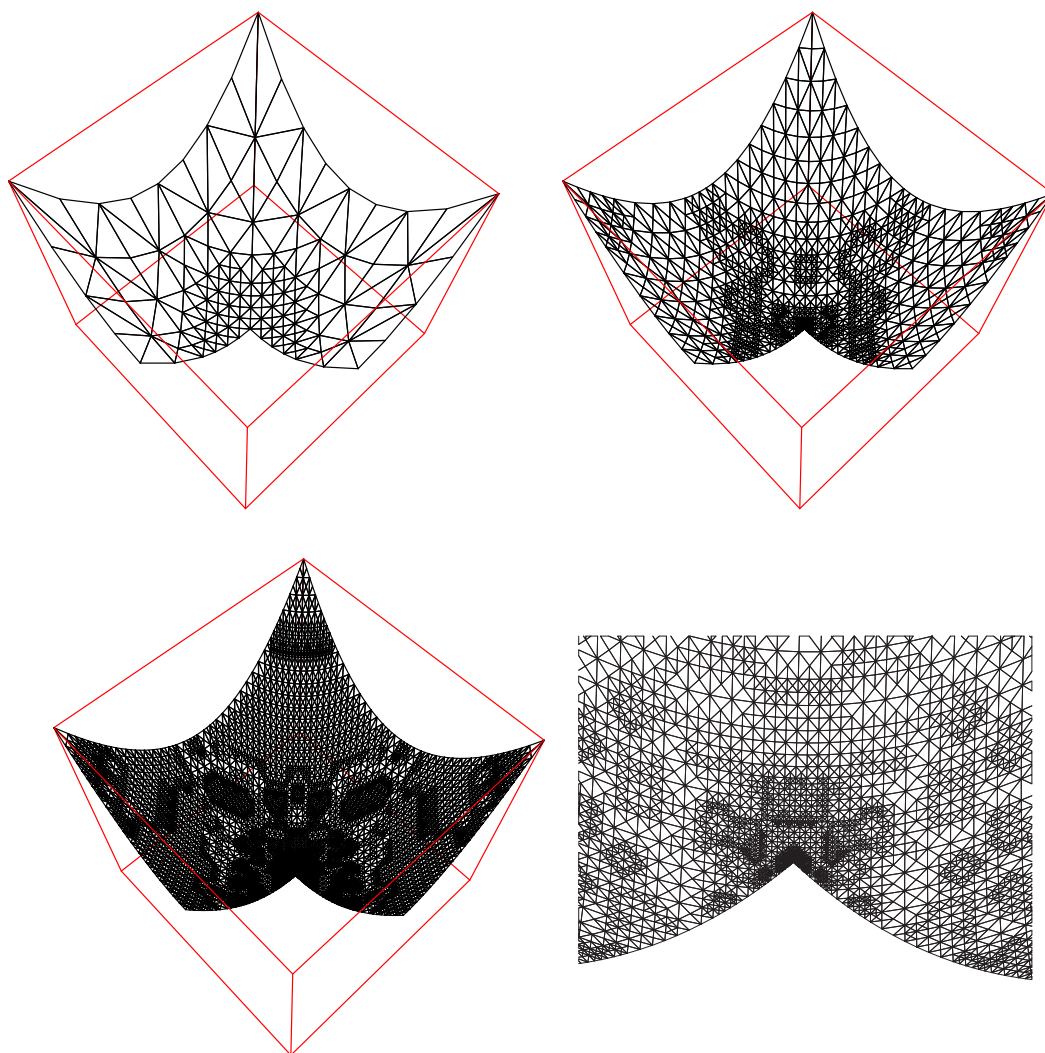Figure 2.5.2: Experiment 1: A sequence of meshes after 1, 3, and 5 iterations (top-left, top-right, bottom left), respectively, and a zoom at the origin after 5 iterations (bottom-right). The meshes show that refinements are adapted according to the corner singularity, namely at the origin, as well as to the surface. The corner singularity the refinement, as can be seen from the bottom-right figure.

2.5.2 Experiment 2: $C^{1,\alpha}$ Surface Singularity.

In contrast to Experiment 1, we now conduct an experiment on a $C^{1,\alpha}$ but not C^2 Surface. We let the surface Γ be the graph of

$$
z(x,y) = \begin{cases} (0.75 - x^2 - y^2)^{1.4} & \text{if} \quad x^2 + y^2 < 0.75, \\[2mm] 0 & \text{otherwise}, \end{cases}
$$

where $(x,y) \in \Omega := [0,1]^2$. It is easy to see that $z \in C^{1,0.4}(\Omega) \setminus C^{1,1}(\Omega)$ due to the singularity of the second derivatives of z on the curve $x^2 + y^2 = 0.75$. We assume the exact solution to be the linear function

$$
u(x,y) = x + y - 0.75,
$$

and the Dirichlet boundary condition and forcing term given by (2.1.6), namely since u is linear

$$
f := -\Delta_\Gamma u = (\nabla u \cdot \nu)(\nabla \cdot \nu),
$$

if z is $C^2(\Omega)$. However, in this example z is $C^{1,0.4}$ and f behaves singularly like $(x^2 + y^2 - 0.75)^{-0.6}$; the singularity does not align with the initial mesh $\mathcal{T}_0(\Omega)$. Note that $f \in L^1(\Gamma) \setminus L^2(\Gamma)$ in neighborhood of this curve, hence $\|f\|_{L^2(\Gamma)}$ is meaningless. However, there is $1 < q < 2$ such that $f \in L^q(\Gamma)$ and we can estimate (if p is Sobolev conjugate exponent of q)

$$
\int_T f(\varphi - \mathcal{I}\varphi) \le C \|f\|_{L^q(T)} \|\varphi - \mathcal{I}\varphi\|_{L^p(T)} \qquad \forall\, T \in \mathcal{T}_k, \ \forall \varphi \in H_0^1(\Gamma),
$$

since $H^1(\Gamma) \subset L^p(\Gamma)$ for $p < \infty$. In short, we can replace $\|f\|_{L^2}$ by $\|f\|_{L^q}$ in a neighborhood of the singularity and follow the same analysis. Set $\alpha = 0.6$,

$$
\gamma := \left\{ (x,y) \ : \ x^2 + y^2 = 0.75 \right\},
$$

and

$$d_T = \mathsf{dist}(T, \gamma).$$

We assume first that $d_T \geq h_T$. Then

$$\|f\|_{L^q(T)} \lesssim d^{-\alpha} h_T^{2/q} \quad \text{and} \quad \|\varphi - \mathcal{I}\varphi\|_{L^p(T)} \lesssim h_T^{2/p} \|\varphi\|_{H^1(\bar\omega_h(T))}.$$

Therefore,

$$\int_T f(\varphi - \mathcal{I}\varphi) \lesssim d_T^{-\alpha} h_T^{2/q+2/p} \|\varphi\|_{H^1(\bar\omega_h(T))}$$

$$= \underbrace{h_T^2 d_T^{-\alpha}}_{\approx \|h_T f\|_{L^2(T)}} \|\varphi\|_{H^1(\bar\omega_h(T))}$$

This implies

$$\int_T f(\varphi - \mathcal{I}\varphi) \lesssim \|h_T f\|_{L^2(T)} \|\varphi\|_{H^1(\bar\omega_h(T))},$$

and nothing change. Therefore, we can compute $\|f\|_{L^q(T)}$ by using $\|f\|_{L^2(T)}$ instead, if T is closed to the singularity curve but not crossing it because they are about the same size. We assume next that $d_T < h_T$. Then

$$\|f\|_{L^q(T)} \approx h_T^{2/q-\alpha}.$$

Hence,

$$\int_T f(\varphi - \mathcal{I}\varphi) \lesssim h^{2-\alpha} \|\varphi\|_{H^1(\bar\omega_h(T))}.$$

In practice we truncate the function $f(\mathbf{x})$ as follows:

$$f_c(\mathbf{x}) = \min\{f(\mathbf{x}), 1.e+15\}.$$

In the first case $d_T \geq h_T$ we never evaluate f in the truncation region because this would require h_T to be very small, namely, we need about 30 iterations. In the
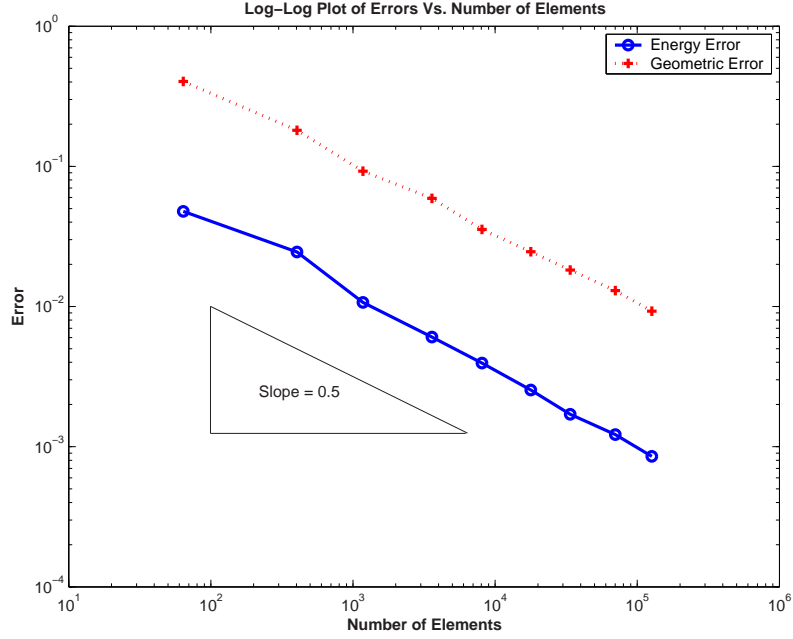
Figure 2.5.3: Experiment 2: Log-log plot of energy and geometric errors vs. the number of elements obtained from AFEM. The decay of these errors are near optimal rate at 0.5, comparing using slopes of plots.

second case, $d_T < h_T$ the quadrature error could be large there are few elements with such a behavior. The implementation works quite well as expected and the errors reduce with nearly optimal rate; see Figure 2.5.3.

In this experiment we study how our AFEM handles this kind of problem. We run the algorithm with parameters $\theta_e = 0.6, \theta_g = \theta_o = 0.5$, and $\theta_\lambda = 0.8$, and a sequence $\{a_k\}$ defined as in Experiment 1. Figure 2.5.3 is a log-log plot of errors vs. the number of elements which displays optimal error decay. The sequence of refined meshes are depicted in Figure 2.5.4. Our observations and comments are as follows.

• According to Figure 2.5.3, the energy and geometric errors decay with a nearly optimal rate of 0.5 after few iterations, despite the fact that f has a singularity along the curve $x^2 + y^2 = 0.75$. The effect of singularity is compensated by massive
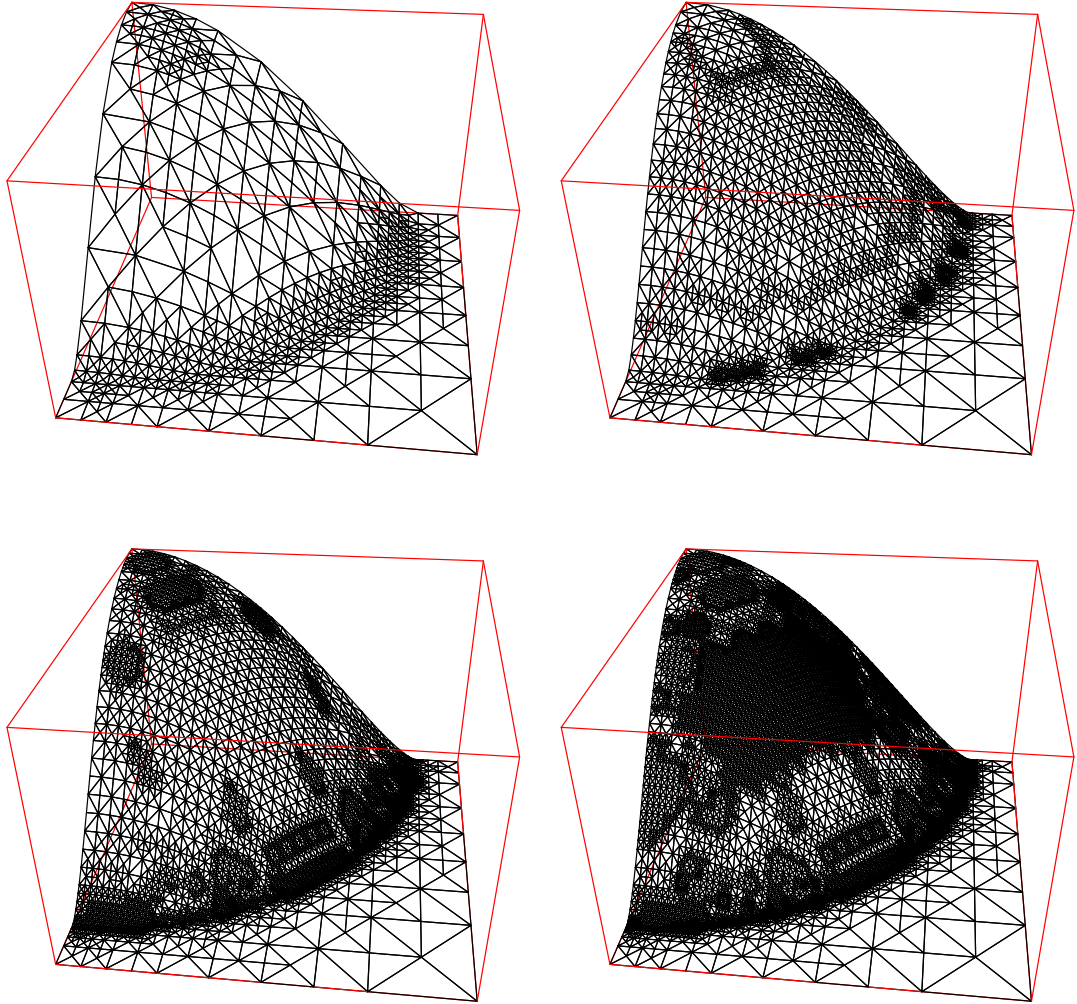
Figure 2.5.4: Experiment 2: A sequence of meshes after 2, 3, 4, and 5 iterations, respectively. The meshes show that refinements are adapted to the line singularity as well as to the surface. The refinements are denser near the line singularity and coarser on the flat part of the surface.

refinement near the singularity. This confirms that our AFEM works fine even if the surface is not $C^{1,1}$, as predicted by theory.

• According to Figure 2.5.4, the refinement produced by AFEM depends on variation of the normal, thereby being quite coarse in the flat part of Γ.

Chapter 3

Design and Convergence of AFEM for the Laplace-Beltrami

Operator on Parametric Surfaces

3.1 Introduction

Let Γ be a $d-1$ dimensional C^1 surface in $\mathbb{R}^d$, $d \geq 2$, either with or without boundaries; Γ is a *closed* surface if it has no boundaries. To represent the Laplace-Beltrami operator on Γ, one needs to describe Γ mathematically using, for example, parametric representations on charts, level sets, distance functions, graphs of functions, etc. Moreover, one usually obtains approximate solutions (finite element solutions) by solving the problem on approximate polyhedral surfaces rather than the surface Γ itself; see [9] for example that exploits the variational structure of the Laplace-Beltrami operator and gives an a priori error analysis. Our present objective is dual to that in [12] in that we introduce an adaptive finite element method (AFEM), derive a posteriori error estimates and use them to prove convergence of adaptive loops.

3.1.1 Geometry of and PDE on Γ.

We assume the surface Γ to be decomposed into several disjoint parts, each represented parametrically. We link this decomposition to a $(d-1)$ dimensional

87

polyhedral surface $\Gamma_0 \subset \mathbb{R}^d$, a piecewise linear interpolant of Γ. We also assume the existence of a continuous piecewise differentiable bijection $\mathcal{P}_0 : \Gamma_0 \to \Gamma$, that is $\mathcal{P}_0$ is differentiable in each face of Γ_0. In this way, the pair $(\Gamma_0, \mathcal{P}_0)$ provides a global description of Γ that will be used to create a sequence $\{\Gamma_k\}_{k=1}^{\infty}$ of polyhedral approximations of Γ. Since Γ_0 is a polyhedral surface, we can write

$$\Gamma_0 = \bigcup_{i=1}^{N} \Gamma_0^i,$$

where N is the number of faces of Γ_0 and Γ_0^i's are distinct faces; we refer to this element Γ_0^i as a *macro-element.* This induces the partition $\{\Gamma^i\}_{i=1}^{N}$ of Γ upon setting

$$\Gamma^i := \mathcal{P}_0(\Gamma_0^i).$$

Since Γ_0 is a linear interpolation of Γ, it follows that $\mathcal{P}_0(\mathbf{v}) = \mathbf{v}$ for all vertices $\mathbf{v}$ of Γ_0^i, $1 \le i \le N$. Since $\Gamma_0^i \subset \mathbb{R}^d$ is a $d-1$ dimensional flat surface, there is a reference element $\Omega \subset \mathbb{R}^{d-1}$ and an affine map $\mathcal{F}_0^i : \mathbb{R}^{d-1} \to \mathbb{R}^d$ such that $\Gamma_0^i = \mathcal{F}_0^i(\Omega)$. For example, if Γ_0^i is a triangle in $\mathbb{R}^3$, then we can take Ω to be the master triangle in $\mathbb{R}^2$ and $\mathcal{F}_0^i$ the affine map that connects the three vertices of Ω with those of Γ_0^i. Hence, we can view Γ^i as a parametric surface on Ω via a parametrization $\mathcal{X}^i := \mathcal{P}_0 \circ \mathcal{F}_0^i$. Since $\mathcal{P}_0$ is differentiable on Γ_0^i, then $\mathcal{X}^i$ is differentiable on Ω, and thus $\Gamma^i = \mathcal{X}^i(\Omega)$ is *regular.*

The structure of map $\mathcal{P}_0$ depends on the application. If Γ^i is described on Γ_0^i via the *distance function* $\mathsf{dist}(x)$, then

$$\Gamma^i \ni \tilde{x} = x - \mathsf{dist}(x)\nabla\mathsf{dist}(x) = \mathcal{P}_0(x) \qquad \forall\, x \in \Gamma_0^i,$$

provided $\mathsf{dist}(x)$ is sufficiently small so that the distance is uniquely defined. If,

88

instead, Γ^i is the *zero level set* $\phi(x) = 0$ of a function ϕ, then

$$\Gamma_0^i \ni x = \tilde{x} + \frac{\nabla\phi(\tilde{x})}{\nabla\phi(\tilde{x})}\,|x - \tilde{x}| = \mathcal{P}_0^{-1}(\tilde{x}) \qquad \forall\, \tilde{x} \in \Gamma^i$$

is the inverse map of $\mathcal{P}_0$. In both cases, dist and ϕ must be twice differentiable for $\mathcal{P}_0$ to be differentiable.

We note that a function $v : \Gamma^i \to \mathbb{R}$ defines uniquely two functions $\hat{v} : \Omega \to \mathbb{R}$ and $\bar{v} : \Gamma_0^i \to \mathbb{R}$ via the maps $\mathcal{X}^i$ and $\mathcal{P}_0$, namely

$$v(\mathcal{X}^i(\hat{x})) = \hat{v}(\hat{x}) \qquad \forall\, \hat{x} \in \Omega \qquad \text{and} \qquad v(\mathcal{P}_0(\bar{x})) = \bar{v}(\bar{x}) \qquad \forall\, \bar{x} \in \Gamma_0^i. \quad (3.1.1)$$

Conversely, given a function $\hat{v} : \Omega \to \mathbb{R}$ (respectively, $\bar{v} : \Gamma_0^i \to \mathbb{R}$) defines uniquely the two functions $v : \Gamma^i \to \mathbb{R}$ and $\bar{v} : \Gamma_0^i \to \mathbb{R}$ (respectively, $v : \Gamma^i \to \mathbb{R}$ and $\hat{v} : \Omega \to \mathbb{R}$.)

We consider, for simplicity, the Laplace-Beltrami operator Δ_Γ on a *closed* surface Γ

$$-\Delta_\Gamma u = f \quad \text{on} \quad \Gamma, \qquad\qquad (3.1.2)$$

where $f \in L^2(\Gamma)$ and $\int_\Gamma f = 0$; the latter is a compatability condition for (3.1.2) to have a solution. However, surfaces with boundary and Dirichlet boundary conditions can be handled as well as shown in section 3.5.2; see also chapter 2 and [12] for graphs.

We denote by $\nu = (\nu_1, \ldots, \nu_d) \in \mathbb{R}^d$ the outer normal vector to Γ. For $v \in C^1(\Gamma)$ we define the tangential gradient of v on Γ by

$$\nabla_\Gamma v = \nabla v - (\nabla v \cdot \nu)\nu \in \mathbb{R}^d,$$

89

where ∇v is the usual gradient of $\mathbb{R}^d$. This definition makes sense provided v is extended to a C^1 function in a neighborhood of Γ, which is possible because Γ is C^1. However, $\nabla_\Gamma v$ does not depend on the extension but only on the value of v on Γ. Likewise, for a vector field $\mathbf{v} \in C^1(\Gamma)$, we define its tangential divergence by

$$\nabla_\Gamma \cdot \mathbf{v} = \nabla \cdot \mathbf{v} - \nu D\mathbf{v}\nu^T,$$

where $D\mathbf{v}$ stands for the differential matrix for $\mathbf{v}$. Therefore, if Γ is C^2, the Laplace-Beltrami operator reads as follows

$$\Delta_\Gamma v = \nabla_\Gamma \cdot \nabla_\Gamma v = \Delta v - (\nabla v \cdot \nu)(\nabla \cdot \nu) - \nu D^2 v\nu^T, \qquad (3.1.3)$$

provided $v \in C^2(\Gamma)$ and $D^2 v$ is the Hessian matrix of v (suitably extended as a C^2 function to a neighborhood of Γ).

To formulate (3.1.2) weakly, we introduce the Sobolev space on the surface Γ:

$$H^1(\Gamma) := \left\{ v \in L^2(\Gamma) \mid v \text{ has weak tangential derivatives in } L^2(\Gamma) \right\}.$$

A weak solution of (3.1.2) is a function $u : \Gamma \to \mathbb{R}$ satisfying

$$u \in H_0^1(\Gamma) : \quad \int_\Gamma \nabla_\Gamma u \cdot \nabla_\Gamma \varphi = \int_\Gamma f\varphi \qquad \forall\, \varphi \in H_0^1(\Gamma). \qquad (3.1.4)$$

3.1.2 The Finite Element Method (FEM) on Parametric Surfaces

We recall that the initial polyhedral surface Γ_0, with nodes lying on Γ, is composed of macro-elements Γ_0^i, each associated to a reference element Ω. We also have the differentiable bijections

$$\mathcal{F}_0^i : \Omega \to \Gamma_0^i, \qquad \mathcal{X}^i : \Omega \to \Gamma^i.$$

We recall that all vertices of the initial linear interpolation Γ_0 of Γ lie on Γ. Note that the surface Γ_0 defines macro-elements Γ_0^i. We separate the surface Γ into several pieces according to these macro-elements Γ_0^i, associate them to a reference element Ω^i and define the maps $\mathcal{X}^i$ and $\mathcal{F}_0^i$ accordingly.

To approximate (3.1.4) via the FEM, we first partition Γ_0 into conforming shape regular simplices; we call this set $\mathcal{T}_h(\Gamma_0)$. Note that each macro-element Γ_0^i induces shape regular simplices on the reference element $\Omega \subset \mathbb{R}^{d-1}$, thereby giving rise to a graded triangulation (or mesh) $\mathcal{T}_h(\Omega)$ of Ω. This triangulation induces a shape regular triangulation $\mathcal{T}_h(\Gamma_h^i)$ of Γ_h^i via the regular parametrization $\mathcal{X}^i$ as follows. Nodes of $\mathcal{T}_h(\Omega)$ are lifted to Γ^i via $\mathcal{X}^i$, and connected by a C^0 piecewise linear function, thereby giving rise to a polyhedral surface Γ_h^i – a piecewise linear approximation of Γ^i. This also induces a unique piecewise affine map $\mathcal{F}_h^i : \Omega \to \Gamma_h^i$ such that $T = \mathcal{F}_h^i(\hat{T})$ where vertices of T are the lifts of vertices of $\hat{T} \in \mathcal{T}_h(\Omega)$. The piecewise linear approximation Γ_h of Γ is just the union of all parts Γ_h^i and, likewise, $\mathcal{T}_h(\Gamma_h)$ denotes the triangulation of Γ_h obtained by combining all elements of $\mathcal{T}_h(\Gamma_h^i)$. The conformity of $\mathcal{T}_h(\Gamma_h)$ follows from that of $\mathcal{T}_h(\Gamma_0)$. We next form a finite element space $\mathbb{V}_h(\Gamma_h)$ of piecewise polynomials of degree n over $\mathcal{T}_h(\Gamma_h)$. Since the analysis on surfaces can be done mostly on each individual macro-element Γ_0^i, we omit the superscript i, namely, Γ stands for either the whole surface Γ or Γ^i; the same notation applies also to $\mathcal{X}$, Γ_h, and $\mathcal{F}_h$.

We formulate an approximation to the Laplace-Beltrami operator on the surface Γ_h as follows. If $F_h \in L^2(\Gamma_h)$, with $\int_{\Gamma_h} F_h = 0$, is a suitable approximation of

f, then the finite element solution $u_h : \Gamma_h \to \mathbb{R}$ solves

$$u_h \in \mathbb{V}_h(\Gamma_h): \qquad \int_{\Gamma_h} \nabla_{\Gamma_h} u_h \cdot \nabla_{\Gamma_h} \varphi_h = \int_{\Gamma_h} F_h \varphi_h \qquad \forall\, \varphi_h \in \mathbb{V}_h(\Gamma_h). \qquad (3.1.5)$$

This yields a symmetric positive definite (SPD) linear system which can be solved

by standard linear solvers such as the (preconditioned) conjugate gradient (CG).

3.1.3   Main Result and Outline

The main purpose of this chapter is to present an AFEM for (3.1.2) for parametric surfaces, thereby extending the idea developed in chapter 2 for graphs. We now briefly state our main result and provide an outline for the chapter.

Let $(\mathbb{V}_k(\Gamma_k), \mathcal{T}_k(\Gamma_k))_{k=1}^{\infty}$ be a sequence created via adaptive loops of the form

$$\text{SOLVE} \to \text{ESTIMATE} \to \text{MARK} \to \text{REFINE} \qquad (3.1.6)$$

as described below. For convenience, if $T \in \mathcal{T}_k(\Gamma_k)$, we denote its corresponding elements $\hat{T} \subset \Omega$ and $\tilde{T} \subset \Gamma$ as follows:

$$\hat{T} := \left\{ \hat{x} \in \Omega \mid \mathcal{F}_k(\hat{x}) \in T \right\}, \qquad \tilde{T} := \left\{ \tilde{x} \in \Gamma \mid \tilde{x} = \mathcal{X} \circ \mathcal{F}_k^{-1}(x),\ x \in T \right\}, \quad (3.1.7)$$

where $\mathcal{F}_k^{-1} : \Gamma_k \to \Omega$ is the inverse map of $\mathcal{F}_k$. To argue about the approximation of Γ by Γ_k in W_∞^1 for parametric surfaces, we introduce the *geometric oscillation* $\lambda_k := \max_{T \in \mathcal{T}_k(\Gamma_k)} \lambda_k(T)$ where

$$\lambda_k(T) := \left\| \nabla_{\hat{x}} \mathcal{X} - \nabla_{\hat{x}} \mathcal{F}_k \right\|_{L^\infty(\hat{T})}. \qquad (3.1.8)$$

We next introduce the *geometric error* $\zeta_k := \left(\sum_{T \in \mathcal{T}_k(\Gamma_k)} \zeta_k^2(T) \right)^{1/2}$ where

$$\zeta_k(T) := \lambda_k(T) \left\| \nabla_\Gamma u_k \right\|_{L^2(\tilde{T})}; \qquad (3.1.9)$$

the presence of the second factor is interesting and shows the interaction between the PDE and the surface. We note that, in contrast with λ_k, the accumulation in ζ_k is in $\ell^2(\mathcal{T}_k(\Gamma_k))$. In defining the *energy error*

$$e_k := \|\nabla_\Gamma(u - u_k)\|_{L^2(\Gamma)}, \tag{3.1.10}$$

and geometric error (3.1.9) we have decided to measure it on Γ and so use ∇_Γ; in doing this, we are implicitly employing the lift; for $v : \Gamma_k \to \mathbb{R}$, its lifts $\tilde{v} : \Gamma \to \mathbb{R}$ and $\hat{v} : \Omega \to \mathbb{R}$ are defined via

$$\tilde{v}(\mathcal{X} \circ \mathcal{F}_k^{-1}(x)) = v(x) = \hat{v}(\mathcal{F}_k^{-1}(x)) \qquad \forall\, x \in \Gamma_k. \tag{3.1.11}$$

Note that (3.1.11) is just the extension of (3.1.1) from Γ_0 to any Γ_k; $\mathcal{P}_0 = \mathcal{X} \circ \mathcal{F}_0^{-1}$. We finally let the *data oscillation* be $\mathsf{osc}_k := \left(\sum_{T \in \mathcal{T}_k(\Gamma_k)} \mathsf{osc}_k(T)^2\right)^{1/2}$ where

$$\mathsf{osc}_k^2(T) = h_T^2 \left\|F_k - \overline{F}_k\right\|_{L^2(T)}^2, \tag{3.1.12}$$

where $\overline{F}_k$ is the L^2-projection of F_k onto $\mathbb{P}_{n-1}(T)$. We are now ready to state the main result of this chapter, the convergence of the adaptive loop (3.1.6).

In sections 3.3 and 3.4 we design an AFEM with the following contraction property. Let $(\Gamma_0, \mathcal{T}_0)$ be an arbitrary initial surface-triangulation pair of Γ for which there is a continuous piecewise differentiable bijection $\mathcal{P}_0 : \Gamma_0 \to \Gamma$, as explained in subsection 3.1.1. Then there exist an integer $k_0 > 0$ and constants $\gamma_g, \gamma_o > 0$, and $\xi < 1$, solely depending on $(\Gamma_0, \mathcal{T}_0)$, shape regularity and the user's parameters of AFEM, such that for any $k \geq k_0$ AFEM satisfies

$$\mathcal{E}_{k+1} \leq \xi\, \mathcal{E}_k, \tag{3.1.13}$$

where $\mathcal{E}_k^2 := e_k^2 + \gamma_g \zeta_k^2 + \gamma_o \mathsf{osc}_k^2$ represents the combined error incurred by AFEM, namely the energy and geometric errors, e_k, ζ_k, as well as information missing in the averaging process osc_k.

The existence of k_0 is related to sufficient resolution of Γ by Γ_k, a condition which is attained by AFEM automatically but not imposed directly on the initial pair $(\Gamma_0, \mathcal{T}_0)$. More precisely, what is needed is that λ_k be below a threshold dictated by the regularity of Γ.

The chapter is organized as follows. The start in §3.2 with a review of differential geometry on parametric surfaces. We explain why the geometric oscillation defined in (3.1.8) is different from that for graphs; see chapter 2, [12]. We discuss the procedure ESTIMATE in §3.3 and the procedures SOLVE, MARK and REFINE in §3.4. We also prove the contraction property, and so convergence in §3.4. We conclude in §3.5 with several numerical experiments on surfaces with or without boundaries that shed light on the theory and document the performance of AFEM.

To simplify the notation, we use the following abbreviations. We write $a \lesssim b$ to denote $a \leq Cb$ for some constant C. We use $\mathbb{V}_h$ and $\mathcal{T}_h$ in stead of $\mathbb{V}_h(\Gamma_h)$ and $\mathcal{T}_h(\Gamma_h)$, respectively. Finally, we denote by v the two lifts $\tilde{v}$ or $\hat{v}$ of $v : \Gamma_k \to \mathbb{R}$.

3.2 Basic Differential Geometry

Let $T \in \mathcal{T}_k$, we define the corresponding regions $\tilde{T} \subset \Gamma$ and $\hat{T} \subset \Omega$ by

$$\tilde{T} := \left\{ \mathcal{X} \circ \mathcal{F}_k^{-1}(x) \mid x \in T \right\} \qquad \text{and} \qquad \hat{T} := \left\{ \mathcal{F}_k^{-1}(x) \mid x \in T \right\}. \qquad (3.2.1)$$

This implies that $T = \mathcal{F}_k(\hat{T})$ is a linear interpolation of $\tilde{T} = \mathcal{X}(\hat{T})$, i.e., $\mathcal{F}_k|_{\hat{T}}$ is the linear map approximating $\mathcal{X}$ over $\hat{T}$. We thus have an estimate for any $1 \le i \le d-1$,

$$\|\mathcal{X}_i - \mathcal{F}_{k,i}\|_{L^\infty(\hat{T})} \le \max_{x,y \in \hat{T}} |\mathcal{X}_i(x) - \mathcal{X}_i(y)| . \tag{3.2.2}$$

For example, if $\mathcal{X}$ is a smooth parametrization, say a $C^{1,\alpha}(\hat{T})$, then

$$\max_{x,y \in \hat{T}} |\mathcal{X}_i(x) - \mathcal{X}_i(y)| \lesssim h_{\hat{T}}{}^\alpha,$$

where $h_{\hat{T}}$ is the diameter of $\hat{T}$. This implies that the difference of $\mathcal{X}$ and $\mathcal{F}_k$ in W^1_∞ is bounded depending on the smoothness of the surface.

To compare surface integrals, we identify the elements of surface area $Q(\hat{x})$ and $Q_k(\hat{x})$ according to the maps $\mathcal{X}$ and $\mathcal{F}_k$, respectively; for example, if $d = 3$ and (u, v) are coordinates for Ω, we use

$$Q := |\mathcal{X}_u(\hat{x}) \times \mathcal{X}_v| \qquad \text{and} \qquad Q_k := |\mathcal{F}_{k,u}(\hat{x}) \times \mathcal{F}_{k,v}| . \tag{3.2.3}$$

Another way to define them is by using the determinant of the first fundamental forms of the maps as will be described later. By changing of surface integrals and according to the lift (3.1.11),

$$\int_T v = \int_{\hat{T}} v Q_k \qquad \text{and} \qquad \int_{\tilde{T}} v = \int_{\hat{T}} v Q.$$

Therefore, we obtain that

$$\int_T v = \int_{\tilde{T}} v \frac{Q_k}{Q} . \tag{3.2.4}$$

To get a connection between ∇_Ω and ∇_Γ, we let a matrix $\mathbf{G} := [\mathcal{X}_1, \dots, \mathcal{X}_{d-1}] \in \mathbb{R}^{d \times d-1}$, where $\mathcal{X}_i \in \mathbb{R}^d$, a column vector, is the derivative of $\mathcal{X}$ with respect to the

95

i^{th} coordinate of Ω; hence, $\mathcal{X}_i$'s are tangent vectors to Γ. Therefore, the chain rule yields the relation

$$\partial_{\hat{x}_i} v = \partial_{\hat{x}_i} v(\mathcal{X}(\hat{x})) = \nabla v \mathcal{X}_i = \nabla_\Gamma v \mathcal{X}_i \quad \text{for } 1 \le i \le d-1,$$

since $\nu \mathcal{X}_i = 0$. Therefore,

$$\nabla_\Omega v(\hat{x}) = \nabla_\Gamma v(\tilde{x}) \mathbf{G}(\hat{x}). \tag{3.2.5}$$

Similar result also holds for Γ_k by replacing $\mathcal{X}$ by $\mathcal{F}_k$, that is

$$\nabla_\Omega v(\hat{x}) = \nabla_{\Gamma_k} v(x) \mathbf{G}_k(\hat{x}).$$

To get the reverse relation, we let a matrix $\widetilde{\mathbf{G}} \in \mathbb{R}^{d \times d}$ be an extension of $\mathbf{G}$ by adding the normal ν the the last column, namely

$$\widetilde{\mathbf{G}} := \left[\mathbf{G}, \nu^T\right] = \left[\mathcal{X}_1, ..., \mathcal{X}_{d-1}, \nu^T\right].$$

Since we assume that $\mathcal{X}$ is a regular parametrization, tangent vectors $\mathcal{X}_1, \ldots, \mathcal{X}_{d-1}$ are linearly independent; hence, $\widetilde{\mathbf{G}}$ is invertible. If $\widetilde{\mathbf{D}} = \widetilde{\mathbf{G}}^{-1}$, then we can write

$$\nabla_\Gamma v = \nabla_\Gamma v \widetilde{\mathbf{G}} \widetilde{\mathbf{D}} = [\nabla_\Omega v, 0] \, \widetilde{\mathbf{D}} = \nabla_\Omega v \, \mathbf{D}, \tag{3.2.6}$$

where $\mathbf{D} \in \mathbb{R}^{d-1 \times d}$ is the restriction of $\widetilde{\mathbf{D}}$ by cutting off the last row. Similarly, by replacing $\mathcal{X}_i$ by $\mathcal{F}_{k,i}$ and ν by ν_k, the normal to Γ_k, and employing $\mathbf{D}_k$ instead of $\mathbf{D}$, we also have

$$\nabla_{\Gamma_k} v = \nabla_\Omega v \, \mathbf{D}_k. \tag{3.2.7}$$

Hence, we have relations

$$\nabla_\Gamma v = \nabla_{\Gamma_k} v \, \mathbf{G}_k \mathbf{D} \quad \text{and} \quad \nabla_{\Gamma_k} v = \nabla_\Gamma v \, \mathbf{G} \mathbf{D}_k.$$

By interchange of surface integrals, we have

$$\langle \nabla_{\Gamma_k} v, \nabla_{\Gamma_k} w \rangle_{\Gamma_k} = \left\langle \nabla_\Gamma v (\mathbf{G} \mathbf{D}_k \mathbf{D}_k^T \mathbf{G}^T) \frac{Q_k}{Q}, \nabla_\Gamma w \right\rangle_\Gamma \tag{3.2.8}$$

where $\langle a, b \rangle_\Gamma := \int_\Gamma a\, b^T$ and $\langle a, b \rangle_{\Gamma_k} := \int_{\Gamma_k} a\, b^T$ for row vectors $a, b \in \mathbb{R}^d$.

Lemma 3.2.1. *Let* $\mathbf{G}$ *and* $\mathbf{D}$ *defined as above. Then we have*

$$\mathbf{G} \mathbf{D} \mathbf{D}^T \mathbf{G}^T = \mathbf{I}_{d \times d} - \nu \otimes \nu. \tag{3.2.9}$$

Proof: Since we know from the extension that

$$\mathbf{I}_{d \times d} = \widetilde{\mathbf{G}}^{-1} \widetilde{\mathbf{G}} = \begin{bmatrix} \mathbf{D} \\ \nu \end{bmatrix} \begin{bmatrix} \mathbf{G} & \nu^T \end{bmatrix} = \begin{bmatrix} \mathbf{D}\mathbf{G} & \mathbf{D}\nu^T \\ \nu\mathbf{G} & \nu \cdot \nu \end{bmatrix},$$

and

$$\mathbf{I}_{d \times d} = \widetilde{\mathbf{G}} \widetilde{\mathbf{G}}^{-1} = \begin{bmatrix} \mathbf{G} & \nu^T \end{bmatrix} \begin{bmatrix} \mathbf{D} \\ \nu \end{bmatrix} = \mathbf{G}\mathbf{D} + \nu \otimes \nu.$$

Therefore, $\mathbf{D}\mathbf{G} = \mathbf{I}_{d-1 \times d-1}$ and $\mathbf{G}\mathbf{D} = \mathbf{I}_{d \times d} - \nu \otimes \nu$. Hence, $\mathbf{G}\mathbf{D}$ is symmetric and we have

$$\mathbf{G} \mathbf{D} \mathbf{D}^T \mathbf{G}^T = \mathbf{G}\mathbf{D}\mathbf{G}\mathbf{D} = \mathbf{G}\mathbf{D} = \mathbf{I}_{d \times d} - \nu \otimes \nu.$$

$\square$

Since $\mathcal{X}$ is a regular parametrization of Γ, the *first fundamental form* reads

$$\mathbf{g} = \left(g_{ij} \right)_{1 \leq i,j \leq d-1} := \left(\mathcal{X}_i^T \mathcal{X}_j \right)_{1 \leq i,j \leq d-1} = \mathbf{G}^T \mathbf{G};$$

this is a symmetric and positive definite matrix. Moreover, since $\mathbf{G}\mathbf{D}$ is symmetric and $\mathbf{D}\mathbf{G} = \mathbf{I}$, we have

$$\mathbf{D} \mathbf{D}^T \mathbf{G}^T \mathbf{G} = \mathbf{D}\mathbf{G}\mathbf{D}\mathbf{G} = \mathbf{I}.$$

97

Therefore, $\mathbf{D}\mathbf{D}^T = \mathbf{g}^{-1}$ which is also symmetric and positive definite.

The results above hold also for the map $\mathcal{F}_k : \Omega \to \Gamma_k$ when computation is restricted to a single element. Namely, we have for $\hat{x} \in \hat{T}$,

$$\mathbf{g}_k(\hat{x}) = \Big(g_{k,ij} \Big)_{1 \le i,j \le d-1} := \Big(\mathcal{F}_{k,i}^T \mathcal{F}_{k,j} \Big)_{1 \le i,j \le d-1} = \mathbf{G}_k^T(\hat{x}) \mathbf{G}_k(\hat{x}),$$

which is constant on $\hat{T}$. We now define the elementary surface area $Q = \sqrt{\det \mathbf{g}}$, and $Q_k = \sqrt{\det \mathbf{g}_k}$ where $\det \mathbf{g}$ stands for the determinant of the matrix $\mathbf{g}$.

With these relations at hand, we can now transform integrals from Γ to Ω and back to Γ_k,

$$\int_{\tilde{T}} \nabla_\Gamma v \cdot \nabla_\Gamma w = \int_{\hat{T}} Q \nabla_\Omega v \mathbf{D}\mathbf{D}^T \cdot \nabla_\Omega w = \int_T \frac{Q}{Q_k} \nabla_{\Gamma_k} v (\mathbf{G}_k \mathbf{D}\mathbf{D}^T \mathbf{G}_k^T) \cdot \nabla_{\Gamma_k} w. \quad (3.2.10)$$

Conversely,

$$\int_T \nabla_{\Gamma_k} v \cdot \nabla_{\Gamma_k} w = \int_{\hat{T}} Q_k \nabla_\Omega v \mathbf{D}_k \mathbf{D}_k^T \cdot \nabla_\Omega w = \int_{\tilde{T}} \frac{Q_k}{Q} \nabla_\Gamma v (\mathbf{G} \mathbf{D}_k \mathbf{D}_k^T \mathbf{G}^T) \cdot \nabla_\Gamma w.$$

$$(3.2.11)$$

This allow us to compare integrals over Γ and Γ_k, namely

$$\int_{\Gamma_k} \nabla_{\Gamma_k} v \cdot \nabla_{\Gamma_k} w - \int_\Gamma \nabla_\Gamma v \cdot \nabla_\Gamma w = \int_\Gamma \nabla_\Gamma v \underbrace{\left(\frac{1}{Q} \mathbf{G} (Q_k \mathbf{D}_k \mathbf{D}_k^T - Q \mathbf{D}\mathbf{D}^T) \mathbf{G}^T \right)}_{=: \mathbf{A}_k} \cdot \nabla_\Gamma w.$$

$$(3.2.12)$$

This is a consequence of (3.2.11) and Lemma 3.2.1, because $\nabla_\Gamma v \cdot \nu = 0$. To estimate the difference we thus have to bound $\mathbf{A}_k$.

Lemma 3.2.2. *For $\hat{T} \in \mathcal{T}_k(\Omega)$, the following estimates are valid.*

$$\| Q - Q_k \|_{L^\infty(\hat{T})} \lesssim \| \nabla_\Omega \mathcal{X} - \nabla_\Omega \mathcal{F}_k \|_{L^\infty(\hat{T})}, \quad \| \mathbf{g} - \mathbf{g}_k \|_{L^\infty(\hat{t})} \lesssim \| \nabla_\Omega \mathcal{X} - \nabla_\Omega \mathcal{F}_k \|_{L^\infty(\hat{T})}.$$

Proof: Since $\mathcal{F}_k|_{\hat{T}}$ is the linear interpolation of a regular parametrization $\mathcal{X}$, we realize that Q and Q_k are bounded and so is

$$Q - Q_k = \frac{\det \mathbf{g} - \det \mathbf{g}_k}{Q + Q_k}.$$

Invoking the definitions of $\mathbf{g}$ and $\mathbf{g}_k$, we can bound

$$|\det \mathbf{g} - \det \mathbf{g}_k| \lesssim \|\nabla_\Omega \mathcal{X} - \nabla_\Omega \mathcal{F}_k\|,$$

where $\|\cdot\|$ is a matrix norm and the constant depends only on the dimension d and smoothness of $\mathcal{X}$. Since Q_k and $\mathbf{g}_k$ are well defined for all interior points of $\hat{T}$, the first estimate thus follows.

Likewise, by definitions of $\mathbf{g}$ and $\mathbf{g}_k$, we obtain

$$|\mathbf{g} - \mathbf{g}_k| \lesssim \|\nabla_\Omega \mathcal{X} - \nabla_\Omega \mathcal{F}_k\|,$$

and thus the second estimate follows. $\qquad\square$

Lemma 3.2.3 (Estimate of $\mathbf{A}_k$). *According to above definition of $\mathbf{A}_k$, we have*

$$\|\mathbf{A}_k\|_{L^\infty(\hat{T})} \lesssim \|\nabla_\Omega \mathcal{X} - \nabla_\Omega \mathcal{F}_k\|_{L^\infty(\hat{T})} \qquad \forall\, \hat{T} \in \mathcal{T}_k(\Omega).$$

Proof: By definition of $\mathbf{A}_k$ given in (3.2.12), and $\mathbf{D}\mathbf{D}^T = \mathbf{g}^{-1}$, we have

$$\|\mathbf{A}_k\|_{L^\infty(\hat{T})} \lesssim \left\| Q_k \mathbf{g}_k^{-1} - Q \mathbf{g}^{-1} \right\|_{L^\infty(\hat{T})}.$$

We note that $\mathbf{G}_k$, being an approximation of $\mathbf{G}$, can be bounded by a constant depending only on the regularity of $\mathcal{X}$. The assertion follows from Lemma 3.2.2 and the fact that

$$Q_k \mathbf{g}_k^{-1} - Q \mathbf{g}^{-1} = (Q_k - Q)\mathbf{g}_k^{-1} + Q\mathbf{g}_k^{-1}(\mathbf{g} - \mathbf{g}_k)\mathbf{g}^{-1},$$

and $\mathbf{g}^{-1}$ can be bounded by a constant depending only on $\mathcal{X}$. $\qquad\square$

Lemma 3.2.4 (Equivalence of norms). *According to above definitions, we have equivalence of norms for functions defined on the surfaces Γ and Γ_k, namely*

$$\|v\|_{L^2(\Gamma)} \sim \|v\|_{L^2(\Gamma_k)}, \tag{3.2.13}$$

$$\|v\|_{H_0^1(\Gamma)} \sim \|v\|_{H^1(\Gamma_k)}. \tag{3.2.14}$$

Proof: We prove the above assertions on a single element $T \in \mathcal{T}_k$ which then implies the result after summing over all the elements.

The first assertion (3.2.13) follows directly from (3.2.4) since $\left\|\frac{Q}{Q_k}\right\|_{L^\infty(\hat{T})}$ is bounded away from 0 for all $\hat{T} \in \mathcal{T}_k(\Omega)$.

To prove (3.2.14) we use the fact that

$$\|v\|_{H^1(\tilde{T})}^2 = \int_{\tilde{T}} \nabla_\Gamma v \cdot \nabla_\Gamma v = \int_T \frac{Q}{Q_k} \nabla_{\Gamma_k} v \mathbf{G}_k \mathbf{DD}^T \mathbf{G}_k^T \cdot \nabla_{\Gamma_k} v.$$

Since $\mathbf{DD}^T$ is positive definite and $(\nabla_{\Gamma_k} v)\mathbf{G}_k$ is non zero unless $\nabla_{\Gamma_k} v = \mathbf{0}$, we thus have

$$c\,\|v\|_{H^1(T)} \leq \|v\|_{H^1(\tilde{T})} \leq C\,\|v\|_{H^1(T)},$$

where c, and C depend on $\|\mathbf{G}_k\|$. Since we can view $\mathbf{G}_k$ as an approximation of $\mathbf{G}$, the second assertion follows by choosing these constants depending only on the surface. □

Remark 3.2.1. It follows from Lemma 3.2.4 above that if $v \in H^1(\Gamma)$, then its lift $v : \Gamma_k \to \mathbb{R}$ is in $H^1(\Gamma_k)$, and vice versa.

3.3   A Posteriori Error Analysis: Procedure ESTIMATE

3.3.1   Error Representation

For convenience in writing, we define bilinear forms as follows

$$\mathcal{B}_\Gamma(v, w) := \int_\Gamma \nabla_\Gamma v \cdot \nabla_\Gamma w \qquad \text{and} \qquad \mathcal{B}_{\Gamma_k}(v, w) := \int_{\Gamma_k} \nabla_{\Gamma_k} v \cdot \nabla_{\Gamma_k} w.$$

According to the weak forms (3.1.4), (3.1.5), the Remark 3.2.1, and integration by parts on each element $T \in \mathcal{T}_k$, we obtain the error representation

$$\mathcal{B}_\Gamma(u - u_k, \varphi) = I_1 + I_2 + I_3 \qquad \forall\, \varphi \in H^1(\Gamma),\ \forall\, \varphi_k \in \mathbb{V}_k,$$

where

$$I_1 := \sum_{T \in \mathcal{T}_k} \int_T \mathcal{R}_T(u_k)(\varphi - \varphi_k) - \sum_{S \in \mathcal{S}_k^o} \int_S \mathcal{J}_S(u_k)(\varphi - \varphi_k),$$

$$I_2 := \mathcal{B}_{\Gamma_k}(u_k, \varphi) - \mathcal{B}_\Gamma(u_k, \varphi),$$

$$I_3 := \int_\Gamma f\varphi - \int_{\Gamma_k} F_k \varphi.$$

Note that

- I_1 is a *standard residual term* obtained by integrating by parts on each $T \in \mathcal{T}_k$ where *element residual* $\mathcal{R}_T$ and *jump residual* $\mathcal{J}_S$ are defined by

$$\mathcal{R}_T(u_k) := (\Delta_{\Gamma_k} u_k + F_k)|_T, \tag{3.3.1}$$

$$\mathcal{J}_S(u_k) := (\nabla_{\Gamma_k} u_k)_S^+ \cdot n_S^+ + (\nabla_{\Gamma_k} u_k)_S^- \cdot n_S^-, \tag{3.3.2}$$

where n_S^+ and n_S^- are outward unit normals to S with respect to T^+ and T^-, on the supporting planes containing T^+ and T^- respectively; T^+ and T^- are elements in
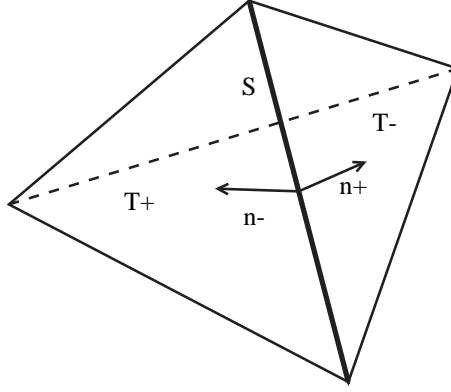
Figure 3.3.1: S is the common side shared by the elements T^+ and T^-, and n^+ and n^- are the normals to the side S on the supporting planes containing T^+ and T^-, respectively.

$\mathcal{T}_k$ that share the side $S \in \mathcal{S}_k^o$ where $\mathcal{S}_k^o$ denotes the set of interior faces of $T \in \mathcal{T}_k$, see Figure 3.3.1. Similarly, $(\nabla_{\Gamma_k} u_k)_S^+$ and $(\nabla_{\Gamma_k} u_k)_S^-$ are tangential gradients of u_k considered on T^+ and T^- restricted to S, respectively. If $\mathbb{V}_k$ is a space of piecewise linear functions, then $\mathcal{R}_T = F_k|_T$ and $\mathcal{J}_S$ is constant on S, since $\nabla_{\Gamma_k} u_k$ is constant on T.

- I_2 is a *geometry consistency term* that accounts for the different between Γ and Γ_k. According to (3.2.12), $I_2 = \int_\Gamma \nabla_\Gamma u_k \mathbf{A}_k \cdot \nabla_\Gamma \varphi$.

- I_3 is a *forcing consistency term* that accounts for the difference of forcing functions f and F_k of the PDE on surfaces Γ and Γ_k, respectively. We choose $F_k \in L^2(\Gamma_k)$ so that $\int_{\Gamma_k} F_k = 0$, thereby making $I_3 = 0$, upon defining

$$F_k(x) := \frac{Q(\hat{x})}{Q_k(\hat{x})} f(\tilde{x}) \qquad \forall\, \hat{x} \in \Omega, \quad x = \mathcal{F}_k(\hat{x}), \quad \tilde{x} = \mathcal{X}(\hat{x}). \qquad (3.3.3)$$

Hence, we arrive at

$$\int_\Gamma \nabla_\Gamma(u - u_k) \cdot \nabla_\Gamma \varphi = \sum_{T \in \mathcal{T}_k} \int_T \mathcal{R}_T(u_k)(\varphi - \varphi_k) - \sum_{S \in \mathcal{S}_k^o} \int_S \mathcal{J}_S(u_k)(\varphi - \varphi_k)$$

$$+ \int_\Gamma \nabla_\Gamma u_k \mathbf{A}_k \cdot \nabla_\Gamma \varphi \quad \forall\, \varphi \in H^1(\Gamma),\ \forall\, \varphi_k \in \mathbb{V}_k. \qquad (3.3.4)$$

3.3.2   Upper Bound

The upper bound for the *energy error* $e_k := \|\nabla_\Gamma(u - u_k)\|_{L^2(\Gamma)}$ is obtained from (3.3.4) and Clement's interpolation of functions defined on a polyhedral surface.

Lemma 3.3.1 (Clemént Interpolation). *There exists a linear interpolation operator*

$\mathcal{I}_k : H^1(\Gamma_k) \to \mathbb{V}_k$ *such that for* $T \in \mathcal{T}_k$ *and* $S \in \mathcal{S}_k^o$ *we have*

$$\|v - \mathcal{I}_k v\|_{L^2(T)} \le C h_T \|\nabla_{\Gamma_k} v\|_{L^2(\bar\omega_k(T))} \quad \forall v \in H^1(\Gamma_k), \qquad (3.3.5)$$

$$\|v - \mathcal{I}_k v\|_{L^2(S)} \le C h_S^{1/2} \|\nabla_{\Gamma_k} v\|_{L^2(\bar\omega_k(T))} \quad \forall v \in H^1(\Gamma_k), \qquad (3.3.6)$$

where C depends only on shape regularity constant, h_T and h_S are diameters of T and S respectively, and $\bar\omega_k(T) := \bigcup \{T' \in \mathcal{T}_k \mid T' \cap T \ne \varnothing\}$.

Note that the mesh $\mathcal{T}_k$ of polyhedral surface Γ_k is conforming and shape regular according to our construction in §3.1.2. Thus, the proof of this Lemma can be found in [5, 6].

On taking $\varphi = u - u_k \in H^1(\Gamma) \sim H^1(\Gamma_k)$, $\varphi_k = \mathcal{I}_k \varphi \in \mathbb{V}_k$ and plugging into (3.3.4), Lemmas 3.2.4 and 3.3.1 yield

$$\|\nabla_\Gamma(u - u_k)\|_{L^2(\Gamma)}^2 \le C_1 \sum_{T \in \mathcal{T}_k} \eta_k^2(T) + C_2 \sum_{T \in \mathcal{T}_k} \|\nabla_\Gamma u_k \mathbf{A}_k\|_{L^2(\tilde T)}^2, \qquad (3.3.7)$$

103

where constants C_1 and C_2 depend only on shape regularity constant and Γ. Here we define the *energy error indicator* $\eta_k(T)$ by

$$\eta_k^2(T) := h_T^2 \left\| \mathcal{R}_T(u_k) \right\|_{L^2(T)}^2 + \sum_{\substack{S \in \mathcal{S}_h^o \\ S \subset \partial T}} h_S \left\| \mathcal{J}_S(u_k) \right\|_{L^2(S)}^2,$$

and the *energy error estimator* $\eta_k := (\sum_{T \in \mathcal{T}_k} \eta_k^2(T))^{1/2}$. As a result of Lemma 3.2.3 and the definition of geometric error (3.1.9), we arrive at the upper bound for the energy error.

Lemma 3.3.2 (Upper Bound). *There exist constants C_1 and C_2 depending only on shape regularity constant and the surface Γ such that*

$$\left\| \nabla_\Gamma (u - u_k) \right\|_{L^2(\Gamma)}^2 \le C_1 \eta_k^2 + C_2 \zeta_k^2. \tag{3.3.8}$$

3.3.3   Lower Bound

We obtain a local lower bound for the energy error by following the idea of bubble functions introduced by Verfürth [23]. By proceeding as in [1, 7, 23] for estimating the local lower bound, we obtain the following result.

Lemma 3.3.3 (Local Lower Bound). *There exist constants $C_3, C_4,$ and C_5, depending on the shape regularity constant and on Γ, such that for $T \in \mathcal{T}_k$*

$$\eta_k^2(T) \le C_3 \left\| \nabla_\Gamma (u - u_k) \right\|_{L^2(\widetilde{\omega_k(T)})}^2 + C_4 \mathsf{osc}_k^2(\omega_k(T)) + C_5 \zeta_k^2(\omega_k(T)), \tag{3.3.9}$$

where $\omega_k(T) := \bigcup \{ T' \in \mathcal{T}_k \mid T' \text{ shares a common side with } T \}$ and $\widetilde{\omega_k(T)} \subset \Gamma$ is a projection of $\omega_k(T)$ to Γ via the map $\mathcal{X} \circ \mathcal{F}_k^{-1}$.

For $T \in \mathcal{T}_k$, let $\mathcal{S}_k^o(T) := \{S \in \mathcal{S}_k^o \mid S \subset \partial T\}$, the oscillation is defined by

$$\mathsf{osc}_k^2(T) := h_T^2 \left\| \mathcal{R}_T(u_k) - \overline{\mathcal{R}}_T \right\|_{L^2(T)}^2 + h_T \sum_{S \in \mathcal{S}_k^o(T)} \left\| \mathcal{J}_S(u_k) - \overline{\mathcal{J}}_S \right\|_{L^2(S)}^2,$$

where $\overline{\mathcal{R}}_T$ and $\overline{\mathcal{J}}_S$ are L^2-projections of $\mathcal{R}_T(u_k)$ and $\mathcal{J}_S(u_k)$ onto $\mathbb{P}_m(T)$ and $\mathbb{P}_m(S)$, respectively, m is a fixed integer; $\mathbb{P}_m(T)$ and $\mathbb{P}_m(S)$ denote spaces of polynomial functions of degree $\le m$ on T and on S, respectively. For $\omega_k(T) \subset \Gamma_k$, we define $\mathsf{osc}_k^2(\omega_k(T)) := \sum_{T' \subset \omega_k(T)} \mathsf{osc}_k^2('T)$, and denote $\mathsf{osc}_k := \mathsf{osc}_k(\Gamma_k)$; the same definition also applies to $\zeta_k^2(\omega_k(T))$.

Remark 3.3.1. If we take $m = n - 1$ where n is the degree of $\mathbb{V}_k$, then by (3.3.1) and (3.3.2), $\mathcal{J}_S(u_k) \in \mathbb{P}_{n-1}(S)$, and $(\Delta_{\Gamma_k} u_k)|_T \in \mathbb{P}_{n-2}(T)$, which imply that

$$\mathsf{osc}_k^2(T) = h_T^2 \left\| F_k - \overline{F}_k \right\|_{L^2(T)}^2, \tag{3.3.10}$$

where $\overline{F}_k$ is L^2-projection of F_k onto $\mathbb{P}_{n-1}(T)$.

According to upper and lower bounds estimates (3.3.8) and (3.3.9), our adaptive algorithm will rely on four local errors indicators $\eta_k(T), \zeta_k(T), \lambda_k(T)$ and $\mathsf{osc}_k(T)$. These indicators are important for designing a converging AFEM algorithm; for example, see [7, 13, 15, 16]. We compute these values for all $T \in \mathcal{T}_k$ and we call this procedure ESTIMATE, namely

$$\boxed{\{\eta_k(T), \zeta_k(T), \lambda_k(T), \mathsf{osc}_k(T)\}_{T \in \mathcal{T}_k} := \mathsf{ESTIMATE}(\Gamma, \Gamma_k, \mathcal{T}_k, F_k, u_k).}$$

3.4 AFEM

As introduced earlier in the introduction, AFEM consists of loops of procedures SOLVE, ESTIMATE, MARK, and REFINE, consecutively. The procedure ESTIMATE

is described in detail in the previous section 3.3, we now describe in detail the other procedures. The discussion on these procedures are similar to those for the case of graphs; see chapter 2, [12].

3.4.1   Procedure SOLVE

This procedure computes approximate solution of a SPD linear system as described in section 3.1.2. This is achieved by employing any standard linear solver such as CG, preconditioned CGs by diagonal, hierarchical basis, or BPX preconditioning. In other words, given a pair of approximate surface-mesh $(\Gamma_k, \mathcal{T}_k)$ and an initial guess for the solution u_{k-1}, SOLVE computes the discrete solution

$$\boxed{u_k := \text{SOLVE}(\Gamma_k, \mathcal{T}_k, u_{k-1}).}$$

3.4.2   Procedure MARK

Following the idea discussed for the graphs discussed in chapter 2, the procedure MARK is designed to choose a subset $\widehat{\mathcal{T}_k} \subset \mathcal{T}_k$ of marked elements according to the relative size of their indicators found by procedure ESTIMATE. Upon setting refining all elements in $\widehat{\mathcal{T}_k}$, we hope to reduce errors and oscillations, and thereby obtain a convergence adaptive algorithm. We describe the marking strategy as follows.

> Marking Strategy: Given parameters $0 < \theta_e, \theta_g, \theta_o < 1$, construct a subset $\widehat{\mathcal{T}_k}$ of $\mathcal{T}_k$ such that the followings hold:
>
> $$(\text{M1}): \qquad \sum_{T \in \widehat{\mathcal{T}_k}} \eta_k^2(T) \geq \theta_e^2 \eta_k^2, \qquad (3.4.1)$$
>
> $$(\text{M2}): \qquad \sum_{T \in \widehat{\mathcal{T}_k}} \zeta_k^2(T) \geq \theta_g^2 \zeta_k^2, \qquad (3.4.2)$$
>
> $$(\text{M3}): \qquad \sum_{T \in \widehat{\mathcal{T}_k}} \operatorname{osc}_k^2(T) \geq \theta_o^2 \operatorname{osc}_k^2. \qquad (3.4.3)$$

We will refer to this procedure as

$$\boxed{\widehat{\mathcal{T}_k} := \mathsf{MARK}(\{\eta_k(T), \zeta_k(T), \operatorname{osc}_k(T)\}_{T \in \mathcal{T}_k}).}$$

The strategy (M1) is for the energy error reduction, (M2) is for geometric error reduction, and (M3) is for oscillation reduction.

3.4.3   Procedure REFINE

This procedure refines all elements in the marked set $\widehat{\mathcal{T}_k}$ of $\mathcal{T}_k$ to obtain a new (finer) pair of approximate surface-mesh $(\Gamma_k, \mathcal{T}_k)$. The refinement step is performed according to two criteria. The first one was introduced by Morin et al [15, 16] to guaranteed energy error reduction.

> Interior Node Property: Refine each marked element $T \in \widehat{\mathcal{T}_k}$ to obtain a new mesh $\mathcal{T}_{k+1}$ compatible with $\mathcal{T}_k$ such that
>
> T and the adjacent elements $T' \in \mathcal{T}_k$ of T, as well as their common
>
> sides, contain a node of the finer mesh $\mathcal{T}_{k+1}$ in their interior.

The second criterium was introduced in chapter 2 for graphs to guarantee the reduction of geometric error.

Geometric Oscillation Property: Given a reduction factor $\theta_\lambda < 1$, refine all $T \in \widehat{\mathcal{T}_k}$ such that for all $T' \in \mathcal{T}_{k+1}(T)$ we have

$$\lambda_{k+1}(T') \leq \theta_\lambda \lambda_k(T),$$

where $\mathcal{T}_{k+1}(T) := \{T' \in \mathcal{T}_{k+1} \mid T' \text{ is obtained by refining } T\}$.

The procedure REFINE may also require additional steps to control the oscillations. We describe the Refining Strategy in several steps as follows.

Refining Strategy: Given a sequence $\{a_k\} \searrow 0$, a marked set $\widehat{\mathcal{T}_k}$, geometric oscillations $\{\lambda_k(T)\}_{T \in \mathcal{T}_k}$, and a fixed reduction rate of element size $0 < \gamma_r < 1$;

1. Refine all $T \in \widehat{\mathcal{T}_k}$ according to Interior Node Property;

2. Refine more if needed for Geometric Oscillation Property;

3. Refine more if needed so that for any $T \in \mathcal{T}_k$

$$\text{all } T' \in \mathcal{T}_{k+1}(T): \qquad \lambda_{k+1}(T') \leq \min\{a_k, \lambda_k(T)\};$$

4. Refine more if needed so that for any $T' \in \mathcal{T}_{k+1}(T)$, $T \in \mathcal{T}_k$,

$$\frac{|T_k'|}{|T'|} \leq \gamma_T \left(\frac{|T|}{|T'|}\right)^{\frac{2}{d-1}} \qquad \text{where} \qquad \gamma_T := \begin{cases} \gamma_r & \text{if } T \in \widehat{\mathcal{T}_k} \\ 1 & \text{if } T \notin \widehat{\mathcal{T}_k} \end{cases}, \qquad (3.4.4)$$

and $T_k' \subset T$ is the projection of T' back to T.

Remark 3.4.1. Since for $T \in \mathcal{T}_k$ is a linear interpolation of $\tilde{T}$, the estimate (3.2.2) implies that Steps 2 and 3 of `Refining Strategy` can be achieved in finite number of steps if $\tilde{T}$ is $C^{1,\alpha}$ surface, $0 < \alpha \leq 1$.

Remark 3.4.2. In Step 3 of `Refining Strategy`, the sequence $a_k \searrow 0$ is needed to guarantee that $\lambda_k \searrow 0$, i.e., Γ_k gets closer and closer to Γ. However, in our results below, Lemma 3.4.3 and Theorem 3.1, we require only that λ_k decreases monotonically and is smaller than some unknown positive threshold. The condition $a_k \searrow 0$ might be stronger than needed. In fact, if Γ is sufficiently smooth, say $C^{1,\alpha}$, then λ_k will reduce monotonically by itself according to (3.2.2), and this refinement step is not required.

Remark 3.4.3. Step 4 of `Refining Strategy` is needed in order to have a reduction of oscillation, see Lemma 3.4.6, especially when we deal with general dimension $d \neq 3$. For $d = 3$, this step is trivial since $T'_k \subset T$, and if $T \in \widehat{\mathcal{T}}_k$ then $|T'_k| \leq \gamma_T |T|$ where $\gamma_T < 1$ depending only on the refinement techniques.

Remark 3.4.4. For the case $d \neq 3$, Step 4 of `Refining Strategy` can be achieved by refining the element $T \in \mathcal{T}_k$ a finite number of times. This is the case because $\frac{|T'_k|}{|T'|}$ is bounded by a constant depending only on $\frac{Q_k}{Q}$. However, $\frac{|T|}{|T'|}$ will increase if we refine more, i.e. when $|T'|$ gets smaller.

Based on ideas developed by Dörfler [7], and Morin, Nochetto, and Siebert [15, 16], the construction of continuous piecewise linear bubble functions used for obtaining *modified local lower bound* is a crucial ingredient for proving convergence of AFEM. To apply the same idea we require that the lift of a continuous piece-

wise polynomial function of degree m defined on Γ_k is also a continuous piecewise polynomial function of degree m on Γ_{k+1}.

The design of refinement technique used here is different from the one given for graphs because the projection $\mathcal{P}_0 : \Gamma_0 \to \Gamma$ can be chosen arbitrarily and might not be linear. We design the refinement in such a way that the lift of functions satisfy the condition above. This can be achieved by refining Γ_k to get Γ_{k+1} based on *macro element/reference element strategy* described as follows.

Let $T \in \mathcal{T}_k$ be an element on Γ_k. To refine T, we first pull back to an element $T_0 \in \mathcal{T}_k(\Gamma_0)$ that corresponds to T, i.e., $T = \mathcal{F}_k(\mathcal{F}_0^{-1}(T_0))$. We next refine T_0 according to the refinement procedure described above to yield a conforming shape-regular mesh on Γ_0. Note that this step may involve more than one macro-element on Γ_0 because the Interior Node Property and completion to conformity require additional refinements on the neighborhood of T_0. We next project all new nodes on Γ_0 to Γ by first mapping nodes to the master element Ω and then mapping to Γ via $\mathcal{X}$. We finally form new elements in $\mathcal{T}_{k+1}$ by enforcing the same connectivity as in Ω; see Figures 3.4.1- 3.4.3. The mesh $\mathcal{T}_{k+1}$ is thus conforming and shape-regular since $\mathcal{X}$ is regular. The new elements $T \in \mathcal{T}_{k+1}$ also induce a new piecewise affine map $\mathcal{F}_{k+1} : \Omega \to \Gamma_{k+1}$. We refer to this procedure as

$$\boxed{(\mathcal{T}_{k+1}, \Gamma_{k+1}, \mathcal{F}_{k+1}) := \mathsf{REFINE}(\widehat{\mathcal{T}_k}, a_k, \{\lambda_k(T)\}_{T \in \mathcal{T}_k}, \mathcal{F}_k).}$$

Remark 3.4.5. Let $T \in \mathcal{T}_k$, denoted by $\Gamma_{k+1}(T)$ a region of Γ_{k+1} consisting of all elements in $\mathcal{T}_{k+1}$ obtained by refining T. With the refinement technique described above, if $v_k : \Gamma_k \to \mathbb{R}$ is a polynomial function of degree m on T, then its lift to
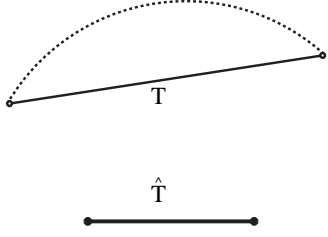
Figure 3.4.1: The element $T \in \mathcal{T}_k$ is corresponding to a reference element $\hat{T} \subset \Omega$ via $T = \mathcal{F}_k(\hat{T})$. The surface Γ is presented by dotted line.
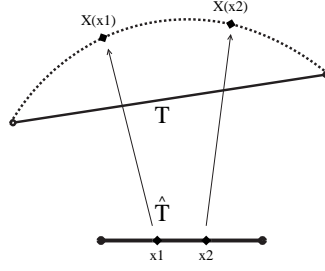
Figure 3.4.2: Refine $\hat{T}$ to obtain new nodes, for example, $x1$ and $x2$. The new nodes are projected to Γ via the map $\mathcal{X}$.
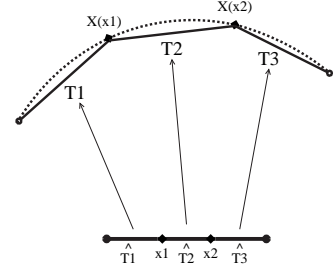
Figure 3.4.3: The new elements $T1$, $T2$, and $T3$ are formed by connecting the new nodes with the old ones according to new elements on Ω.

Γ_{k+1} is a piecewise polynomial function of degree m on $\Gamma_{k+1}(T)$. This is the case because lifting polynomial functions via affine maps preserves their degree.

3.4.4 Lemmas

For convenience we will use the following notation. For any $\omega \subset \Gamma$,

$$ e_k(\omega) := \|\nabla_\Gamma (u - u_k)\|_{L^2(\omega)}, \qquad \varepsilon_{k+1}(\omega) := \|\nabla_\Gamma (u_{k+1} - u_k)\|_{L^2(\omega)}, $$

and use e_k, respectively ε_{k+1} when $\omega = \Gamma$. The following results are consequences of procedures MARK and REFINE described above.

Geometric Error Reduction

As a direct outcome of the `Refining Strategy` Step 3, we have the reduction of geometric error.

Lemma 3.4.1 (Geometric oscillation reduction). *For a sequence $\{a_k\}$ converg-*

ing monotonically to 0 as $k \to \infty$ as used by procedure REFINE. *Then we have*

$$\lambda_k \to 0 \ as \ k \to \infty \ monotonically.$$

Employing Marking Strategy (M2), Refining Strategy, and Lemma 3.4.1 above, we obtain the geometric error reduction. The proof is the same as for graphs and we omit here; see Chapter 2, [12].

Lemma 3.4.2 (Geometric error reduction). *There exist constants $0 < \rho_1 < 1$ and $\rho_2 > 0$ such that for any $k \geq 0$*

$$\zeta_{k+1}^2 \leq \rho_1 \zeta_k^2 + \rho_2 \lambda_k^2 \varepsilon_{k+1}^2. \tag{3.4.5}$$

Quasi-Orthogonality

The quasi-orthogonality replaces the usual orthogonality because the approximating surfaces Γ_k and Γ_{k+1} are different, whence the pairs of associated finite element space-mesh $(\mathbb{V}_k, \mathcal{T}_k)$ and $(\mathbb{V}_{k+1}, \mathcal{T}_{k+1})$ are no longer nested. We state here the Lemma and stress that its proof is the same as for graphs; see Chapter 2.

Lemma 3.4.3 (Quasi-orthogonality). *The exist constants $C_6, C_7 > 0$ and a number $k_* \geq 0$ such that $\Lambda_0 := (\frac{1}{2} - \rho_2 C_6 \lambda_{k_*}^2) \in [\frac{1}{4}, \frac{1}{2})$, and for any $k \geq k_*$*

$$e_{k+1}^2 \leq e_k^2 - \Lambda_0 \varepsilon_{k+1}^2 + C_7 \zeta_k^2. \tag{3.4.6}$$

Remark 3.4.6 (Threshold for λ_k). For quasi-orthogonality to hold we require that λ_k is sufficiently small (k is bigger than some k_*) or, equivalently, that Γ_k be sufficiently closed to Γ. This is a natural a priori condition [9]. Since we do not have a

procedure to quantify a posteriori when such a condition is achieved, let sequence $\{a_k\}_k$ take care of this matter: it guarantees the eventual validity of the threshold for λ_k regardless of the resolution of the initial mesh-surface approximation.

Energy Error Reduction

It is well documented that the reduction of energy error relies on the *upper bound*, *modified local lower bound*, `Marking Strategy (M1)`, and `Interior Node Property`, see [13, 15, 16]. We discuss here the modified local lower bound which is conceptually similar to the case of graphs; see chapter 2, [12]. The main difference is that for parametric surfaces lifting of functions from Γ_k to Γ_{k+1} may not preserve polynomial functions, which is trivially the case for graphs, unless we design the refinement technique as describe in the previous section. The proof of the modified local lower bound is thus the same as for graphs and we omit here; see chapter 2.

Lemma 3.4.4 (Modified Local lower bound). *For any $T \in \widehat{\mathcal{T}}_k$, we have*

$$\eta_k^2(T) \leq C_3 \varepsilon_{k+1}^2(\tilde{\omega}_k(\tilde{T})) + C_4 \zeta_k^2(\omega_k(T)) + C_5 \mathsf{osc}_k^2(\omega_k(T)). \qquad (3.4.7)$$

Applying the upper bound (3.3.8) and `Marking Strategy (M1)`, we have

$$e_k^2 \leq C_1 \eta_k^2 + C_2 \zeta_k^2 \leq \frac{C_1}{\theta_e^2} \sum_{T \in \widehat{\mathcal{T}}_h} \eta_k^2(T) + C_2 \zeta_k^2.$$

Estimating $\eta_k^2(T)$ using (3.4.7), we have a corollary.

Corollary 3.4.5. *There are constants $\Lambda_1, \Lambda_2, \Lambda_3 > 0$ depending on $\theta_e, C_1, C_2, C_3, C_4$ and C_5, such that*

$$e_k^2 \leq \Lambda_1 \varepsilon_{k+1}^2 + \Lambda_2 \zeta_k^2 + \Lambda_3 \mathsf{osc}_k^2. \qquad (3.4.8)$$

Oscillation Reduction

According to Remark 3.3.1, the oscillation have the form

$$\mathsf{osc}_k^2(T) = h_T^2 \left\| F_k - \overline{F}_k \right\|_{L^2(T)}^2,$$

where $\overline{F}_k$ is the L^2-projection of F_k on $\mathbb{P}_{n-1}(T)$. Since it is convenient to work with area (measure) of the element T when we have to deal with surfaces that are different, we thus define the oscillation

$$\mathsf{osc}_k^2(T) = |T|^{\frac{2}{d-1}} \left\| F_k - \overline{F}_k \right\|_{L^2(T)}^2,$$

since $h_T^2 \sim |T|^{\frac{2}{d-1}}$, where $d \geq 2$ denotes the dimension. With this definition and following the `Refining Strategy` Step 4, we obtain the reduction of the oscillation. We state here the Lemma but its proof is exactly the same as for graphs and we omit it; see Chapter 2, [12].

Lemma 3.4.6 (Oscillation reduction). *There exists a constant $0 < \hat{\alpha} < 1$ depending on Γ and a parameter θ_o from* `Marking Strategy` (M3) *such that*

$$\mathsf{osc}_{k+1}^2 \leq \hat{\alpha}\mathsf{osc}_k^2. \tag{3.4.9}$$

3.4.5 Algorithm and Convergence

Given parameters $\theta_e, \theta_g, \theta_o, \theta_\lambda, \gamma_r$, a sequence $\{a_k\}_k$, the adaptive algorithm consists of consecutive loops of procedures SOLVE, ESTIMATE, MARK, and REFINE:

<div style="border:1px solid black;padding:1em;">

AFEM

Choose parameters $0 < \theta_e, \theta_g, \theta_o, \theta_\lambda < 1$, a sequence $\{a_k\} \searrow 0$, and let $u_{-1} = 0$.

1. Pick a suitable initial linear interpolation Γ_0 and a suitable projection $\mathcal{P}_0$ to describe Γ. Let $\mathcal{T}_0$ be a mesh for Γ_0, pick a macro reference element Ω for each element in $\mathcal{T}_0$, and obtain parametrizations $\mathcal{X}$ and $\mathcal{F}_0$ for Γ and Γ_0. Set $k = 0$.

2. $u_k = \mathsf{SOLVE}(\Gamma_k, \mathcal{T}_k, u_{k-1})$;

3. $\{\eta_k(T), \zeta_k(T), \lambda_k(T), \mathsf{osc}_k(T)\}_{T \in \mathcal{T}_k} = \mathsf{ESTIMATE}(\Gamma, \Gamma_k, \mathcal{T}_k, F_k, u_k)$;

4. $\widehat{\mathcal{T}}_k = \mathsf{MARK}(\{\eta_k(T), \zeta_k(T), \mathsf{osc}_k(T)\}_{T \in \mathcal{T}_k})$;

5. $(\mathcal{T}_{k+1}, \Gamma_{k+1}, \mathcal{F}_{k+1}) = \mathsf{REFINE}(\widehat{\mathcal{T}}_k, a_k, \{\lambda_k(T)\}_{T \in \mathcal{T}_k}, \mathcal{F}_k)$;

6. Set $k = k + 1$ and go to Step 2.

</div>

Theorem 3.1 (Convergence of AFEM). *Let $(\Gamma_0, \mathcal{T}_0)$ be an initial approximating surface-mesh pair of Γ. There exist a number $k_0 \geq 0$, and positive constants γ_g, γ_o, and $\xi < 1$, such that for any $k \geq k_0$, AFEM satisfies*

$$\mathcal{E}_{k+1} \leq \xi \, \mathcal{E}_k, \tag{3.4.10}$$

where $\mathcal{E}_k^2 := e_k^2 + \gamma_g \zeta_k^2 + \gamma_o \mathsf{osc}_k^2$.

Proof: According to Lemma 3.4.3, there is k_* such that (3.4.6) holds, namely

$$e_{k+1}^2 \leq e_k^2 - \Lambda_0 \varepsilon_{k+1}^2 + C_7 \zeta_k^2 \qquad \forall k \geq k_*, \tag{3.4.11}$$

where $\frac{1}{4} \leq \Lambda_0 < \frac{1}{2}$. Since ε_{k+1} and ζ_k are coupled according to Lemma 3.4.2 and (3.4.8), we split the term $\Lambda_0 \varepsilon_{k+1}^2$ into two parts

$$\Lambda_0 \varepsilon_{k+1}^2 = \beta \Lambda_0 \varepsilon_{k+1}^2 + (1 - \beta) \Lambda_0 \varepsilon_{k+1}^2,$$

where the constant $\beta \in (0, 1)$ will be chosen later.

Step 1. Using (3.4.8), we can eliminate $\beta \Lambda_0 \varepsilon_{k+1}^2$ by the estimate

$$\frac{\beta \Lambda_0}{\Lambda_1} e_k^2 \leq \beta \Lambda_0 \varepsilon_{k+1}^2 + \frac{\Lambda_0 \Lambda_2}{\Lambda_1} \beta \zeta_k^2 + \frac{\Lambda_0 \Lambda_3}{\Lambda_1} \beta \mathsf{osc}_k^2,$$

and (3.4.11) becomes

$$e_{k+1}^2 \leq \alpha e_k^2 - (1 - \beta) \Lambda_0 \varepsilon_{k+1}^2 + (C_7 + \Lambda_4 \beta) \zeta_k^2 + \Lambda_5 \beta \mathsf{osc}_k^2, \tag{3.4.12}$$

where $\alpha := 1 - \frac{\beta \Lambda_0}{\Lambda_1} < 1$, $\Lambda_4 := \frac{\Lambda_0 \Lambda_2}{\Lambda_1} > 0$, and $\Lambda_5 := \frac{\Lambda_0 \Lambda_3}{\Lambda_1} > 0$.

Step 2. To get rid of $(1 - \beta) \Lambda_0 \varepsilon_{k+1}^2$, we use (3.4.5) in Lemma 3.4.2, namely

$$\frac{(1 - \beta) \Lambda_0}{\rho_2 \lambda_{k_0}^2} \zeta_{k+1}^2 \leq \frac{\rho_1 (1 - \beta) \Lambda_0}{\rho_2 \lambda_{k_0}^2} \zeta_k^2 + (1 - \beta) \Lambda_0 \varepsilon_{k+1}^2 \qquad \forall k \geq k_0,$$

where $k_0 \geq k_*$ will be chosen later. Therefore, (3.4.12) becomes

$$e_{k+1}^2 + \gamma_g \zeta_{k+1}^2 \leq \alpha e_k^2 + \mu_0 \gamma_g \zeta_k^2 + \Lambda_5 \beta \mathsf{osc}_k^2, \tag{3.4.13}$$

where $\gamma_g := \frac{(1-\beta) \Lambda_0}{\rho_2 \lambda_{k_0}^2}$ and μ_0 satisfies

$$\mu_0 \gamma_g = C_7 + \Lambda_4 \beta + \rho_1 \gamma_g. \tag{3.4.14}$$

Step 3. From (3.4.14), writing γ_g in terms of β and solving for β, we have

$$\beta = \frac{\beta_0 - C_7}{\beta_0 + \Lambda_4} \qquad \text{where} \qquad \beta_0 := \frac{\Lambda_0 (\mu_0 - \rho_1)}{\rho_2 \lambda_{k_0}^2}.$$

Since $\rho_1 < 1$, we first choose $\rho_1 < \mu_0 < 1$ which gives $\beta_0 > 0$. Since $\lambda_k \searrow 0$, we can then choose $k_0 \geq k_*$ so that $\beta_0 > C_7$, which implies that $0 < \beta < 1$. Therefore, γ_g defined in (3.4.13) is a positive constant.

Step 4. Using (3.4.9) of Lemma 3.4.6, we can write (3.4.13) as

$$e_{k+1}^2 + \gamma_g \zeta_{k+1}^2 + \gamma_o \mathsf{osc}_{k+1}^2 \leq \alpha e_k^2 + \mu_0 \gamma_g \zeta_k^2 + \mu_1 \gamma_o \mathsf{osc}_k^2,$$

where γ_o is a constant to be determined and μ_1 satisfies

$$\mu_1 \gamma_o = \gamma_o \hat{\alpha} + \Lambda_5 \beta.$$

Since $\hat{\alpha} < 1$, we can choose $\hat{\alpha} < \mu_1 < 1$, which implies that $\gamma_o = \frac{\Lambda_5 \beta}{\mu_1 - \hat{\alpha}} > 0$. The assertion follows by setting $\xi = \sqrt{\max\{\alpha, \mu_0, \mu_1\}} < 1$. $\qquad\square$

3.5 Numerical Experiments

We now illustrate our theory developed in this chapter by showing some numerical experiments. These experiments are implemented based on the AFEM described above. The implementation is performed within the FEM toolbox ALBERT developed by Schmidt and Siebert [20, 21].

For convenience of presentation, we use the following notation:

- e_k and ζ_k denote the energy and geometric errors, respectively, after k iterations.

- $|\mathcal{T}_k|$ denotes the number of elements in triangulation $\mathcal{T}_k$.

- $\mathsf{EOC}_e(k)$ and $\mathsf{EOC}_g(k)$ denote the experimental orders of convergence after k iterations, namely

$$\mathsf{EOC}_e(k) := \frac{\log(e_{k-1}/e_k)}{\log(|\mathcal{T}_k|/|\mathcal{T}_{k-1}|)} \quad \text{and} \quad \mathsf{EOC}_g(k) := \frac{\log(\zeta_{k-1}/\zeta_k)}{\log(|\mathcal{T}_k|/|\mathcal{T}_{k-1}|)}.$$

117

3.5.1 Experiment 1: Smooth Closed Surface

In this experiment we test our algorithm by considering a smooth surface Γ as a zero level set of a smooth function:

$$\Gamma := \left\{ (x, y, z) \in \mathbb{R}^3 \mid (x - z^2)^2 + y^2 + z^2 - 1 = 0 \right\}$$

as proposed in [9]. We solve the Laplace-Beltrami operator on Γ using our AFEM assuming the exact solution is known;

$$u(x, y, z) = xy \qquad \forall\, (x, y, z) \in \Gamma.$$

We then prescribe the forcing term to satisfy $f = -\Delta_\Gamma u$ and $\int_\Gamma f = 0$, where $\Delta_\Gamma u$ is computed according to (3.1.3).

The AFEM starts by first choosing a suitable pair of $(\Gamma_0, \mathcal{P}_0)$ as described in section 3.1.1. Here, the projection $\mathcal{P}_0$ lifts a point $(x, y, z) \in \Gamma_0$ to Γ along the normal of the function

$$\phi(x, y, z) := (x - z^2)^2 + y^2 + z^2 - 1$$

at (x, y, z); the projection $\mathcal{P}_0$ is thus not orthogonal to Γ We implement AFEM with parameters $\theta_e = 0.6$, $\theta_g = \theta_o = 0.5$, and $\theta_\lambda = 0.8$. We present our results as follows. Table 3.5.1 shows the reduction of the energy error and the rate of convergence. Figure 3.5.2 presents the meshes and their refinements. We now describe and comment the results in detail.

● Table 3.5.1 shows that our AFEM performs as expected for smooth surfaces, AFEM gives the decay of the energy error at the optimal rate of about 0.5 as one

k	$|\mathcal{T}_k|$	e_k	$\mathsf{EOC}_e(k)$
0	320	7.03e-01	—
1	584	5.42e-01	0.431
2	1124	4.00e-01	0.466
3	2080	3.07e-01	0.431
4	3776	2.50e-01	0.341
5	7016	1.77e-01	0.555
6	11096	1.28e-01	0.717
7	21664	1.00e-01	0.365
8	38632	7.62e-02	0.472

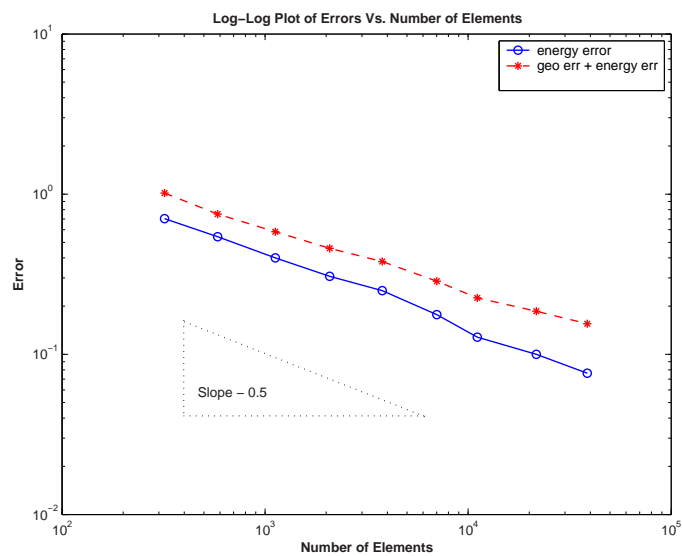Table 3.5.1: Experiment 1: The decay of the energy error. AFEM gives the decay for the energy error at the optimal rate of about 0.5.

Figure 3.5.1: Experiment 1: Log-log plot of errors Vs. number of elements. The energy error and the sum of geometric and energy errors decay nearly optimal at the rate about 0.5.

would expect by uniform refinement FEM. Moreover, Figure 3.5.1 shows that the sum of geometric and energy errors also decays nearly optimal at the rate about 0.5.

• Figure 3.5.2 displays several meshes which are more refined on region of rapid variation but are quasi-uniform. This is the correct refinement for a smooth problem. See the next Experiment when a singularity is considered.
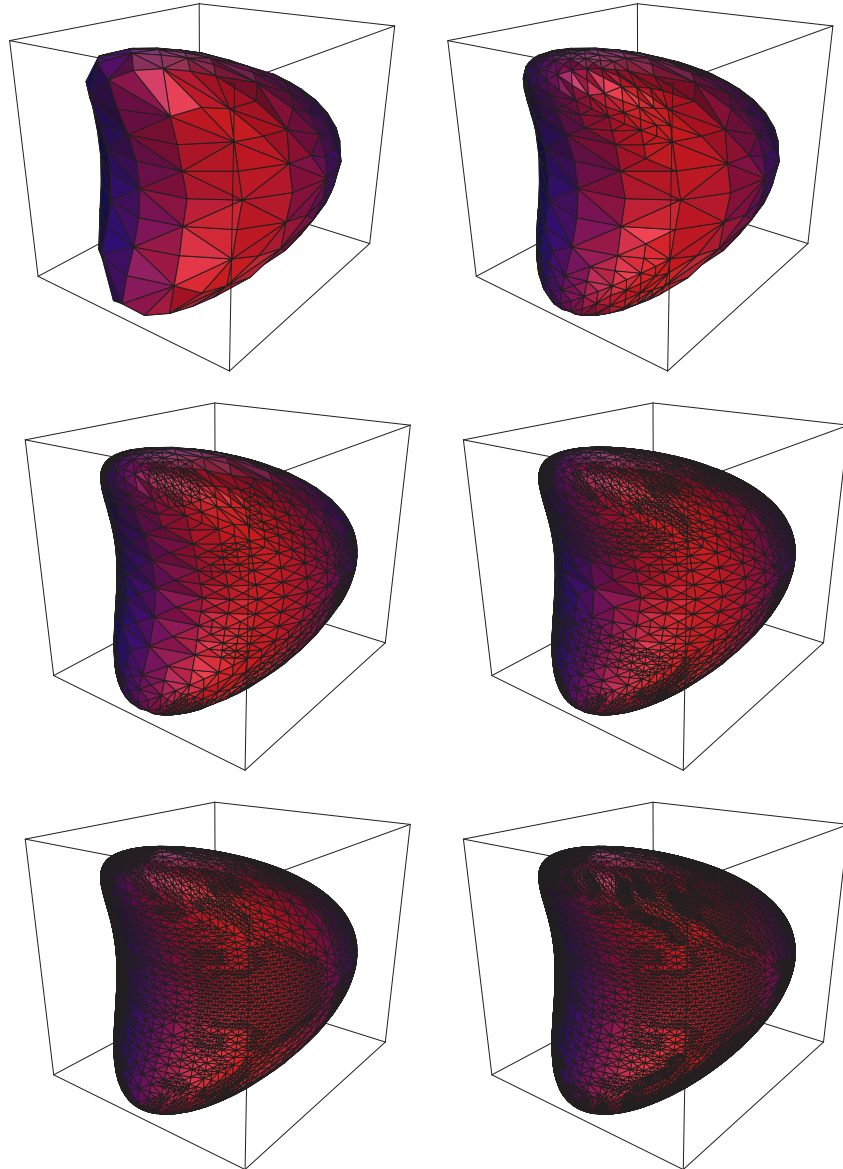
Figure 3.5.2: Experiment 1: A sequence of triangulations-surfaces produced by AFEM. Starting from left to right and top to bottom, Γ_0 (the initial surface), Γ_2, Γ_4, Γ_5, Γ_6, and Γ_7, respectively. Despite the face that the surface is smooth, the refinement seems to be denser where the surface has larger curvature. However, the refinement seems to be quasi-uniform overall.

3.5.2 Experiment 2: Corner Singularity

In this experiment we consider a surface with boundary to illustrate that our

AFEM is still valid in this case. In fact our theory developed above can be extended

to any parametric surface with smooth boundary and Dirichlet boundary condition.

We consider the surface as part of a unit sphere described by

$$\Gamma := \left\{ (x, y, z) \in \mathbb{R}^3 \mid x^2 + y^2 + z^2 = 1; \ (x, y) \in [-1, 1]^2 \setminus (0, 1) \times (-1, 0) \right\};$$

it is obtained by cutting off the parts on the unit sphere in the octans 4 and 8. We assume that the exact solution is known and given by

$$u(x, y, z) = u(r, \phi) = r^{2/3} \sin(2\phi/3),$$

where $r := \sqrt{x^2 + y^2}$ and $\phi = \tan^{-1}(y/x)$, and $(x, y, z) \in \Gamma$. We prescribed the boundary condition $g = u$ and the forcing term $f = -\Delta_\Gamma u$ according to (3.1.3).

We first start by choosing a suitable pair of $(\Gamma_0, \mathcal{P}_0)$, an initial piecewise linear interpolant of Γ and a projection. We take the projection $\mathcal{P}_0$ that lifts a point from Γ_0 to Γ along the normal

$$\nu(x, y, z) := \frac{1}{\sqrt{x^2 + y^2 + z^2}}(x, y, z).$$

We implemented AFEM with parameters $\theta_e = \theta_g = 0.5$, $\theta_o = 0.4$, and $\theta_\lambda = 0.8$. The results are presented in Table 3.5.2 for the decay of the errors vs. the number of elements, and in Figure 3.5.3 for the sequence of meshes obtained from AFEM. The results of the same experiment performed by standard FEM also given in Table 3.5.3. We describe and comment our results as follows.

• With the presence of corner singularities, Table 3.5.2 and Figure 3.5.3 show that AFEM reduces both the energy and geometric errors at the optimal rate of about 0.5. This is not the case for a standard FEM with uniform refinement, see Table 3.5.3.

k	$|\mathcal{T}_k|$	e_k	$\mathsf{EOC}_e(k)$	ζ_k	$\mathsf{EOC}_g(k)$
0	24	8.32e-01	—	1.03e+00	—
1	124	4.59e-01	0.362	7.72e-01	0.174
2	504	2.48e-01	0.439	3.71e-01	0.522
3	1424	1.59e-01	0.429	2.55e-01	0.363
4	3480	1.07e-01	0.441	1.75e-01	0.416
5	7896	7.51e-02	0.434	1.28e-01	0.382
6	18264	4.76e-02	0.543	8.71e-02	0.462
7	38944	3.30e-02	0.482	5.94e-02	0.504
8	73856	2.46e-02	0.457	4.49e-02	0.437
9	156324	1.66e-02	0.529	3.19e-02	0.455
10	328320	1.18e-02	0.462	2.03e-02	0.612

Table 3.5.2: Experiment 2: AFEM. The decays of the energy and geometric errors are nearly optimal of order 0.5 despite the fact that the solution has corner singularities; compared with Table 3.5.3 where standard FEM is used.

k	$|\mathcal{T}_k|$	e_k	$\mathsf{EOC}_e(k)$	ζ_k	$\mathsf{EOC}_g(k)$
0	24	8.32e-01	—	1.03e+00	—
1	96	5.16e-01	0.345	7.93e-01	0.187
2	384	2.89e-01	0.417	4.10e-01	0.476
3	1536	1.71e-01	0.380	2.09e-01	0.485
4	6144	1.02e-01	0.371	1.05e-01	0.496
5	24576	6.21e-02	0.359	5.27e-02	0.499
6	98304	3.82e-02	0.351	2.64e-02	0.500
7	393216	2.37e-02	0.344	1.32e-02	0.500

Table 3.5.3: Experiment 2: Standard FEM. The standard FEM with uniform refinement does not give the decays of the energy error at the optimal rate due to the corner singularities. However, the geometric error still decays at the optimal rate since the surface is smooth.
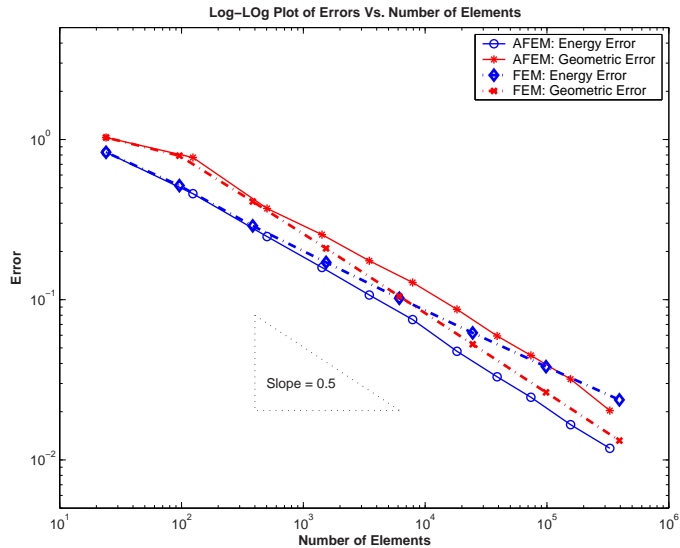
Figure 3.5.3: Experiment 2: Log-log plot of errors Vs. number of elements. The decay rates of both energy and geometric errors are nearly optimal of order about 0.5 for AFEM, whereas FEM only exhibits the expected rate of 0.33 for the energy error due to the corner singularities; FEM performs optimally in term of the geometric error since the surface is C^2.

• Figure 3.5.4 displays graded meshes produced by AFEM to compensate the effect of the corner singularities at points $(0, 0, 1)$ and $(0, 0, -1)$. The massive refinements near the singularities reduce that effect and lead to nearly optimal rate of convergence of the energy error. The refinements on the other parts are almost uniform due to geometric oscillation, however they are still coarser than those near the singularities.

3.5.3   Experiment 3: $C^{1,\alpha}$ Surface Singularity.

In this section we conduct an experiment on the $C^{1,\alpha}$ Surface Γ. We let Γ be the closed surface of revolution of the curve $\gamma := \gamma_1 \cup \gamma_2 \cup \gamma_3 \cup \gamma_4$ around the z-axis
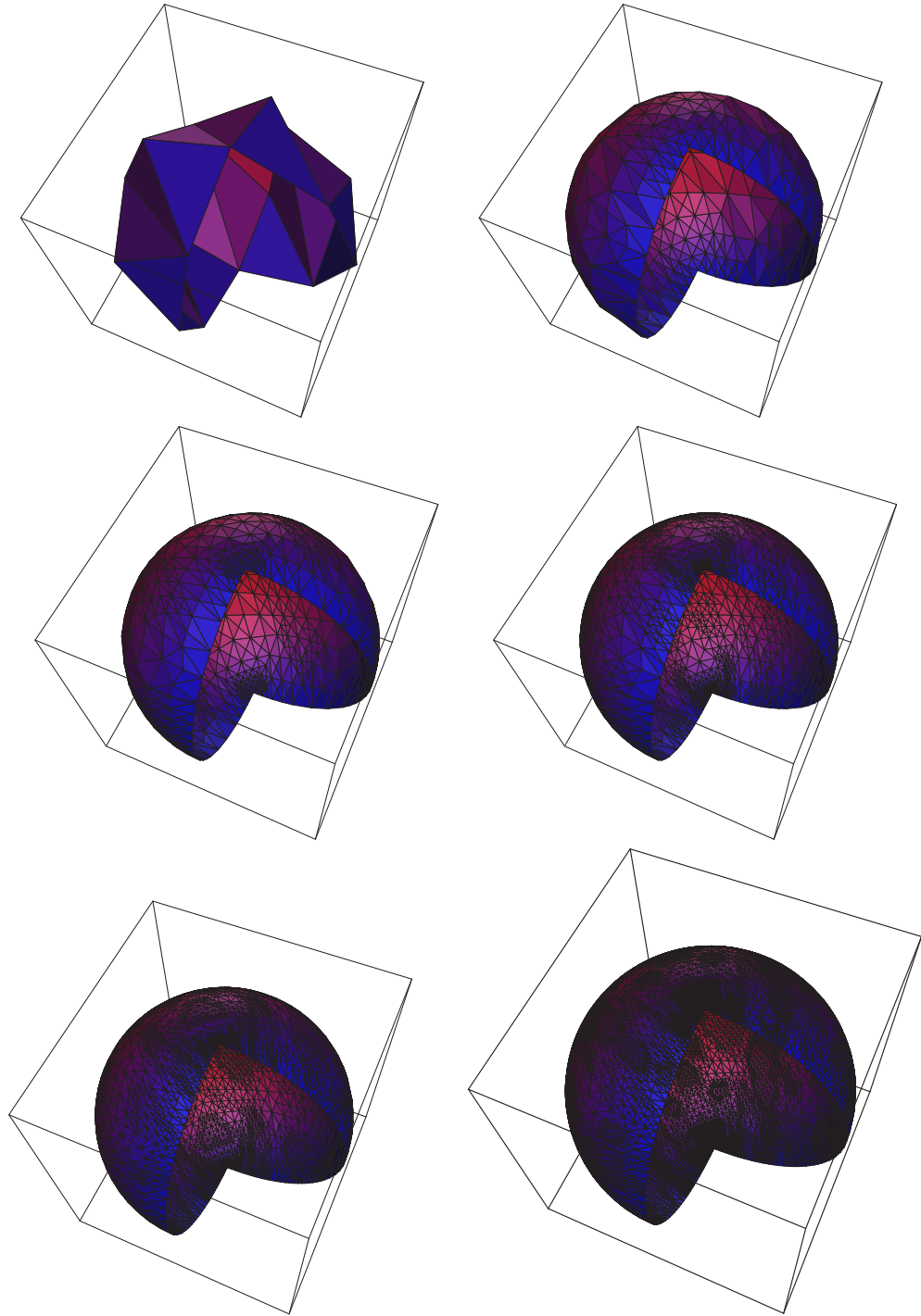
Figure 3.5.4: Experiment 2: A sequence of triangulations-surfaces produced by AFEM. Starting from left to right and top to bottom, Γ_0 (the initial surface), Γ_2, Γ_3, Γ_4, Γ_5, and Γ_6, respectively. The refinement is adapted according to the corner singularities; it is denser near the corners at the points $(0, 0, 1)$ and $(0, 0, -1)$. This leads to optimal rates of convergence of the energy error whereas uniform refinement yield a suboptimal rate. Refinement is mostly uniform on the other part to resolve geometric oscillation.

where

$$\gamma_1 := \left\{ (r,z) \mid z = (.25 - r^2)^{1.4}, r \in [0, 0.5) \right\},$$

$$\gamma_2 := \left\{ (r,z) \mid z = 0, r \in [0.5, 1] \right\},$$

$$\gamma_3 := \left\{ (r,z) \mid r = 1 + \sqrt{.25 - (z + 0.5)^2}, z \in (-1, 1) \right\},$$

$$\gamma_4 := \left\{ (r,z) \mid z = -1, r \in [0, 1] \right\},$$

and $r = \sqrt{x^2 + y^2}$ on Γ; see Figure 3.5.5. Therefore, the curve γ is $C^{1,0.4}$ which implies that Γ is a $C^{1,0.4}$ but not $C^{1,1}$ surface. Note that Γ has two flat parts; the bottom where $z = -1, r \leq 1$, and on the top where $z = 0, 0.5 \leq r \leq 1$. We let
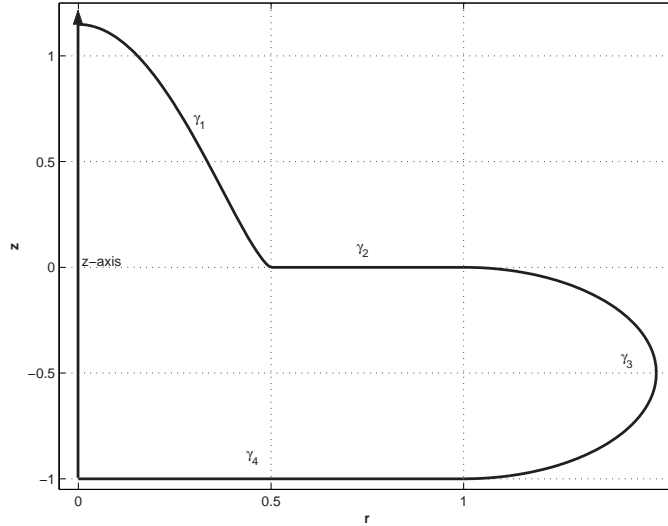

Figure 3.5.5: Experiment 3: Γ is the revolution surface of the curve $\gamma := \gamma_1 \cup \gamma_2 \cup \gamma_3 \cup \gamma_4$.

the exact solution $u : \Gamma \to \mathbb{R}$ of (3.1.2) be a linear function

$$u(x, y, z) = x + 2y.$$

We define the forcing term $f = -\Delta_\Gamma u$ and, since u is linear, (3.1.3) implies

$$f = (\nabla u \cdot \nu)(\nabla \cdot \nu).$$

125

We start AFEM by choosing a suitable pair $(\Gamma_0, \mathcal{P}_0)$ to describe Γ as introduced in §3.1.1. We define the projection $\mathcal{P}_0 : \Gamma_0 \to \Gamma$ as follows. For $(x, y, z) \in \Gamma_0$, if $r := \sqrt{x^2 + y^2}$, $\mathcal{P}_0$ maps

$$(x, y, z) \mapsto (x, y, z(x, y)) \quad \text{if} \quad r < 0.5, z > -0.5;$$

$$(x, y, z) \mapsto (x, y, 0) \quad \text{if} \quad 0.5 < r \leq 1, z > -0.5;$$

$$(x, y, z) \mapsto (x, y, -1) \quad \text{if} \quad r \leq 1, z < -0.5;$$

$$(x, y, z) \mapsto \left(\frac{x}{r} + (x - \frac{x}{r})\frac{0.5}{d_0}, \frac{y}{r} + (y - \frac{y}{r})\frac{0.5}{d_0}, (z + 0.5)\frac{0.5}{d_0} - 0.5 \right) \quad \text{if} \quad r > 1.0,$$

where $d_0 := \sqrt{(r-1)^2 + (z+0.5)^2}$. Note that $\mathcal{P}_0$ is continuous on Γ_0 but $\nabla \mathcal{P}_0$ may have jumps on the curves $r = 0.5$ or $r = 1$ that may not align with boundaries of macro-elements. In this experiment, we show that AFEM performs quite well in this situation given that the jumps of $\nabla \mathcal{P}_0$ goes to zero as Γ_k goes to Γ.

Remark 3.5.1. In theory we require that $\mathcal{P}_0$ is differentiable on macro-elements T so that $\lambda_k(T)$ defined in (3.1.8) goes to zero as Γ_k goes to Γ, which is needed for the theory to hold. Here we design Γ_0 such that the curves $r = 0.5$ or $r = 1$ do not align with boundaries of macro-elements, hence $\mathcal{P}_0$ may not be differentiable on some macro-elements. However, the convergence of AFEM still holds since the jumps of $\nabla \mathcal{P}_0$ goes to zero, hence λ_k also goes to zero, as Γ_k goes to Γ. We verify this claim by computing $\nabla \mathcal{P}_0$ directly as follows. On the curve $r = 0.5$,

$$\nabla \mathcal{P}_0 |_{r=0.5^-} - \nabla \mathcal{P}_0 |_{r=0.5^+} = \begin{bmatrix} 0 & 0 & 0 \\ 0 & 0 & 0 \\ \partial z/\partial x & \partial z/\partial x & 0 \end{bmatrix} = \mathbf{0},$$

k	$\lvert \mathcal{T}_k \rvert$	e_k	$\mathrm{EOC}_e(k)$	ζ_k	$\mathrm{EOC}_g(k)$
0	224	1.62e+00	—	2.90e+00	—
1	600	8.89e-01	0.606	1.73e+00	0.525
2	1324	6.34e-01	0.428	1.29e+00	0.367
3	2016	5.53e-01	0.326	1.04e+00	0.509
4	3692	3.95e-01	0.555	7.64e-01	0.515
5	6548	2.55e-01	0.763	5.29e-01	0.641
6	12600	1.90e-01	0.448	4.13e-01	0.380
7	23836	1.36e-01	0.525	2.97e-01	0.518
8	39048	1.01e-01	0.611	2.25e-01	0.557
9	68876	7.91e-02	0.427	1.74e-01	0.454
10	124616	5.95e-02	0.480	1.31e-01	0.478

Table 3.5.4: Experiment 3: AFEM performs nearly optimal where both energy and geometric errors decay at the rate about 0.5 despite the fact that Γ is a $C^{1,0.4}$ surface.

since $\partial z/\partial x|_{r=0.5^-} = \partial z/\partial y|_{r=0.5^-} = 0$. Similarly, on the curve $r = 1$,

$$
\nabla \mathcal{P}_0|_{r=1^+} - \nabla \mathcal{P}_0|_{r=1^-} = \begin{bmatrix} x^2(\frac{0.5}{d_0} - 1) & xy(\frac{0.5}{d_0} - 1) & 0 \\ xy(\frac{0.5}{d_0} - 1) & y^2(\frac{0.5}{d_0} - 1) & 0 \\ 0 & 0 & 0 \end{bmatrix},
$$

since $d_0|_{r=1^+} = |z + 0.5|$. Since $d_0 \to 0.5$ as $\Gamma_k \to \Gamma$, this implies the claim.

Remark 3.5.2. As in Experiment 2 of Chapter 2, the forcing term f behaves like $(0.5 - r)^{-0.6}$ if $r < 0.5$, and in fact, $f \in L^1(\Gamma) \setminus L^2(\Gamma)$. As explain before for graphs, calculation of $\lVert f \rVert_{L^2}$ is implemented via a truncation

$$
f_c(x) = \min \{f(x), 1.e + 15\} ;
$$

see Chapter 2, Experiment 2.

We implement AFEM with parameters $\theta_e = \theta_g = \theta_o = 0.5$. The results are shown in Table 3.5.4 and Figures 3.5.6-3.5.9. We describe and comment our results as follows.
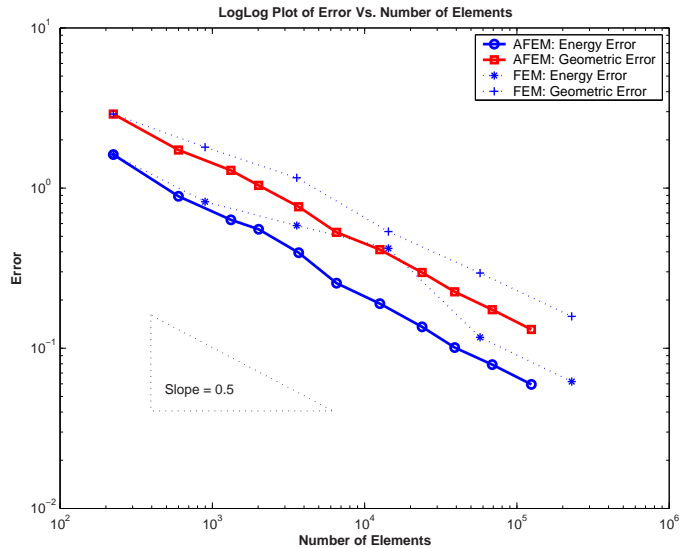
Figure 3.5.6: Experiment 3: Log-log plot of errors Vs. number of elements shows the comparison between AFEM and standard FEM.

- AFEM performs nearly optimal which gives the reduction of both energy and geometric errors at the rate about 0.5; see Table 3.5.4, despite the fact that Γ is just a $C^{1,0.4}$ surface. Figure 3.5.6 also shows that the AFEM performed better than standard uniform refinement FEM.

- According to Remark 3.5.1, AFEM performs quite well and λ_k decrease monotonically after first few iterations as expected.

- According to Figure 3.5.7 AFEM refines adaptively according to the smoothness of the surface given that the solution is smooth, u is linear in this case. There are no refinements where the surface is flat, i.e., the bottom of the surface in Figure 3.5.8, and the top part where $0.5 < r < 1$. The refinement is more dense near the singularity curve, $r = 0.5$, where the right-hand side f exhibits an unbounded but integrable discontinuity; see the zooms 3.5.9. The refinement on other smooth parts that are not flat, are done mostly uniform due to the geometric oscillation.
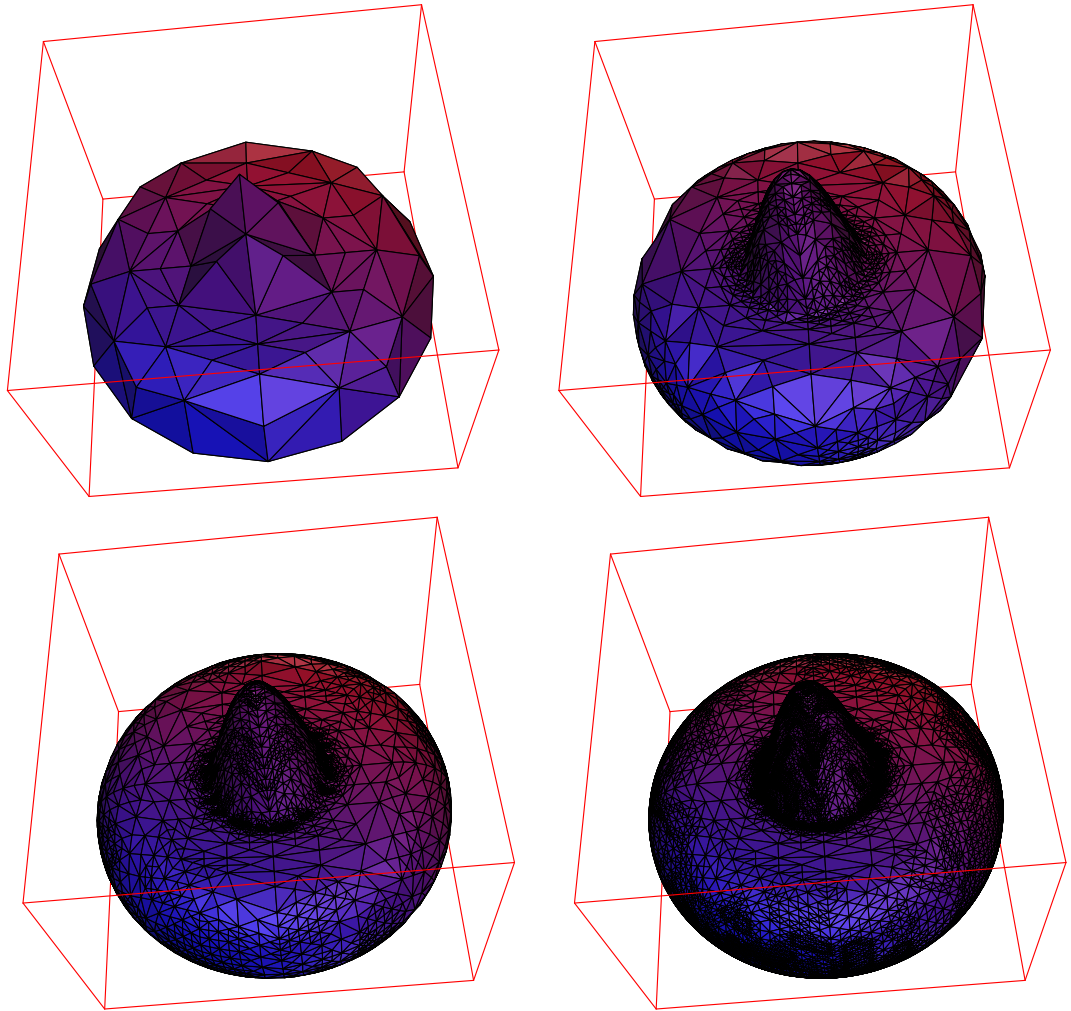
128

Figure 3.5.7: Experiment 3: The sequence of meshes Γ_3, Γ_5, and Γ_7 produced by AFEM starting from the macro-mesh Γ_0.
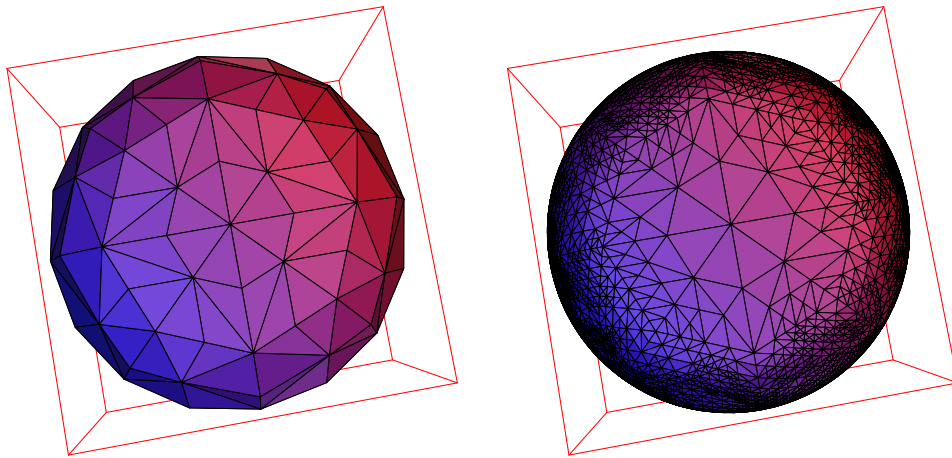
Figure 3.5.8: Experiment 3: The AFEM adapts according to the surface given that the solution is smooth, u is linear in this case; there are no refinements on the bottom part and on the top part where the surface is flat, the other parts are refined according to the shape of the surface.
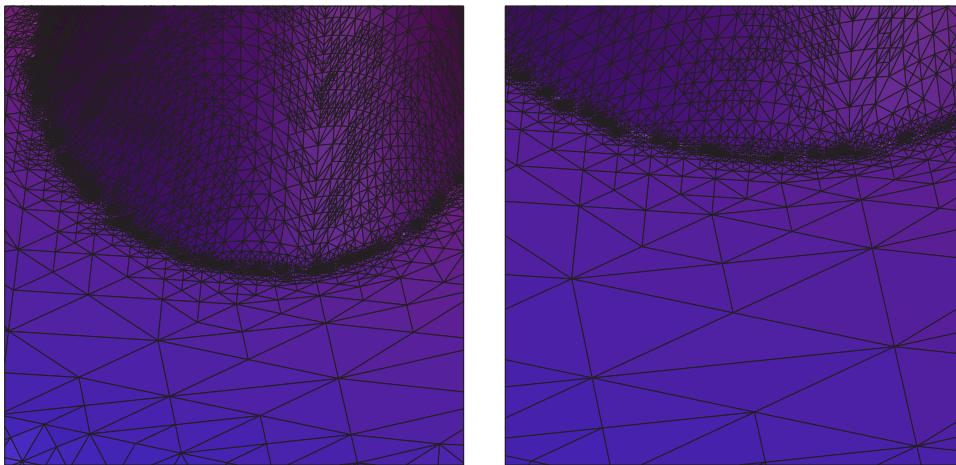

Figure 3.5.9: Experiment 3: The zooms of meshes for Γ_8 and Γ_9 near the curve $r = 0.5$ where the surface is singular in that the second derivatives exhibit and unbounded but integrable discontinuity. AFEM adapts and refines massively near this curve to resolve the effect of this singularity, and gives nearly optimal results; see also Table 3.5.4.

BIBLIOGRAPHY

[1] M. Ainsworth and J.T. Oden, *A Posteriori Error Estimation in Finite Element Analysis*, John Wiley & Sons, Inc., 2000.

[2] I. Babuška and M. Vogelius, *Feedback and adaptive finite element solution of one dimensional boundary value problems*, Numer. Math. 44 (1984), pp.75-102

[3] E. Bänsch, P. Morin, and R.H. Nochetto, *Surface diffusion of graphs: variational formulation, error anlysis and simulation*, SIAM J. Numer. Anal., 42, 2 (2004), pp.773-799.

[4] Z. Chen and F. Jia, *An adaptive finite element algorithm with reliable and efficient error control for linear parabolic problems*, Math. Comp., 73 (2004), pp.1163-1197.

[5] Ph. Ciarlet, *The Finite Element Method for Elliptic Problems.*, North-Holland, Amsterdam, 1978; reprinted, Classics Appl. Math. 40, SIAM, Philadelphia, 2002.

[6] P. Clément, *Approximation by finite element functions using local regularizations*, RAIRO Modél. Math. Anal. Numér., 2 (1975) pp.77-84.

[7] W. Dörfler, *A convergent adaptive algorithm for Poisson's equation*, SIAM J. Numer. Anal., 33 (1996), pp.1106-1124.

[8] W. Dörfler and M. Rumpf, *An adaptive strategy for elliptic problems including a posteriori controlled boundary approximation*, Math. Comp., 67 (1998) pp.1361-1382.

[9] G. Dziuk, *Finite elements for the Beltrami operator on arbitrary surfaces*, Partial Differential Equations and Calculus of Variations, Lecture Notes in Mathematics 1357, Springer Berlin Heidelberg New York London Paris Tokyo 1988, pp.142-155.

[10] P. Grisvard, *Elliptic Problems in Nonsmooth Domains*, Pitman, Boston, 1985.

[11] R.B. Kellogg, *On the Poisson equation with intersecting interfaces*, Applicable Analysis, 4 (1975), pp.101-129.

[12] K. Mekchay, P. Morin, and R.H. Nochetto, *AFEM for Laplace-Beltrami operator on graphs: a posteriori error estimate and convergence.*, Preprint.

[13] K. Mekchay and R.H. Nochetto, *Convergence of adaptive finite element methods for general second order linear elliptic PDE*, SIAM J. Numer. Anal., To appear.

[14] K. Mekchay, P. Morin and R.H. Nochetto, *AFEM for the Laplace-Beltrami operator on parametric surfaces*, (in preparation).

[15] P. Morin, R.H. Nochetto, and K.G. Siebert, *Data oscillation and convergence of adaptive FEM*, SIAM J. Numer. Anal., 38, 2 (2000), pp.466-488.

[16] P. Morin, R.H. Nochetto, and K.G. Siebert, *Convergence of adaptive finite element methods*, SIAM Review, 44 (2002), pp.631-658.

[17] P. Morin, R.H. Nochetto, and K.G. Siebert, *Local problems on stars: a posteriori error estimation, convergence and performance*, Math. Comp., 72 (2003) pp.1067-1097.

[18] R.H. Nochetto, *Removing the saturation assumption in a posteriori error analysis*,Istit. Lombardo Sci. Lett. Rend. A, 127 (1993), pp.67-82.

[19] A.H. Schatz, *An observation concerning Ritz-Galerkin methods with indefinite bilinear forms*, Math. Comp. 28 (1974), pp.959-962.

[20] A. Schmidt and K.G. Siebert, *ALBERT: an adaptive hierarchical finite element toolbox*, Documentation, Preprint 06/2000, Universität Freiburg.

[21] A. Schmidt and K.G. Siebert, *ALBERT - software for scientific computations and applications*, Acta Mathematica Universitatis Comenianae 70 (2001), pp.105-122.

[22] A. Schmidt and K.G. Siebert, *Design of Adaptive Finite Element Software : The Finite Element Toolbox ALBERTA*, Lecture Note in Computational Science and Engineering, Springer, 2005.

[23] R. Verfürth, *A Review of A Posteriori Error Estimation and Adaptive Mesh-Refinement Technique*, Wiley-Teubner, Chichester, 1996.